



# Discovery of Small-Molecule Autophagy Modulators in Mammalian Systems

## Citation

Kuo, Szu-Yu. 2016. Discovery of Small-Molecule Autophagy Modulators in Mammalian Systems. Doctoral dissertation, Harvard University, Graduate School of Arts & Sciences.

## Permanent link

<http://nrs.harvard.edu/urn-3:HUL.InstRepos:33840641>

## Terms of Use

This article was downloaded from Harvard University's DASH repository, and is made available under the terms and conditions applicable to Other Posted Material, as set forth at <http://nrs.harvard.edu/urn-3:HUL.InstRepos:dash.current.terms-of-use#LAA>

## Share Your Story

The Harvard community has made this article openly available.  
Please share how this access benefits you. [Submit a story](#).

[Accessibility](#)

**Discovery of Small-Molecule Autophagy Modulators  
in Mammalian Systems**

A dissertation presented

by

Szu-Yu Kuo

to

The Department of Molecular and Cellular Biology

in partial fulfillment of the requirements

for the degree of

Doctor of Philosophy

in the subject of

Biology

Harvard University

Cambridge, Massachusetts

May 2016

© 2016 Szu-Yu Kuo

All rights reserved

## Discovery of Small-Molecule Autophagy Modulators in Mammalian Systems

### Abstract

Autophagy is an evolutionarily conserved catabolic process in eukaryotes, which involves the formation of double-membrane vesicles that enclose cellular components and fuse with lysosomes. Autophagy is critical to the maintenance of cellular homeostasis by degrading cytosolic materials and redistributing biological building blocks to essential metabolic pathways. Furthermore, autophagy selectively clears cytosolic components, including protein aggregates, damaged organelles and invasive pathogens, to alleviate cellular stresses caused by these components. The importance of autophagy has been underscored by relationships between compromised autophagy and the pathogenesis of various human diseases. These observations have motivated us to explore whether autophagy enhancement can introduce beneficial effects in the context of these diseases.

Here I describe our efforts to study effects of autophagy enhancement in cellular models of human diseases using small-molecule probes. We identified 998 probes from screening 59,541 small molecules prepared by stereoselective, diversity oriented chemical synthesis. We further prioritized five probes based on their activities, chemical structures and toxicities to mammalian cells, and tested them in cellular models of various human diseases. One probe, BRD5631, elicited beneficial effects, which supports our hypothesis that enhancing autophagy is a promising strategy to rescue disease phenotypes related to defective autophagy. We also discovered BRD1240, a potent probe that suppressed the maturation of autophagy by disrupting lysosomal functions. An unbiased approach using bioactivity profiling suggested that BRD1240 might share the same MoA of a known V-ATPase inhibitor, bafilomycin A1, which was confirmed *in vitro*.

In parallel, I explored the potential to use small-molecule probes to directly modulate a variant of autophagic core protein ATG16L1 (T300A), which is associated with increased risk for Crohn's disease due to susceptibility to caspase-3 cleavage. I developed an assay for screening small molecules that protect ATG16L1 T300A from caspase-3 cleavage and identified small molecules that elicited desirable effects. I also present plans to further study their mechanisms and effects of these small molecules on Crohn's disease phenotypes.

Together, these findings provide more understanding of autophagy enhancement in the context of diseases. Moreover, small-molecule probes we discover can serve as valuable tools for studying autophagy in the context of cellular homeostasis and disease.

## Table of Contents

<b>Abstract</b> .....	<b>iii</b>
<b>Table of Contents</b> .....	<b>v</b>
<b>Acknowledgements</b> .....	<b>viii</b>
<b>List of Abbreviations</b> .....	<b>x</b>
<b>Chapter I: Overview</b> .....	<b>1</b>
1.1 Autophagy and its regulatory mechanism.....	2
1.2 Selective autophagy.....	4
1.3 Relevance of autophagy to human diseases .....	5
1.4 Small-molecule probes for autophagy .....	8
1.5 Target-based and phenotypic-based screening strategies in chemical biology and drug discovery.....	11
1.6 Concluding remarks .....	12
1.7 References.....	14
<b>Chapter II: Small-molecule enhancers of autophagy modulate cellular disease phenotypes suggested by human genetics</b> .....	<b>21</b>
<b>2.1 Introduction</b> .....	<b>23</b>
2.1.1 Small-molecule autophagy modulators in disease relevant cellular assays .....	23
2.1.2 Small-molecule screening for autophagy modulators .....	24
<b>2.2 Identification of small-molecule modulators of autophagy in a high-throughput phenotypic screen</b> .....	<b>26</b>
2.2.1 High-throughput screening identifies small-molecule modulators of autophagy .....	26
2.2.2 Effects of small-molecule hits on cell viability are tested .....	27
2.2.3 Autophagy flux assay distinguishes inhibitors of autophagosome turnover from activators of autophagosome formation.....	27
2.2.4 Alkyl amines and lipophilic moieties are enriched among hits of the LC3 punctae formation assays.....	29
2.2.5 Prioritized compounds do not disrupt lysosomal functions .....	33
<b>2.3 Mechanistic and functional characterization of novel small-molecule enhancers of autophagy</b> .....	<b>35</b>
2.3.1 Measuring levels of LC3-II by Western blot validates the results of microscopy-based assays .....	35
2.3.2 Autophagy modulators do not disrupt mTOR kinase activity .....	35
2.3.3 BRD5631 decreases the presence of aggregates in cells expressing poly-Q repeats (eGFP-HDQ74).....	36
2.3.4 A subset of autophagy modulators suppress NPC1-induced cell death in a hiPSC-derived neuronal model of Niemann–Pick Type C1 disease.....	38

2.3.5 A subset of autophagy modulators enhances bacterial clearance in an autophagy-dependent manner.....	39
2.3.6 A subset of autophagy modulators suppresses IL-1 $\beta$ secretion in an autophagy-dependent manner.....	43
<b>2.4 Conclusion and discussion .....</b>	<b>44</b>
<b>2.5 Materials and methods .....</b>	<b>48</b>
<b>2.6 References.....</b>	<b>57</b>
<b>Chapter III: Discovery of a small-molecule probe for V-ATPase function .....</b>	<b>63</b>
3.1 Introduction .....	65
3.2 BRD1240 increases autophagosome number by inhibiting autophagosomal turnover ..	67
3.3 BRD1240 modulates lysosomal function .....	70
3.4 BRD1240 has notable structure-activity relationships .....	71
3.5 BRD1240 kills a similar subset of cancer cells as the V-ATPase inhibitor, Bafilomycin A1 .....	73
3.6 BRD1240 suppresses V-ATPase function in biochemical assays using membrane fractions .....	74
3.7 Conclusion .....	76
3.8 Experimental methods .....	77
3.9 Reference .....	82
<b>Chapter IV: Identification of small-molecule modulators of caspase-3 processing of ATG16L1 T300A .....</b>	<b>85</b>
4.1 Introduction .....	87
4.2 Validation of a knockout-reconstitution system expressing ATG16L1 T300A in HeLa cells.....	89
4.3 Development of the AlphaLISA assay for assessing the level of full-length ATG16L1 protein .....	91
4.4 Primary screening of 20,876 compounds and confirmation of hits in dose in the AlphaLISA assay.....	94
4.5 Conclusion and future directions.....	96
4.6 Experiment methods .....	98
4.7 References.....	101
<b>Chapter V: Summary and discussion.....</b>	<b>103</b>
5.1 Summary of research presented.....	104
5.2 Discussion and future directions .....	106
5.3 References.....	109
<b>Appendix A: Supplementary materials for chapter II.....</b>	<b>111</b>
<b>Appendix B: Supplementary materials for chapter III.....</b>	<b>121</b>
<b>Appendix C: Supplementary materials for chapter IV .....</b>	<b>127</b>

*In the mountains of truth you will never climb in vain:  
either you will get up higher today,  
or you will exercise your strength  
so as to be able to get up higher tomorrow.*

- Friedrich Nietzsche



## Acknowledgements

I would like to first and foremost thank my advisor, Dr. Stuart Schreiber, for his guidance and support along my journey towards a PhD. Stuart has introduced me to the realm of chemical biology, led me to the collaborative environment at Broad, and last but certainly not least, inspired me to tackle challenging questions aiming to impact human health. I am always grateful to have this opportunity to work so closely with my role model of a scientist and a mentor. I would like to thank Dr. Ramnik Xavier for providing critical scientific guidance and extraordinary opportunities to work on projects that are on the cutting edge of the field. Special thanks to my committee members, Dr. Rachele Gaudet and Dr. Emily Balskus for mentoring me, supporting me and providing helpful feedbacks and suggestions. Also, I would never be able to go this far without numerous helps from my mentor, Dr. Aly Shamji, and my colleagues, Dr. Adam Castoreno and Dr. Leslie Aldrich. Thank you for being with me from my first day in the lab, and teaching me everything from day-to-day lab techniques to priceless graduate school survival guides.

I would like to extend my sincere gratitude to my colleagues, Dr. Kara Lassen, Dr. Kim Carey, Dr. Daniel O'Connell, Dr. Liza Leshchiner, Dr. Isabel Latorre, Dr. Tom Sundberg, Dr. Michael Durney, Dr. Jason Rush, Dr. Caline Matar, Lupe Jasso, Doug Kenny, Liv Johannessen, Ariel Lefkovith, Sydney Alnemy, Adam Petrone and all other current and former members in the Schreiber group and the Xavier group. You have helped me growing up as a scientist with valuable discussions and your instrumental advises on experiment design, lab techniques, data interpretation and scientific writing. And of course, my daily life in the lab would have been unbearably stressful without times when we shared laughter and free foods in the kitchen along with meaningful or nonsense conversations, science jokes and everything.

Thanks to all my friends around me during these years. Doing science is a bittersweet process, but having you as my companions and being able to share with you even the most trivial ups and downs in graduate school have made my experience sweeter than bitterer.

Special thanks to my roommates, Ilse, I-Tzu and Kevin Chen, to be my family in Cambridge, to tolerate those moments when I almost lost my sanity and to share critical but always warm and loving advises in all aspects of life.

I would like to thank my friends in the class of B95B01 at NTU. Times with you in college largely shaped my personality and attitudes toward life, and made me a more lovable human being (for most of the time). You have also taught me that true friendships would not be worn by time and distance. Finally, I would like to express my deepest appreciation to my family. Your unconditional love and support have given me courage to face challenges and overcome obstacles throughout my journey. Being part of our family has been and will be the most precious portion of my life.

## List of Abbreviations

<b>APP</b>	amyloid precursor protein
<b>ASM</b>	acid sphingomyelinase
<b>AUC</b>	area under the curve
<b>BafA1</b>	bafilomycin A1
<b>BCP</b>	build/couple/pair
<b>BMDM</b>	bone marrow derived macrophage
<b>CBZ</b>	carbamazepine
<b>CD</b>	Crohn's disease
<b>CP</b>	chloramphenicol
<b>CQ</b>	chloroquine
<b>CRISPR</b>	clustered regularly interspaced short palindromic repeats
<b>Dex</b>	dexamethasone
<b>DMEM</b>	Dulbecco's modified Eagle's medium
<b>DMSO</b>	dimethyl sulfoxide
<b>DOS</b>	diversity-orientated synthesis
<b>FDA</b>	Food and Drug Administration
<b>FRET</b>	fluorescence resonance energy transfer
<b>GWAS</b>	genome-wide association study
<b>hESC</b>	human embryonic stem cells
<b>hiPSC</b>	human induced pluripotent stem cells
<b>HTS</b>	high-throughput screen
<b>iBMDM</b>	immortalized bone marrow derived macrophage
<b>IMDM</b>	Iscove's modified Dulbecco's medium
<b>iTRAQ</b>	isobaric tags for relative and absolute quantitation
<b>LAP</b>	LC3-associated phagocytosis
<b>LIR</b>	LC3-interacting region
<b>LPS</b>	lipopolysaccharide
<b>MDP</b>	muramyl dipeptide
<b>MEF</b>	mouse embryonic fibroblast
<b>MoA</b>	mechanism-of-actions
<b>Mtb</b>	<i>Mycobacterium tuberculosis</i>
<b>mTOR</b>	the mechanistic target of rapamycin

<b>NPC1</b>	Niemann-Pick type C1 disease
<b>OPTN</b>	Optineurin
<b>p.i.</b>	post-infection
<b>PAINS</b>	pan assay interference compounds
<b>PBS</b>	phosphate buffered saline
<b>PE</b>	phosphatidylethanolamine
<b>pepA</b>	pepstatin A
<b>PFA</b>	paraformaldehyde
<b>PI3K</b>	phosphatidylinositol-3 kinase
<b>PI3P</b>	phosphatidylinositol-3-phosphate
<b>PRR</b>	pathogen recognition receptor
<b>S6K1</b>	p70 S6 kinase 1
<b>SAR</b>	structure-activity relationship
<b>SCV</b>	<i>Salmonella</i> -containing vacuole
<b>SILAC</b>	stable isotope labeling by amino acid in cell culture
<b>STA</b>	staurosporine
<b>TFP</b>	trifluoperazine
<b>UBA</b>	ubiquitin-binding domain
<b>V-ATPase</b>	vacuole-type H <sup>+</sup> -ATPases

*Page left intentionally blank*

# **Chapter I**

## **Overview**

## 1.1 Autophagy and its regulatory mechanism

Autophagy is a highly-regulated cellular pathway in eukaryotes by which intracellular components are degraded in a lysosome-dependent manner. Three different types of autophagy have been defined based on the routes through which components are directed to degradation. Microautophagy and chaperone-mediated autophagy deliver components directly into lysosomes. In contrast, macroautophagy involves the formation of double-membrane vesicles that encapsulate cellular components and fuse with lysosomes (1).

In most cell types, macroautophagy (referred as autophagy hereafter) occurs at a basal level to maintain cellular homeostasis by degrading cytosolic materials and redistributing nutrients to essential metabolic pathways (1). Autophagy is initiated by the activation of a class III phosphatidylinositol-3 kinase (PI3K) complex, VPS34 complex, which in turn activates the production of phosphatidylinositol-3-phosphate (PI3P) on pre-autophagosomal structures (2). PI3P recruits proteins that facilitate the nucleation and elongation of pre-autophagosomal structures, including the ATG5-ATG12-ATG16L1 complex (2). The ATG5-ATG12-ATG16L1 complex specifies the site of LC3 recruitment and catalyzes the covalent conjugation of LC3-I to the lipid phosphatidylethanolamine (PE) and forms LC3-II, which plays a role in the elongation and closure of membranes and specifically labels autophagic vesicles (3, 4). Autophagosomes then fuse with lysosomes and form autolysosomes. Lysosomes contain components that are critical to maintain the acidic lumen environment and hydrolases that degrade contents in autolysosomes. The fate of autolysosomes following the degradation process is not well understood. Products generated via the degradation of lumen contents are released to complement cytosolic nutrient pools (5). The regeneration of lysosomes directly from autolysosomes has also been reported (6). (Figure 1.1)

Autophagy initiation can be regulated through distinct signaling cascades. Many signals, including nutrient and energy levels, are coordinated by the kinase activity of the mechanistic target of rapamycin (mTOR) (7). When activated by nutrients, mTOR suppresses autophagy by

phosphorylating components in the ULK1-complex (8). When mTOR kinase activity is blocked in response to nutrient deprivation or other energy-low conditions, ULK1 becomes activated and induces autophagy by phosphorylating Beclin 1, which in turn activates VPS34 (9). Signaling pathways that are independent to mTOR suppression have also been identified. For example, the binding of Beclin 1 by its negative regulator, GAPR-1, inhibits autophagy. Disrupting their interaction by Tat-beclin 1, a peptide derived from the fragment of Beclin 1, can enhance autophagy (10). As lysosomes are critical for the degradative capacity of autolysosomes, proper lysosomal functions are also essential for autophagy machinery. Acidic pH in lysosomes is mainly maintained by the activity of the vacuole-type H<sup>+</sup>-ATPases (V-ATPases). Blocking the activity of V-ATPases negatively regulates autophagy by disrupting the degradative activity of autophagy (11).

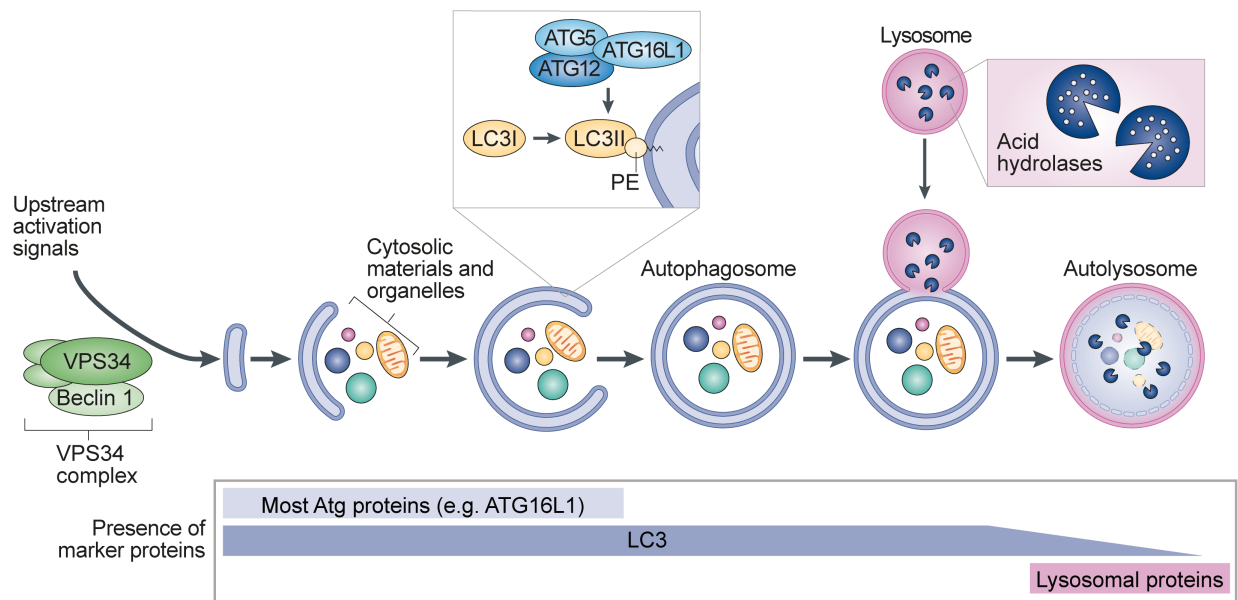


**Figure 1.1. The process of autophagy.** The process of autophagy and key regulators of the process are highlighted. Once the autophagosome forms, the ATG5-ATG12-ATG16L1 complex dissociates from the surface of autophagosome. It has also been reported that a hydrolytic enzyme, ATG4, can cleave LC3 molecules on the outer membrane, while LC3 molecules remain on the inner membrane of autophagosomes until degraded after the formation of the autolysosome (12). The figure is modified from refs. 13 and 14.



Furthermore, many studies have indicated that some regulatory mechanisms can enhance efficiencies of both autophagy initiation and autophagosome-lysosome fusion, so the two steps can be orchestrated. For example, nutrient deprivation not only activates autophagy via suppressing mTOR kinase activity, but also stimulates the relocalization of lysosomes from peripheral to perinuclear location to facilitate autophagosome-lysosome fusion (15). Also, mTOR is reported to localize on lysosomes under nutrient-rich conditions via mechanisms depending on the V-ATPase (16, 17). Lysosome-associated mTOR can recruit and phosphorylate TFEB, the master transcription factor of lysosome- and autophagy-related genes (18), and restrain TFEB from translocating to nucleus. Under nutrient-deprivation conditions, mTOR disassociates from lysosomes and loses its kinase activity, and therefore TFEB can translocate to nucleus to promote the transcription of genes essential for lysosome biogenesis and autophagy (19, 20).

## **1.2 Selective autophagy**

Autophagy has long been considered to be non-selective, until studies discover that various cargos can be targeted specifically to pre-autophagosomal structures for degradation, including aggregate proteins, damaged organelles and invasive pathogens (21). In mammalian systems, the most well known autophagy-targeting signal is the modification of cargos with ubiquitin. To selectively target cargos, it is necessary to have adaptor proteins that interact with both ubiquitylated cargos and proteins on pre-autophagosomal structures. To date, several adaptors that contain ubiquitin-binding (UBA) domains and LC3-interacting region (LIR) motifs have been identified, including p62, NBR-1, NDP52, TAX1BP1 and Optineurin (OPTN) (22). Among various cargos, the selective clearance of mitochondria is the most extensively studied one. Parkin is an E3 ubiquitin ligase that ubiquitylates outer membrane proteins on damaged mitochondria. This process is dependent on the activity of PINK1, which accumulates on the surface of damaged mitochondria (23). Ubiquitin-labeled damaged mitochondria can be

targeted by NDP52, OPTN and in some cases, TAX1BP1, and subsequently recruited to autophagy machinery (24, 25). In the context of aggregate clearance, ubiquitylated protein aggregates can be targeted by p62 and NBR-1 and degraded by autophagy (26-28).

Autophagy machinery is able to clear many medically important bacteria including *Salmonella enterica*, *Mycobacterium tuberculosis* (Mtb), *Shigella flexneri* and *Listeria monocytogenes* (29). *Salmonella enterica* serotype Typhimurium (hereafter *Salmonella*) is often used as a model for studying this mechanism (30). Upon cellular invasion into non-phagocytic cells, *Salmonella* are localized in intracellular compartments termed *Salmonella*-containing vacuoles (SCVs) and proliferate in SCVs (31). Previous research indicates that both damaged SCVs and *Salmonella* that escape into the cytosol from damaged SCVs can be ubiquitylated by an E3 ligase LRSAM1 and be targeted by adaptor proteins that deploy LC3-interacting regions and recruit pathogens to nascent autophagosomes (32, 33). P62, NDP52, OPTN and TAX1BP1 have been identified to be involved in *Salmonella* targeting and have non-redundant contributions (34-37). Notably, NDP52 can also interact with galectin-8, the protein that labels damaged SCVs, and facilitate the targeting of damaged SCV to autophagy (38). The importance of the autophagy machinery in the control of *Salmonella* infection has been well established; however, its complexity has also been revealed, which motivates our focus on developing genetic and molecular probes for research into mechanisms for how antibacterial autophagy is regulated.

### **1.3 Relevance of autophagy to human diseases**

Besides being a fundamental cellular process, autophagy has also been implicated in several human diseases, including neurodegenerative diseases, inflammatory disorders such as Crohn's disease (CD) and infectious diseases (39).

Most adult-onset neurodegenerative diseases are characterized by the accumulation of toxic protein aggregates in neurons; for instance, mutant huntingtin aggregates for Huntington's

disease and mutant  $\alpha$ -synuclein for Parkinson's disease. Autophagy has been implicated in the clearance of cytosolic neurodegenerative disease-associated protein aggregates (40). In cellular models of Huntington's disease, for example, autophagy inhibition by genetic or pharmacological manipulations suppresses the clearance of toxic aggregates, while autophagy activation enhances the clearance (41-43). Activating autophagy by suppressing mTOR kinase activities in *Drosophila melanogaster* and mouse models of Huntington's disease alleviates symptoms of neurodegeneration (41). In the context of familial Parkinson's disease, autophagy can clear aggregated mutant  $\alpha$ -synuclein (44, 45) and is also implicated in the clearance of damaged mitochondria (46). Mutations in *Parkin* and *PINK1* have been long linked to increased risk of familial Parkinson's disease (47, 48). Accumulated understanding of *Parkin* and *PINK1* functions has supported the connections between dysfunctional mitochondria and Parkinson's disease, and highlight the importance of autophagy-based mitochondria clearance (49).

Similarly, genetic variants in genes regulating autophagy and antibacterial autophagy have been linked to increase incidence of CD (50). Further studies have linked the disease-associated alleles to CD phenotypes that reflect high microbial load and uncontrolled anti-microbial immune responses in intestinal epithelium and cytokine-producing innate immune cells (51). More specifically, the CD-associated risk allele of *NOD2* abrogates NF- $\kappa$ B activation induced by bacterial cell wall components in human cell lines and the induction of antibacterial autophagy in human cell lines and murine bone marrow derived macrophages (BMDMs) (52, 53). Cells harboring CD-associated risk allele of *IRGM* fail to control the expression level of *IRGM* when challenged by CD-related stresses, which affect the efficiency of autophagic flux and antibacterial autophagy (54). Furthermore, expression of a coding variant in *ATG16L1* (T300A) correlates with compromised bacterial defense, increased release of inflammatory cytokines (IL-1 $\beta$  and IL-6), and reduced formation of antimicrobial granules in gut Paneth cells (55-57).

Defects in autophagy can also result in systematic effects as in the context of infectious diseases. Autophagy serves as one of innate immune mechanisms that regulate the responses to invasive pathogens. Its importance is highlighted by the observation that knockout of *Atg5* or *Atg16L1* in mouse intestinal epithelial cells results in diminished resistance to *Salmonella* (58, 59). In cells that produce inflammatory responses in response to pathogens, autophagy can prevent the responses from being excessive through degrading precursors of inflammatory cytokines (60) or through removing cytosolic components that activate inflammasome, which is critical for the maturation of inflammatory cytokines (61). Also, autophagy is involved in the delivery of endogenous microbial antigens to MHC class II antigen-presenting molecules. Proper antigen presentation is critical for the activation of CD4<sup>+</sup> T lymphocytes (62, 63). At the whole organism levels, knockdown of proteins important for autophagy initiation decreases the host survival rates after infection with *Staphylococcus aureus* in *Caenorhabditis elegans* (64). Similar results are observed in *Drosophila melanogaster* infected with *Listeria monocytogenes* (65).

Notably, many proteins critical for autophagy also have non-canonical roles in other cellular pathways. For example, some autophagic core proteins, including LC3, are known to be recruited to phagosomal membranes to facilitate the degradation of pathogens in phagosomes in the process of LC3-associated phagocytosis (LAP) in phagocytic cells (66-68). Recruitment of LC3 in LAP requires Beclin 1, VPS34 and the ATG12-ATG5-ATG16L1 complex but not the ULK1 complex (69). Phenotypes observed in disease models utilizing genetic modulations of functions of autophagy core components may reflect combined effects on autophagy and LAP or other non-canonical autophagy pathways and should therefore be interpreted carefully.

## 1.4 Small-molecule probes for autophagy

Small-molecule probes have proven to be valuable tools for studying biological processes including autophagy. In addition to forming the basis for medicines and pharmacology studies, their ability to selectively target specific functions of multifunction protein complexes and cell circuitry also makes them important tools in basic life science research (70). For example, rapamycin was instrumental to the discovery of mTOR and the understanding of many mTOR-regulated mechanisms, including autophagy (71). Rapamycin binds the immunophilin FKBP12 to form a drug-protein complex that allosterically blocks the activity of mTORC1, leading to the activation of autophagy (71-73). Many other small molecules also activate autophagy by suppressing mTOR kinase activity (Figure 1.2). Torin1 and its analogs suppress mTOR via direct ATP-competition (74). PI-103 selectively inhibits class I PI3Ks and mTOR in an ATP-competitive manner (75). Balgi and colleagues reported that perhexiline, niclosamide, amiodarone and rottlerin activate autophagy by inhibiting mTORC1 signaling (76).

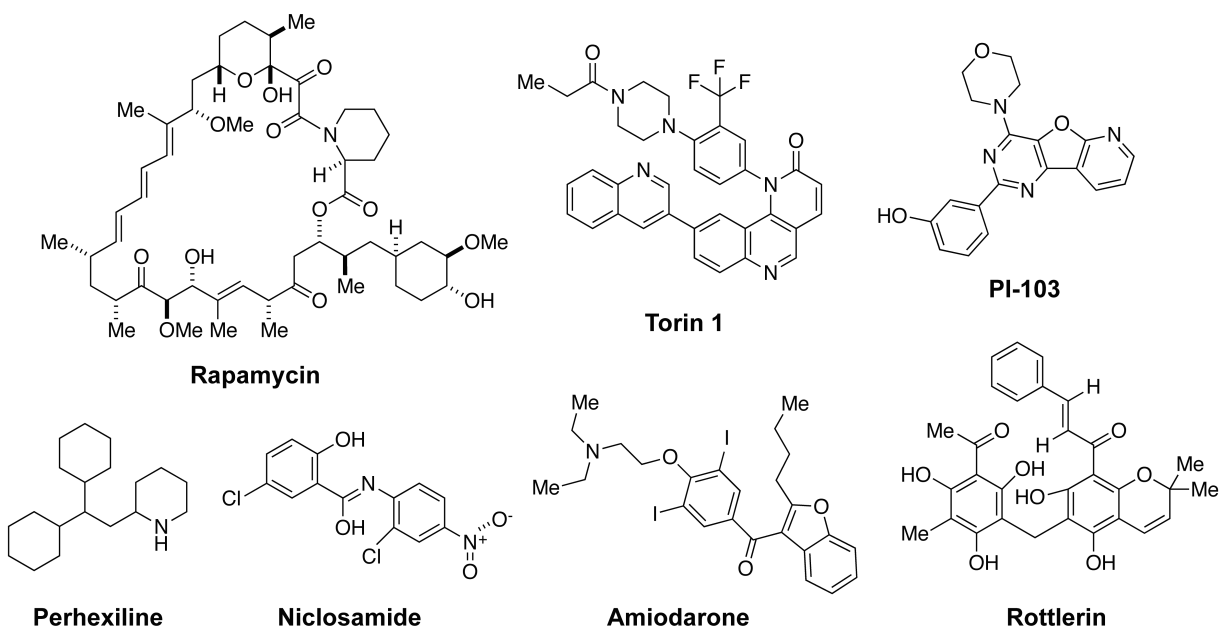


**Figure 1.2. Small-molecule activators of autophagy that disrupts mTOR activity.**

Many small molecules activate autophagy without disrupting mTOR kinase activity (Figure 1.3). The discovery of them has contributed to the identification of novel mTOR-independent mechanisms of autophagy activation, or the validation of previously identified mechanisms (39, 42). For example, trifluoperazine (TFP), a calmodulin antagonist that increases cytosolic  $\text{Ca}^{2+}$  concentration (77), was identified to promote GFP-LC3 punctae formation and the clearance of a known autophagic target, aggregated mutant huntingtin (78). This discovery echoed another study that proposed the roles of  $\text{Ca}^{2+}$  and calmodulin in regulating autophagy (79). In some cases, small molecules that induced favorable phenotypes in disease models related to deficient autophagy were deeply investigated, and subsequently revealed regulatory mechanisms of autophagy. Lithium is used as a mood-stabilizing drug and is able to suppress the level of aggregated mutant huntingtin in models of Huntington's disease (80). Follow-up studies discovered that the protective effects of lithium depend on its activity to activate autophagy by suppressing intracellular inositol level. Other small molecules that suppress inositol levels, such as carbamazepine (CBZ) and valproic acid can elicit similar effects, emphasizing the link between inositol signaling pathway and autophagy activation(45).

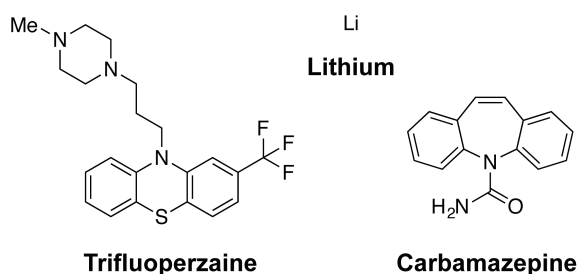


**Figure 1.3. Small-molecule activators of autophagy that does not disrupt mTOR activity.**

Likewise, many researchers have shown that autophagy can be inhibited pharmacologically by targeting the upstream or late-stage autophagy process. Commonly used inhibitors that target the upstream pathway of autophagy are 3-methyladenine (81), wortmannin and LY294002 (82) (Figure 1.4A). All of them target PI3K and therefore are able to inhibit the

activity of the class III PI3K, VPS34. These three compounds target all three classes of PI3K; therefore are known to have side effects other than autophagy activation. SAR405, a highly selective VPS34 inhibitor was recently discovered (83). Besides kinase inhibitors, spautin-1 was recently discovered as an autophagy inhibitor that promotes the proteasomal degradation of VPS34 complex (84). Compounds that disrupt lysosomal functions can serve as inhibitors of the late-stage of autophagy (Figure 1.4B). For example, compounds that disrupt lysosomal acidification [bafilomycin A1 (BafA1) (11) and chloroquine (CQ) (85)] or lysosomal protease inhibitors [pepstatin A (pepA) and E64d (86)] can block autophagic turnover by suppressing autophagosome-lysosome fusion and/or by disrupting the digestive activity of lysosomes.

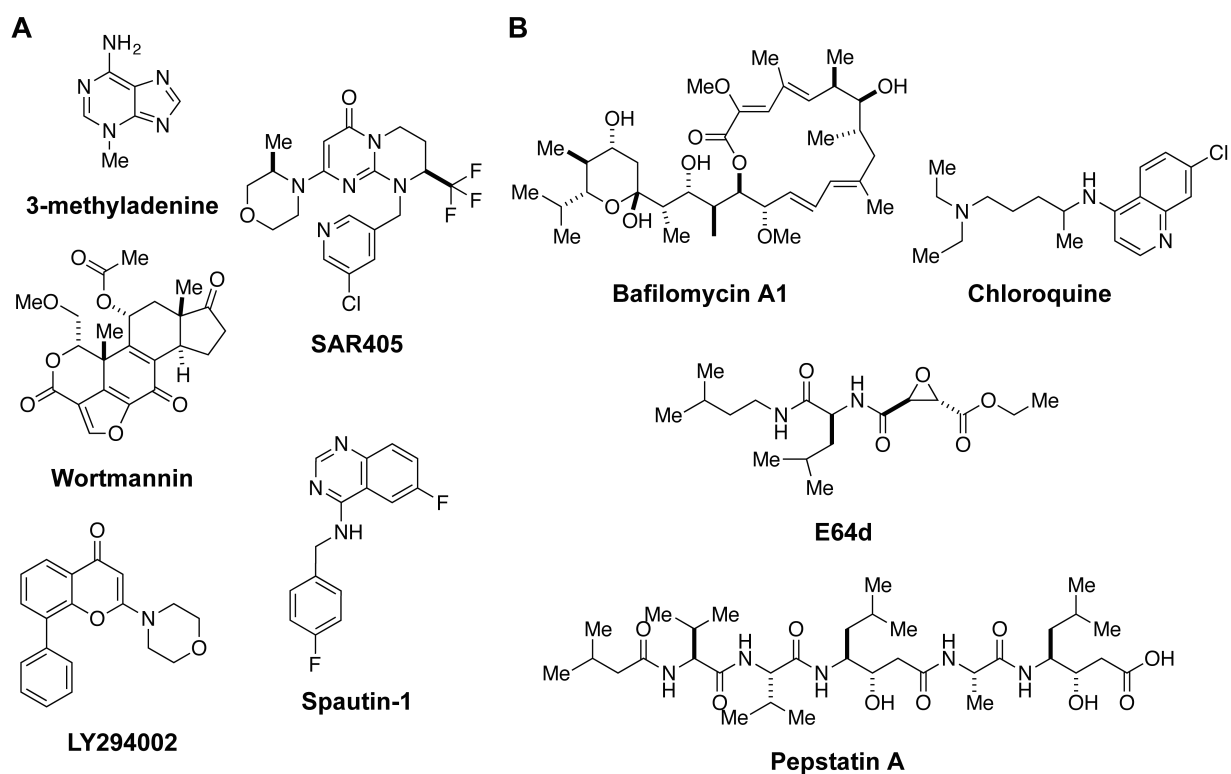


**Figure 1.4. Small-molecule inhibitors of autophagy.** (A) Small molecules that inhibit the initiation of autophagy. (B) Small molecules that inhibit the late stage of autophagy.

Although many small-molecule probes have been identified and utilized in autophagy research, a majority of them have moderate potency, and may have multiple targets and

functions. In order to have a better understanding of the autophagy process, developing more efficient and selective molecular probes is crucial.

## **1.5 Target-based and phenotypic-based screening strategies in chemical biology and drug discovery**

High-throughput small-molecule screening is commonly utilized to discover biologically active probes and drug candidates in academia and pharmaceutical industry. Approaches of small-molecule screening can be broadly classified into two categories: discovery of small molecules that modulate the activity of specific biological targets (target-based screens) and discovery of small molecules that elicit desired phenotypes in relevant cell or animal models (phenotypic screens) (87). In brief, a target-based screen requires the identification of disease-associate biological targets to enable the search of small-molecule probes that bind or modulate the activities of targets of interest in biochemical assays, which usually involve purified targets (88, 89). Follow-up efforts are necessary to validate that effects of small molecules can be recapitulated in cellular environments, and that such effects can elicit favorable biological phenotypes (90). On the contrary, phenotypic screens allow scientists to study directly if small molecules are able to modulate cellular or physiological phenotypes in more biologically relevant contexts than target-based screens (87). Molecular targets associated with phenotypes elicited by bioactive small molecules need to be deconvoluted to enable medicinal chemistry efforts for probe optimization and drug development (91).

The understanding of the human genome and insights into disease mechanisms have significantly accelerated the progress of disease-relevant target identification in the past few decades, and therefore have made target-based screens a popular approach in probe and drug development (92). With the advances in screening technologies, more and more probes were successfully identified to modulate targets that were previously considered 'undruggable', such



as protein-protein interactions (93). An analysis published recently (94) presented the importance of target-based screening strategies in drug development, as the majority (43%) of new drugs approved by US Food and Drug Administration (FDA) between 1999 and 2008 were from target-based screens, while 25% were from phenotypic screens. Notably, the same article also pointed out that phenotypic-based screens had more success in identifying first-in-class drugs than target-based approaches. This observation highlights the potential of phenotypic screens as an unbiased approach to reveal new therapeutic targets, which makes it particularly appealing for areas in which detailed mechanistic understanding is not yet available (95). Recent advancements in the sophistication of phenotypic assays and mechanism-of-action (MoA) determination have facilitated the success of phenotypic screening strategies and will continue to make these strategies more attractive (96). Like all scientific methods, target-based and phenotypic-based screen each has its own strengths and weaknesses. The choice of screening method should be made on a case-by-case basis. Level of mechanistic understanding in the area of interest, techniques available and the purpose of the study all have to be considered before a particular screening strategy is chosen.

## **1.6 Concluding remarks**

Autophagy is a critical cellular process that plays an important role in the context of various human diseases. However, our understanding of autophagy, its regulatory pathways and how this machinery plays a role in disease pathogenesis is still limited. In order to improve our understanding, we sought to discover small-molecule autophagy modulators to study the effects and therapeutic implications of autophagy enhancement in human diseases associated with defective autophagy. We identified novel modulators of autophagy using a phenotypic-based high-throughput screen (HTS) of 59,541 small molecules prepared by stereoselective diversity-oriented chemical synthesis and demonstrated that representative hits promoted autophagy without perturbing lysosomal functions. Representative hits were further tested in

several disease-related models, as well as in assays aiming to unravel their mechanisms (**Chapter II**). **Chapter III** describes the characterization of a potent inhibitor of autophagosome turnover that emerged from the HTS, and highlights the potency of combining hypothesis-orientated strategies and unbiased bioactivity profiling in MoA determination. In **Chapter IV**, I present the progress-to-date of an alternative approach aiming to identify small molecules that target the risk allele of CD, ATG16L1 T300A, using a target-based HTS. Lastly, **Chapter V** presents possible strategies for the target deconvolution of small-molecule autophagy modulators emerging from the HTS, compares insights gained from conducting both phenotypic-based and target-based screens and discusses the potential of autophagy enhancement as a therapeutic strategy.

## 1.7 References

1. B. Ravikumar *et al.*, Regulation of mammalian autophagy in physiology and pathophysiology. *Physiol Rev* **90**, 1383-1435 (2010).
2. A. Simonsen, S. A. Tooze, Coordination of membrane events during autophagy by multiple class III PI3-kinase complexes. *J Cell Biol* **186**, 773-782 (2009).
3. N. Fujita *et al.*, The Atg16L complex specifies the site of LC3 lipidation for membrane biogenesis in autophagy. *Mol Biol Cell* **19**, 2092-2100 (2008).
4. C. Otomo, Z. Metlagel, G. Takaesu, T. Otomo, Structure of the human ATG12~ATG5 conjugate required for LC3 lipidation in autophagy. *Nat Struct Mol Biol* **20**, 59-66 (2013).
5. Z. Yang, D. J. Klionsky, Eaten alive: a history of macroautophagy. *Nat Cell Biol* **12**, 814-822 (2010).
6. L. Yu *et al.*, Termination of autophagy and reformation of lysosomes regulated by mTOR. *Nature* **465**, 942-946 (2010).
7. M. Laplante, D. M. Sabatini, mTOR signaling in growth control and disease. *Cell* **149**, 274-293 (2012).
8. J. Kim, M. Kundu, B. Viollet, K. L. Guan, AMPK and mTOR regulate autophagy through direct phosphorylation of Ulk1. *Nat Cell Biol* **13**, 132-141 (2011).
9. R. C. Russell *et al.*, ULK1 induces autophagy by phosphorylating Beclin-1 and activating VPS34 lipid kinase. *Nat Cell Biol* **15**, 741-750 (2013).
10. S. Shoji-Kawata *et al.*, Identification of a candidate therapeutic autophagy-inducing peptide. *Nature* **494**, 201-206 (2013).
11. A. Yamamoto *et al.*, Bafilomycin A<sub>1</sub> Prevents Maturation of Autophagic Vacuoles by Inhibiting Fusion between Autophagosomes and Lysosomes in Rat Hepatoma Cell Line, H-4-II-E Cells. *Cell Structure and Function* **23**, 33-42 (1998).
12. I. Tanida *et al.*, HsAtg4B/HsApg4B/Autophagin-1 Cleaves the Carboxyl Termini of Three Human Atg8 Homologues and Delipidates Microtubule-associated Protein Light Chain 3- and GABAA Receptor-associated Protein-Phospholipid Conjugates. *Journal of Biological Chemistry* **279**, 36268-36276 (2004).
13. G. Marino, M. Niso-Santano, E. H. Baehrecke, G. Kroemer, Self-consumption: the interplay of autophagy and apoptosis. *Nat Rev Mol Cell Biol* **15**, 81-94 (2014).
14. N. Mizushima, T. Yoshimori, B. Levine, Methods in mammalian autophagy research. *Cell* **140**, 313-326 (2010).
15. V. I. Korolchuk *et al.*, Lysosomal positioning coordinates cellular nutrient responses. *Nat Cell Biol* **13**, 453-460 (2011).

16. Y. Sancak *et al.*, Ragulator-Rag complex targets mTORC1 to the lysosomal surface and is necessary for its activation by amino acids. *Cell* **141**, 290-303 (2010).
17. R. Zoncu *et al.*, mTORC1 senses lysosomal amino acids through an inside-out mechanism that requires the vacuolar H(+)-ATPase. *Science* **334**, 678-683 (2011).
18. C. Settembre *et al.*, TFEB links autophagy to lysosomal biogenesis. *Science* **332**, 1429-1433 (2011).
19. A. Rocznik-Ferguson *et al.*, *The Transcription Factor TFEB Links mTORC1 Signaling to Transcriptional Control of Lysosome Homeostasis*. (2012), vol. 5, pp. ra42-ra42.
20. C. Settembre *et al.*, A lysosome-to-nucleus signalling mechanism senses and regulates the lysosome via mTOR and TFEB. *EMBO J* **31**, 1095-1108 (2012).
21. A. Stolz, A. Ernst, I. Dikic, Cargo recognition and trafficking in selective autophagy. *Nat Cell Biol* **16**, 495-501 (2014).
22. A. B. Birgisdottir, T. Lamark, T. Johansen, The LIR motif - crucial for selective autophagy. *J Cell Sci* **126**, 3237-3247 (2013).
23. L. A. Kane *et al.*, PINK1 phosphorylates ubiquitin to activate Parkin E3 ubiquitin ligase activity. *J Cell Biol* **205**, 143-153 (2014).
24. M. Lazarou *et al.*, The ubiquitin kinase PINK1 recruits autophagy receptors to induce mitophagy. *Nature* **524**, 309-314 (2015).
25. B. Richter *et al.*, Phosphorylation of OPTN by TBK1 enhances its binding to Ub chains and promotes selective autophagy of damaged mitochondria. *Proc Natl Acad Sci U S A*, (2016).
26. G. Bjorkoy *et al.*, p62/SQSTM1 forms protein aggregates degraded by autophagy and has a protective effect on huntingtin-induced cell death. *J Cell Biol* **171**, 603-614 (2005).
27. M. Filimonenko *et al.*, The selective macroautophagic degradation of aggregated proteins requires the PI3P-binding protein Alfy. *Mol Cell* **38**, 265-279 (2010).
28. V. Kirkin *et al.*, A role for NBR1 in autophagosomal degradation of ubiquitinated substrates. *Mol Cell* **33**, 505-516 (2009).
29. J. Huang, J. H. Brumell, Bacteria-autophagy interplay: a battle for survival. *Nat Rev Microbiol* **12**, 101-114 (2014).
30. T. Noda, S. Kageyama, N. Fujita, T. Yoshimori, Three-Axis Model for Atg Recruitment in Autophagy against Salmonella. *Int J Cell Biol* **2012**, 389562 (2012).
31. E. J. McGhie, L. C. Brawn, P. J. Hume, D. Humphreys, V. Koronakis, Salmonella takes control: effector-driven manipulation of the host. *Curr Opin Microbiol* **12**, 117-124 (2009).
32. C. L. Birmingham, A. C. Smith, M. A. Bakowski, T. Yoshimori, J. H. Brumell, Autophagy controls Salmonella infection in response to damage to the Salmonella-containing vacuole. *J Biol Chem* **281**, 11374-11383 (2006).

33. A. Huett *et al.*, The LRR and RING domain protein LRSAM1 is an E3 ligase crucial for ubiquitin-dependent autophagy of intracellular *Salmonella Typhimurium*. *Cell Host Microbe* **12**, 778-790 (2012).
34. T. L. Thurston, G. Ryzhakov, S. Bloor, N. von Muhlinen, F. Randow, The TBK1 adaptor and autophagy receptor NDP52 restricts the proliferation of ubiquitin-coated bacteria. *Nat Immunol* **10**, 1215-1221 (2009).
35. D. A. Tumbarello *et al.*, The Autophagy Receptor TAX1BP1 and the Molecular Motor Myosin VI Are Required for Clearance of *Salmonella Typhimurium* by Autophagy. *PLoS Pathog* **11**, e1005174 (2015).
36. P. Wild *et al.*, Phosphorylation of the autophagy receptor optineurin restricts *Salmonella* growth. *Science* **333**, 228-233 (2011).
37. Y. T. Zheng *et al.*, The adaptor protein p62/SQSTM1 targets invading bacteria to the autophagy pathway. *J Immunol* **183**, 5909-5916 (2009).
38. T. L. Thurston, M. P. Wandel, N. von Muhlinen, A. Foeglein, F. Randow, Galectin 8 targets damaged vesicles for autophagy to defend cells against bacterial invasion. *Nature* **482**, 414-418 (2012).
39. D. C. Rubinsztein, P. Codogno, B. Levine, Autophagy modulation as a potential therapeutic target for diverse diseases. *Nat Rev Drug Discov* **11**, 709-730 (2012).
40. S. Sarkar, Regulation of autophagy by mTOR-dependent and mTOR-independent pathways: autophagy dysfunction in neurodegenerative diseases and therapeutic application of autophagy enhancers. *Biochem Soc Trans* **41**, 1103-1130 (2013).
41. B. Ravikumar *et al.*, Inhibition of mTOR induces autophagy and reduces toxicity of polyglutamine expansions in fly and mouse models of Huntington disease. *Nat Genet* **36**, 585-595 (2004).
42. A. Williams *et al.*, Novel targets for Huntington's disease in an mTOR-independent autophagy pathway. *Nat Chem Biol* **4**, 295-305 (2008).
43. A. Yamamoto, M. L. Cremona, J. E. Rothman, Autophagy-mediated clearance of huntingtin aggregates triggered by the insulin-signaling pathway. *J Cell Biol* **172**, 719-731 (2006).
44. S. Sarkar, J. E. Davies, Z. Huang, A. Tunnacliffe, D. C. Rubinsztein, Trehalose, a novel mTOR-independent autophagy enhancer, accelerates the clearance of mutant huntingtin and alpha-synuclein. *J Biol Chem* **282**, 5641-5652 (2007).
45. S. Sarkar *et al.*, Lithium induces autophagy by inhibiting inositol monophosphatase. *J Cell Biol* **170**, 1101-1111 (2005).
46. D. Feng, L. Liu, Y. Zhu, Q. Chen, Molecular signaling toward mitophagy and its physiological significance. *Exp Cell Res* **319**, 1697-1705 (2013).

47. T. Kitada *et al.*, Mutations in the parkin gene cause autosomal recessive juvenile parkinsonism. *Nature* **392**, 605-608 (1998).
48. E. M. Valente *et al.*, Hereditary Early-Onset Parkinson's Disease Caused by Mutations in PINK1. *Science* **304**, 1158-1160 (2004).
49. K. Yamano, N. Matsuda, K. Tanaka, The ubiquitin signal and autophagy: an orchestrated dance leading to mitochondrial degradation. *EMBO Rep* **17**, 300-316 (2016).
50. P. Lapaquette, P. Brest, P. Hofman, A. Darfeuille-Michaud, Etiology of Crohn's disease: many roads lead to autophagy. *J Mol Med (Berl)* **90**, 987-996 (2012).
51. P. Kuballa, W. M. Nolte, A. B. Castoreno, R. J. Xavier, Autophagy and the immune system. *Annu Rev Immunol* **30**, 611-646 (2012).
52. C. R. Homer, A. L. Richmond, N. A. Rebert, J. P. Achkar, C. McDonald, ATG16L1 and NOD2 interact in an autophagy-dependent antibacterial pathway implicated in Crohn's disease pathogenesis. *Gastroenterology* **139**, 1630-1641, 1641 e1631-1632 (2010).
53. L. H. Travassos *et al.*, Nod1 and Nod2 direct autophagy by recruiting ATG16L1 to the plasma membrane at the site of bacterial entry. *Nat Immunol* **11**, 55-62 (2010).
54. P. Brest *et al.*, A synonymous variant in IRGM alters a binding site for miR-196 and causes deregulation of IRGM-dependent xenophagy in Crohn's disease. *Nat Genet* **43**, 242-245 (2011).
55. K. Cadwell *et al.*, A key role for autophagy and the autophagy gene Atg16l1 in mouse and human intestinal Paneth cells. *Nature* **456**, 259-263 (2008).
56. K. G. Lassen *et al.*, Atg16L1 T300A variant decreases selective autophagy resulting in altered cytokine signaling and decreased antibacterial defense. *Proc Natl Acad Sci U S A* **111**, 7741-7746 (2014).
57. T. S. Plantinga *et al.*, Crohn's disease-associated ATG16L1 polymorphism modulates pro-inflammatory cytokine responses selectively upon activation of NOD2. *Gut* **60**, 1229-1235 (2011).
58. J. L. Benjamin, R. Sumpter, Jr., B. Levine, L. V. Hooper, Intestinal epithelial autophagy is essential for host defense against invasive bacteria. *Cell Host Microbe* **13**, 723-734 (2013).
59. K. L. Conway *et al.*, Atg16l1 is required for autophagy in intestinal epithelial cells and protection of mice from Salmonella infection. *Gastroenterology* **145**, 1347-1357 (2013).
60. J. Harris *et al.*, Autophagy controls IL-1beta secretion by targeting pro-IL-1beta for degradation. *J Biol Chem* **286**, 9587-9597 (2011).
61. S. T. Shibutani, T. Saitoh, H. Nowag, C. Munz, T. Yoshimori, Autophagy and autophagy-related proteins in the immune system. *Nat Immunol* **16**, 1014-1024 (2015).

62. C. Munz, Antigen processing via autophagy--not only for MHC class II presentation anymore? *Curr Opin Immunol* **22**, 89-93 (2010).
63. C. Paludan *et al.*, Endogenous MHC Class II Processing of a Viral Nuclear Antigen After Autophagy. *Science* **307**, 593-596 (2005).
64. O. Visvikis *et al.*, Innate host defense requires TFEB-mediated transcription of cytoprotective and antimicrobial genes. *Immunity* **40**, 896-909 (2014).
65. T. Yano *et al.*, Autophagic control of listeria through intracellular innate immune recognition in drosophila. *Nat Immunol* **9**, 908-916 (2008).
66. G. Y. Lam, M. Cemma, A. M. Muise, D. E. Higgins, J. H. Brumell, Host and bacterial factors that regulate LC3 recruitment to *Listeria monocytogenes* during the early stages of macrophage infection. *Autophagy* **9**, 985-995 (2013).
67. X. Li, M. Prescott, B. Adler, J. D. Boyce, R. J. Devenish, Beclin 1 is required for starvation-enhanced, but not rapamycin-enhanced, LC3-associated phagocytosis of *Burkholderia pseudomallei* in RAW 264.7 cells. *Infect Immun* **81**, 271-277 (2013).
68. J. Martinez *et al.*, Molecular characterization of LC3-associated phagocytosis reveals distinct roles for Rubicon, NOX2 and autophagy proteins. *Nat Cell Biol* **17**, 893-906 (2015).
69. N. T. Ktistakis, S. A. Tooze, Digesting the Expanding Mechanisms of Autophagy. *Trends Cell Biol*, (2016).
70. C. J. O'Connor, L. Laraia, D. R. Spring, Chemical genetics. *Chem Soc Rev* **40**, 4332-4345 (2011).
71. S. N. Sehgal, Sirolimus: its discovery, biological properties, and mechanism of action. *Transplantation Proceedings* **35**, S7-S14 (2003).
72. E. J. Brown *et al.*, A mammalian protein targeted by G1-arresting rapamycin-receptor complex. *Nature* **369**, 756-758 (1994).
73. T. Noda, Y. Ohsumi, Tor, a Phosphatidylinositol Kinase Homologue, Controls Autophagy in Yeast. *Journal of Biological Chemistry* **273**, 3963-3966 (1998).
74. C. C. Thoreen *et al.*, An ATP-competitive mammalian target of rapamycin inhibitor reveals rapamycin-resistant functions of mTORC1. *J Biol Chem* **284**, 8023-8032 (2009).
75. F. I. Raynaud *et al.*, Pharmacologic characterization of a potent inhibitor of class I phosphatidylinositide 3-kinases. *Cancer Res* **67**, 5840-5850 (2007).
76. A. D. Balgi *et al.*, Screen for chemical modulators of autophagy reveals novel therapeutic inhibitors of mTORC1 signaling. *PLoS One* **4**, e7124 (2009).
77. S. Gilroy, W. A. Hughes, A. J. Trewavas, Calmodulin antagonists increase free cytosolic calcium levels in plant protoplasts in vivo. *FEBS Letters* **212**, 133-137 (1987).

78. L. Zhang *et al.*, Small molecule regulators of autophagy identified by an image-based high-throughput screen. *Proc Natl Acad Sci U S A* **104**, 19023-19028 (2007).
79. M. Hoyer-Hansen *et al.*, Control of macroautophagy by calcium, calmodulin-dependent kinase kinase-beta, and Bcl-2. *Mol Cell* **25**, 193-205 (2007).
80. J. Carmichael, K. L. Sugars, Y. P. Bao, D. C. Rubinsztein, Glycogen synthase kinase-3beta inhibitors prevent cellular polyglutamine toxicity caused by the Huntington's disease mutation. *J Biol Chem* **277**, 33791-33798 (2002).
81. P. O. Seglen, P. B. Gordon, 3-Methyladenine: Specific inhibitor of autophagic/lysosomal protein degradation in isolated rat hepatocytes. *Proceedings of the National Academy of Sciences* **79**, 1889-1892 (1982).
82. E. F. C. Blommaert, U. Krause, J. P. M. Schellens, H. Vreeling-Sindelárová, A. J. Meijer, The Phosphatidylinositol 3-Kinase Inhibitors Wortmannin and LY294002 Inhibit Autophagy in Isolated Rat Hepatocytes. *European Journal of Biochemistry* **232**, 240-246 (1997).
83. B. Ronan *et al.*, A highly potent and selective Vps34 inhibitor alters vesicle trafficking and autophagy. *Nat Chem Biol* **10**, 1013-1019 (2014).
84. J. Liu *et al.*, Beclin1 controls the levels of p53 by regulating the deubiquitination activity of USP10 and USP13. *Cell* **147**, 223-234 (2011).
85. R. K. Amaravadi *et al.*, Autophagy inhibition enhances therapy-induced apoptosis in a Myc-induced model of lymphoma. *J Clin Invest* **117**, 326-336 (2007).
86. D. J. Klionsky *et al.*, Guidelines for the use and interpretation of assays for monitoring autophagy (3rd edition). *Autophagy* **12**, 1-222 (2016).
87. U. S. Eggert, The why and how of phenotypic small-molecule screens. *Nat Chem Biol* **9**, 206-209 (2013).
88. J. Inglese *et al.*, High-throughput screening assays for the identification of chemical probes. *Nat Chem Biol* **3**, 466-479 (2007).
89. G. Kauselmann, A. Dopazo, W. Link, Identification of Disease-Relevant Genes for Molecularly-Targeted Drug Discovery. *Current Cancer Drug Targets* **12**, 1-13 (2012).
90. G. W. Paul, H. G. Ian, D. R. Kevin, H. F. Alan, Target Validation: Linking Target and Chemical Properties to Desired Product Profile. *Current Topics in Medicinal Chemistry* **11**, 1275-1283 (2011).
91. M. Schenone, V. Dancik, B. K. Wagner, P. A. Clemons, Target identification and mechanism of action in chemical biology and drug discovery. *Nat Chem Biol* **9**, 232-240 (2013).
92. M. A. Lindsay, Target discovery. *Nat Rev Drug Discov* **2**, 831-838 (2003).



93. L. C. Cesa, A. K. Mapp, J. E. Gestwicki, Direct and Propagated Effects of Small Molecules on Protein-Protein Interaction Networks. *Front Bioeng Biotechnol* **3**, 119 (2015).
94. D. C. Swinney, J. Anthony, How were new medicines discovered? *Nat Rev Drug Discov* **10**, 507-519 (2011).
95. D. C. Swinney, The contribution of mechanistic understanding to phenotypic screening for first-in-class medicines. *J Biomol Screen* **18**, 1186-1192 (2013).
96. Bridget K. Wagner, Stuart L. Schreiber, The Power of Sophisticated Phenotypic Screening and Modern Mechanism-of-Action Methods. *Cell Chemical Biology* **23**, 3-9 (2016).

# Chapter II

## **Small-Molecule Enhancers of Autophagy Modulate Cellular Disease Phenotypes Suggested by Human Genetics**

Partly adapted from S.-Y. Kuo *et al.*, Small-molecule enhancers of autophagy modulate cellular disease phenotypes suggested by human genetics. *Proceedings of the National Academy of Sciences* **112**, E4281-E4287 (2015). (1)

## Collaborator Contributions

- **Dr. Adam Castoreno** conducted the primary screen with my assistance and conducted the toxicity assay.
- **Dr. Leslie Aldrich** synthesized DOS compounds.
- **Dr. Gautam Goel** and **Dr. Vlado Dančik** analyzed data of the primary screen and the autophagy flux assay.
- **Dr. Vlado Dančik** assisted in the chemical moiety enrichment analysis.
- **Dr. Leslie Aldrich** assisted in assays measuring lysosomal functions and *Salmonella* clearance.
- **Dr. Sovan Sarkar** and **Dr. Dorothea Maetzel** conducted the Huntingtin aggregate clearance assays and NPC1 assays.
- **Dr. Adam Castoreno** and **Dr. Kara Conway** conducted assays measuring inflammatory cytokine secretion.

## 2.1 Introduction

### 2.1.1 Small-molecule autophagy modulators in disease relevant cellular assays

Small-molecule enhancers of autophagy are increasingly being tested for their beneficial effects on disease phenotypes in relevant cell types (2). For example, different enhancers exhibit distinct profiles of activity in innate and adaptive immune pathways, including host defense against pathogens (3). Phenothiazine-derived antipsychotics (prochlorperazine edisylate) and first-line antibiotics (isoniazid and pyrazinamide) promote autophagy-dependent activity against Mtb, the latter involving modulation of proinflammatory responses in Mtb-infected macrophages (4, 5). Likewise, the microtubule depolymerizing compound flubendazole and the autophagy-inducing peptide Tat-beclin 1 both induce the release of Beclin 1 and enhance autophagy-dependent antiviral and anti-microbial activity in cell models (6, 7). In the context of protein aggregation disorders, CBZ-induced autophagy reduces accumulation of  $\alpha$ 1-antitrypsin in liver cells and rescues hepatic fibrosis in mice (8), whereas rapamycin- or trehalose-induced autophagy clears  $\alpha$ -synuclein and mutant huntingtin aggregates in neurodegenerative disease models, among others (9). Autophagy defects linked to the lysosomal storage disorder Niemann–Pick type C1 disease (NPC1; caused by mutation in the NPC1 protein) can be restored by stimulating autophagy with rapamycin or CBZ, which is cytoprotective in NPC1 disease-relevant cells (10, 11). In the context of CD, small molecules have been shown to promote favorable immune phenotypes. Treatment with the PDK1 inhibitor AR-12 in macrophages (12) or rapamycin in epithelial cells (13) promotes bacterial clearance, and treatment with rapamycin leads to reduced IL-1 $\beta$  levels in innate immune cells and animals, possibly via degradation of pro-IL-1 $\beta$  or its processing machinery (14).

### 2.1.2 Small-molecule screening for autophagy modulators

Small-molecule modulators of canonical and selective autophagy with novel and distinct MoA are critical for studying the relevance of autophagy in diseases and for exploring the potentials of autophagy enhancement as a therapeutic strategy. Various approaches, including target-based and phenotypic-based strategies have been applied to identify small-molecule autophagy modulators. For target-based approaches, assays have been developed to target components involved in the initiation of autophagy. ATG4 is a protease that cleaves pro-LC3 and thus essential for autophagosome formation (15). Biochemical assays using fluorophore-tagged LC3 as FRET substrate (16) or synthetic fluorogenic peptide substrate of ATG4 (17) were utilized to discover small molecules that inhibit ATG4 protease activity. As another example, the kinase activity of ULK1 is critical to the initiation of autophagy (18). A biochemical assay that used purified ULK-1 and its substrate ATG13 was developed and inhibitors of ULK1 kinase activity were identified (19). In both cases, same assays can be adapted for identifying enhancers of ATG4 or ULK1 as autophagy activators. In theory, compounds that enhance ATG4 activity will decrease levels of the LC3 FRET substrate or the fluorogenic peptide substrate. Compounds that activate ULK1 will increase the level of ATG13 phosphorylation. Both ATG4 and ULK1 activators were identified in pilot screens of the Sigma LOPAC library in each study (16, 17, 19). However, further confirmation studies are needed to validate if these compounds are putative activators of ATG4 or ULK1, or merely false positives.

Among phenotypic-based strategies, assays that measure changes in subcellular localization of LC3 are most widely used. LC3 normally displays a diffuse cytosolic pattern (LC3-I), but upon induction of autophagy, LC3 is post-translationally modified (LC3-II) and accumulates on autophagosome membranes. This change can be visualized and quantified by counting the number of LC3 punctae in cells by microscopy (20). With the expression of GFP-tagged LC3, numbers of fluorescent punctae can be scored in a high-throughput manner with automated imaging and analysis systems. Compounds that increase the number of GFP-LC3

punctae have been identified in various HTS (21-23). However, a limitation of the GFP-LC3 assay is its inability to distinguish autophagy activation from inhibition of late stages of autophagy, since both of these mechanisms can lead to an increase in GFP-LC3 punctae numbers (24). One strategy used to overcome this limitation was to measure not only numbers of punctae, but also other parameters, such as area, intensity and localization of GFP-LC3 punctae. These parameters were used to facilitate annotating small molecules as autophagy activators or inhibitors of late steps (23). Compounds emerging from GFP-LC3 based HTS could also be tested in secondary assays that monitor the degradation of known substrates of autophagy, such as long-lived proteins and LC3, as LC3 molecules that localize on autophagosome inner membrane are eventually degraded in autolysosome (21, 23). Alternatively, the mCherry-GFP-LC3 reporter system could measure autophagosome formation and maturation (autophagic flux), and was utilized to identify small-molecule enhancers of autophagy in HTS (3, 7).

In this study, our goal was to study effects of autophagy enhancement in the contexts of various diseases. It is likely that autophagy plays different roles and is regulated differently in each disease of interest. Therefore, we decided to screen for activators of canonical autophagy, rather than search for modulators of any specific component of autophagy machinery.

Phenotypic-based strategies would enable an unbiased identification of canonical autophagy modulators that acted through various and potentially novel MoAs. Once small-molecule autophagy activators were identified, we planned to test them in different disease-relevant assays and identify autophagy activators that could elicit favorable phenotypes in each assay.

## 2.2 Identification of small-molecule modulators of autophagy in a high-throughput phenotypic screen

### 2.2.1 High-throughput screening identifies small-molecule modulators of autophagy

To discover novel small-molecule modulators of canonical autophagy, we performed an HTS of 59,541 stereochemically and skeletally diverse compounds derived from diversity-oriented synthesis (DOS). These molecules are enriched for  $sp^3$ -hybridized atoms relative to conventional commercial libraries (25-27), resulting in topographically rich 3D structures. The primary HTS measured autophagosome number induced by 4-hour compound treatment in HeLa cells stably expressing GFP-LC3. Numbers of GFP-LC3 punctae per cell were counted by automated microscopy and scored by image analysis software (Figure 2.1). Significance of changes was assessed by computing an empirical test statistic termed ‘prevalence’, which compared the distribution of punctae per cell for each compound (test distribution) to that of the negative control, DMSO (null distribution). Specifically, prevalence was computed as the area under the curve of the test distribution beyond the critical value corresponding to 95% confidence of the null distribution. Prevalence is useful for assessing significance when comparing two populations that do not follow a normal distribution pattern, which is the case for punctae per cell in the GFP-LC3 assay.

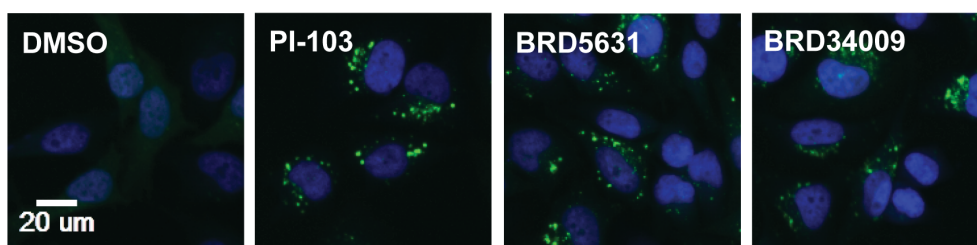


**Figure 2.1. HTS identifies DOS-derived small-molecule autophagy modulators.** HeLa cells stably expressing GFP-LC3 were treated with compounds for 4 hours, and the number of GFP punctae per cell was quantified by fluorescence microscopy and automated image analysis. Representative images of cells treated with DMSO, PI-103 (2.5  $\mu$ M), BRD5631 (10  $\mu$ M), or BRD34009 (10  $\mu$ M) are shown.

To assess data quality, we computed the prevalence score induced by positive control (PI-103) of each plate, and only included plates in which the score were  $\geq 0.5$  for further analysis. For most plates, the prevalence values were about 0.7. Z' scores were calculated for overall assay performance using prevalence scores from 32 wells of negative control (DMSO) and 32 wells of positive control (PI-103) on each plate and were typically between 0.6-0.8 for all plates screened. We identified about 2,000 hits that increased the average number of GFP-LC3 punctae per cell to a level  $\geq 30\%$  of the positive control (background-subtracted). 998 hits were prioritized after their prevalence values were also taken into consideration.

### **2.2.2 Effects of small-molecule hits on cell viability are tested**

Activation of autophagy has been associated with induction of cell death in certain circumstances (28). In the context of pathogen clearance and modulating disease phenotypes of our interest, a preferred small-molecule probe would be able to activate autophagy at low concentration (low  $EC_{50}$ ) without affecting cell viability (high  $IC_{50}$ ). The 998 hits from the primary screen were tested for effects on viability of HeLa cells. We treated cells for 72 hours with each compound and used CellTiter-Glo to measure ATP levels as a surrogate for cell viability. 85% of hits showed little to modest toxicity (<25% effect) at 10  $\mu\text{M}$  (data not shown). We ranked compounds by the ratio of the  $EC_{50}$  of autophagy activation to the  $IC_{50}$  of cytotoxicity and compounds that have smaller ratio values were preferred.

### **2.2.3 Autophagy flux assay distinguishes inhibitors of autophagosome turnover from activators of autophagosome formation**

The number of GFP-LC3 punctae in the cell can be increased by either activating autophagy or by inhibiting autophagy at late steps in the process, such as by disrupting lysosome functions. We prioritized 400 representative hits based on potency and chemical structure for testing in a secondary assay for autophagic flux that relies on visualizing LC3



protein tagged with both mCherry and GFP. The GFP signal is attenuated in autolysosomes, while the mCherry signal remains stable (29); as a result, autophagosomes (GFP<sup>+</sup>/mCherry<sup>+</sup>) and autolysosomes (GFP<sup>-</sup>/mCherry<sup>+</sup>) can be distinguished and counted by high-throughput imaging (Figure 2.2). In the process of assay development, we noticed that a longer period of treatment was required for robust changes induced by positive controls. Therefore, 400 representative hits were treated to cells for 24 hours and their effects were measured with automated microscope and image analysis systems. The number of GFP<sup>-</sup>/mCherry<sup>+</sup> punctae (presumed autolysosomes) was increased by 250 hits (putative activators) and decreased by 80 hits (putative late-stage inhibitors) from the primary screen (Figure S2.1).

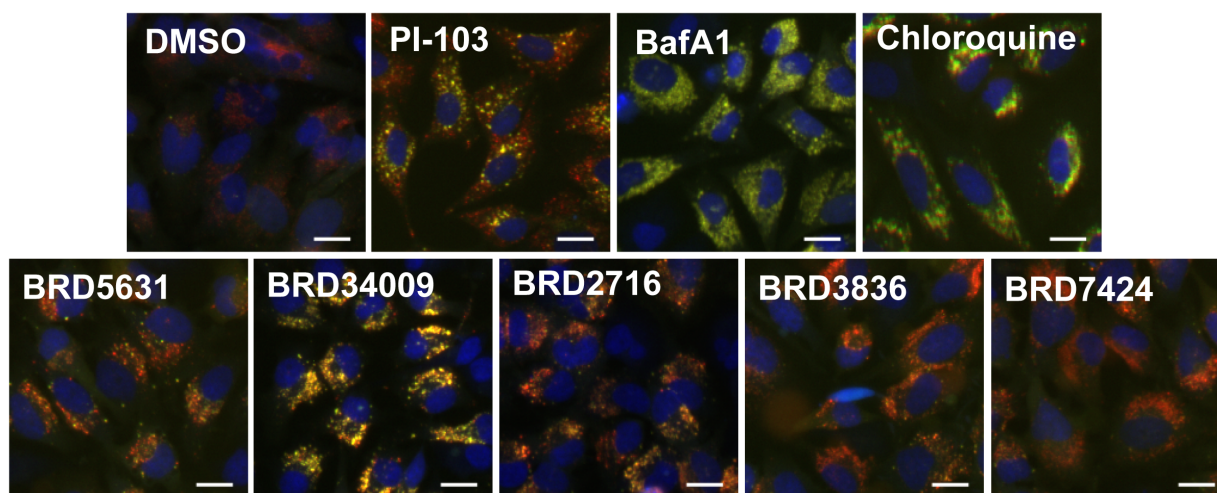


**Figure 2.2. DOS compounds promote autophagic flux to various extents.** HeLa cells stably expressing mCherry-GFP-LC3 were treated with compounds for 24 hours, after which cells were fixed and stained with Hoechst 33342 and punctae number was quantified by fluorescence microscopy and automated image analysis. Representative images of DMSO, PI-103 (5  $\mu$ M), chloroquine (60  $\mu$ M), BafA1 (100 nM) and BRD5631, BRD34009, BRD2716, BRD3836, and BRD7424 (each 10  $\mu$ M) are shown. GFP<sup>+</sup>/mCherry<sup>+</sup> (yellow) punctae represent presumed autophagosomes and GFP<sup>-</sup>/mCherry<sup>+</sup> (red) punctae represent presumed autolysosomes. Scale bars represent 10 $\mu$ m.

#### **2.2.4 Alkyl amines and lipophilic moieties are enriched among hits of the LC3 punctae formation assays**

The primary screening data for 59,541 DOS compounds were studied to identify structural moieties associated with increased activity in the GFP-LC3 punctae formation assay. This systematic analysis was enabled by the design of the DOS collection, which includes common building blocks and structural elements across a range of diverse scaffolds. Using a 30% increase of punctae number relative to the positive control as the cutoff, the hit rate among small molecules that contained an alkyl amine was 7%, which was about 2-fold higher than the overall hit rate of the primary screen (3%), suggesting that containing an alkyl amine moderately associated with inducing GFP-LC3 punctae formation (Figure 2.3A and Table S2.1). Lipophilic moieties further increased the likelihood of activity in the assay, as the hit rates of small molecules containing an alkyl amine and one lipophilic moiety (diphenyl alkyne, biphenyl, cyclohexane or naphthalene) increased to 20-60% in this collection (Figures 2.3 A-C and Table S2.1). Interestingly, the association of these structural moieties with autophagy-modulating activity was observed across several distinct skeletons.

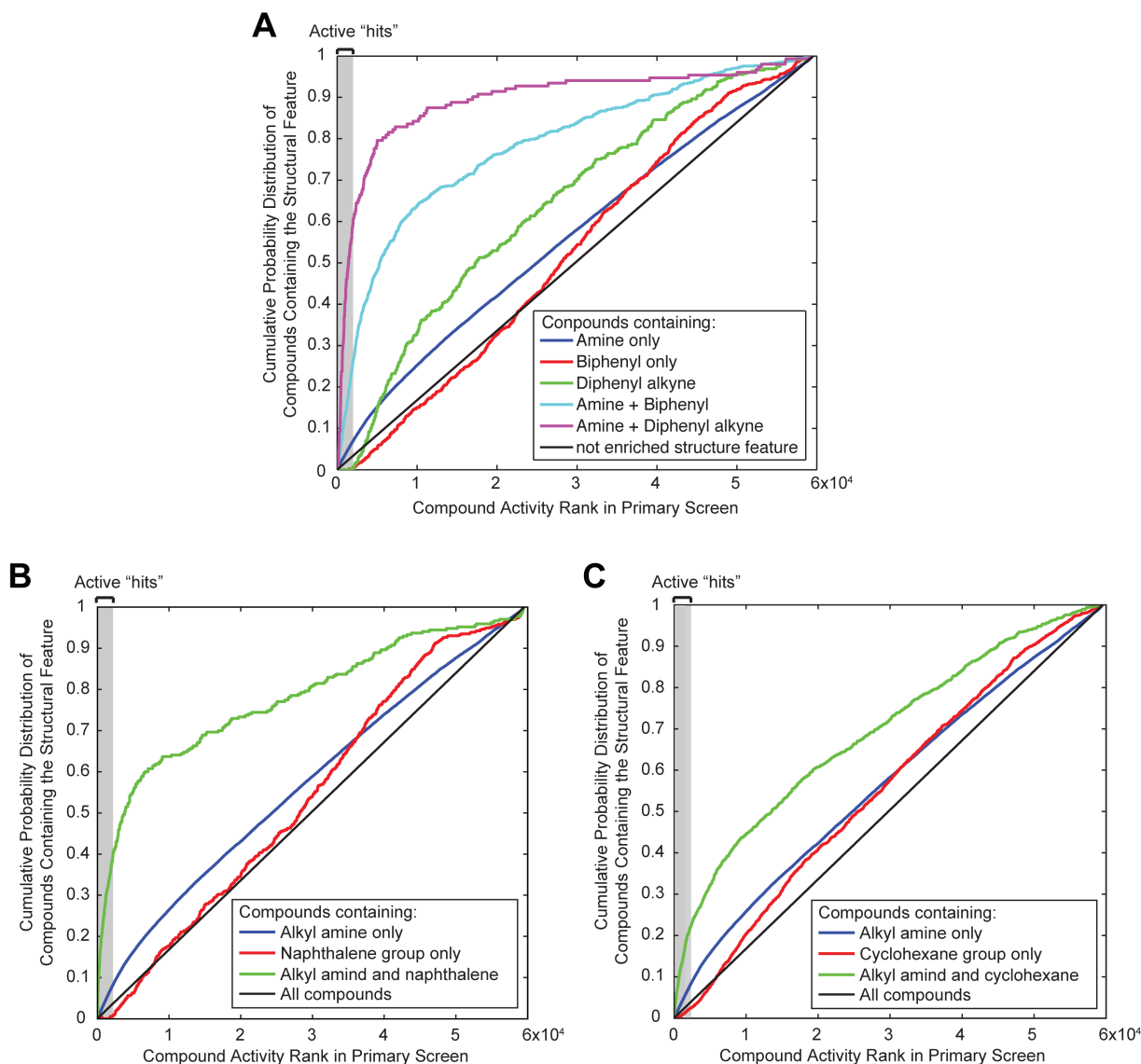


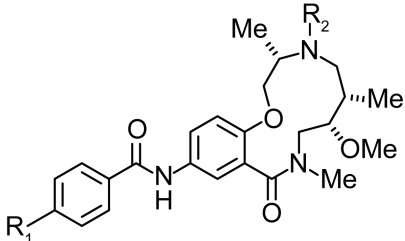
**Figure 2.3. Chemical moieties are enriched among hits that induce GFP-LC3 punctae formation.** 59,541 DOS compounds were ranked based on their activities in the primary screen. Compounds containing alkyl amine (A-C), biphenyl, diphenyl alkyne (A), naphthalene (B), cyclohexane (C) or the combination of alkyl amine and each of lipophilic group were selected and the cumulative probability distribution of each class was plotted.

To investigate these structure-activity relationships (SAR) further, we prepared and tested a focused library of analogs of BRD5631 (Table 2.1), a potent enhancer of punctae formation containing two structural features significantly enriched among autophagy activators, a secondary dialkyl amine and a biphenyl group. We found that only analogs that contained an amine (secondary dialkyl amine, BRD5631, or tertiary dialkyl methyl amine, BRD1239) at this

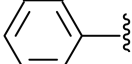
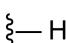
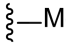
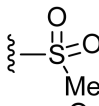
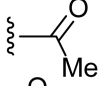
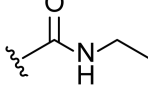
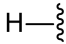
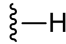
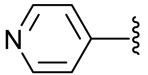
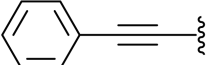
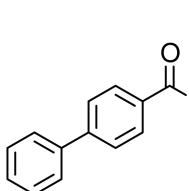
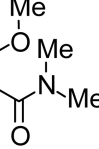
position retained activity, with the secondary dialkyl amine (BRD5631) being the most potent. We also found that removal of a single phenyl group (BRD6426) or replacing the terminal phenyl group with a pyridyl group (BRD0781), eliminated the biological activity of BRD5631, highlighting the importance of this group and its lipophilicity. Though critical, the lipophilic biphenyl moiety was not sufficient for activity, since the acyclic analog BRD6721 was completely inactive. Consistent with the observation that diphenyl alkynes were enriched among screening hits, we found that replacing the biphenyl group of BRD5631 with a diphenyl alkyne yielded another compound (BRD5131) with equal potency.

Similar analyses were undertaken to associate structural elements with activity in the dual-tagged mCherry-GFP-LC3 assay. Given that the alkyl amine structural moiety was associated with activity in the primary screen, the majority of these compounds contained an alkyl amine. We further found that small molecules containing a secondary dialkyl amine were enriched among the compounds that increased numbers of presumed autolysosomes (GFP<sup>-</sup>/mCherry<sup>+</sup>), while those containing a tertiary dimethyl alkyl amine were enriched among the compounds that reduced the number of presumed autolysosomes (Figure S2.2). These results highlight the necessity of certain structural features for optimal activity in the assays measuring LC3 punctae formation, although it is unclear whether these features are required for enhancement of specific molecular interactions or physicochemical properties to LC3 punctae formation.

**Table 2.1. Results of GFP-LC3 punctae formation assay show that BRD5631 analogs corroborate structure-activity relationship trends observed in the primary HTS. Data are the mean  $\pm$  SD of three independent experiments.**



The chemical structure shows a central benzene ring substituted with a methyl piperazine ring (with methyl groups at the 2 and 6 positions and a methoxy group at the 4 position), a methyl amide group (-NHMe), and an amide group (-NH-C(=O)-R1). The R1 and R2 substituents are defined in the table below.

Compound	R <sub>1</sub>	R <sub>2</sub>	GFP-LC3 Punctae EC <sub>50</sub> ( $\mu$ M)
BRD5631			3.1 $\pm$ 0.6
BRD1239	“		11.1 $\pm$ 2.4
BRD1246	“		>20
BRD6426	“		>20
BRD2443	“		>20
BRD9467			>20
BRD0781		“	>20
BRD5131		“	3.6 $\pm$ 0.5
BRD6721			>20

### 2.2.5 Prioritized compounds do not disrupt lysosomal functions

Compounds containing a lipophilic group and a basic amine can accumulate within lysosomes (lysosomotropism) and potentially interfere with lysosomal function, cell viability, and autophagy (30, 31). To determine whether our hits disrupt lysosomal function, we first tested their effect on lysosomal proteases by measuring processing of a fluorogenic substrate (DQ-BSA)(32). For these experiments, we selected four structurally representative hits, including BRD5631, as well as one hit lacking an amine (Figure 2.4), that display a range of activities in the GFP-LC3 assay (Figures 2.1 and S2.3A) and mCherry-GFP-LC3 assay (Figure 2.2). As expected, control compounds that inhibit lysosomal proteases directly (E64d/pepA) or indirectly by increasing lysosomal pH (BafA1 and CQ) significantly decreased both DQ-BSA punctae number and intensity. In contrast, none of the selected hits reduced either the number or intensity of DQ-BSA punctae at doses that induce GFP-LC3 punctae (Figures 2.5A and S2.3B). Furthermore, the compounds did not disrupt accumulation of a fluorescent basic amine probe used to stain acidic compartments (LysoTracker Red; Figures 2.5B and S2.3C) or significantly affect viability at autophagy-modulating doses (<10% effect; Figure S2.3D) (33). These data suggest that BRD5631 and other hits do not increase GFP-LC3 punctae formation by broadly disrupting lysosomal function, motivating us to further characterized these hits more deeply in mechanistic and functional assays for autophagy.

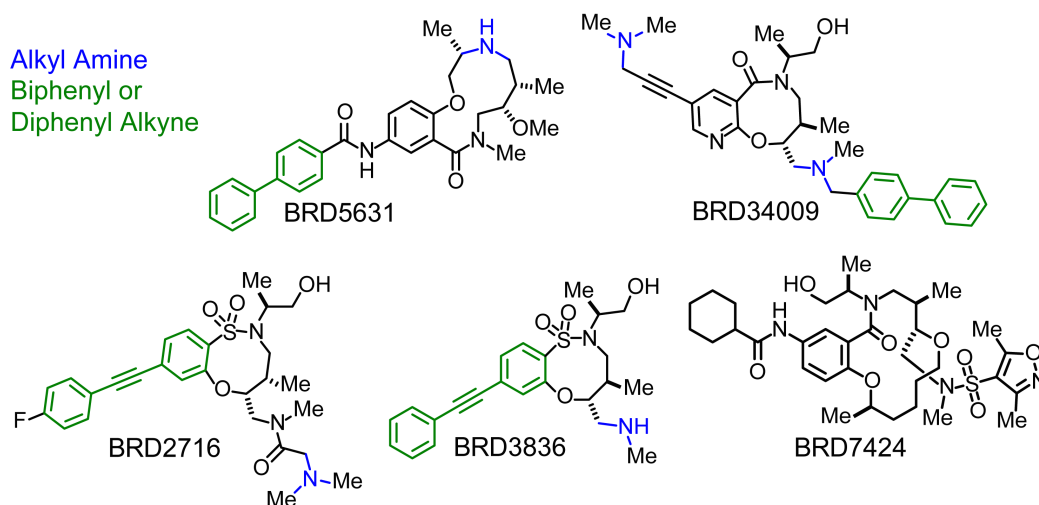


**Figure 2.4. Chemical structures of five prioritized compounds.**

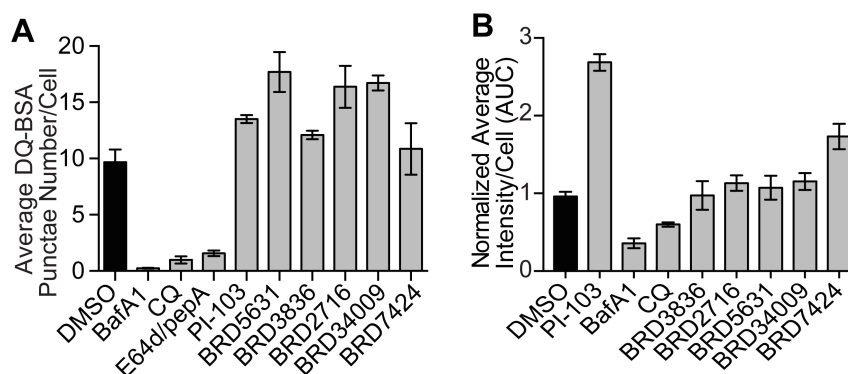


**Figure 2.5. Autophagy modulators do not disrupt lysosomal functions.** (A) Compounds were evaluated in the DQ-BSA assay. BafA1 (100 nM), CQ (50  $\mu$ M), E64d/pepA (10  $\mu$ g/mL each), PI-103 (10  $\mu$ M), and DOS compounds (10  $\mu$ M each). Data are presented as mean  $\pm$  SD,  $n = 3$ . (B) Compounds were evaluated in the LysoTracker assay in 8-point dose by two-fold serial dilution from the following starting concentrations: PI-103 and DOS compounds (20  $\mu$ M each), BafA1 (200 nM), CQ (100  $\mu$ M). Data are presented as average area under the curve  $\pm$  SD,  $n = 2$ . Data are representative of multiple experiments.

## 2.3 Mechanistic and Functional Characterization of Novel Small-Molecule Enhancers of Autophagy

### 2.3.1 Measuring levels of LC3-II by Western blot validates the results of microscopy-based assays

We first validated results in GFP-LC3 and mCherry-GFP-LC3 assays by measuring levels of LC3-II by Western blot. Consistent with the results from microscopy-based assays, we found that BRD5631 treatment led to increased levels of LC3-II (Figure 2.6). When cotreated with the V-ATPase inhibitor BafA1 (a known late-stage inhibitor of autophagy), BRD5631 was able to increase LC3-II levels above those observed with BafA1 alone, suggesting that BRD5631 stimulated formation of new autophagosomes (Figure 2.6). These data were consistent with its ability to increase numbers of autolysosomes (mCherry<sup>+</sup>/GFP<sup>-</sup>) in the mCherry-GFP-LC3 assay. Similar results were observed with other screening hits to a lesser degree (Figure 2.6), with the exception of BRD34009, which induced LC3-II formation but showed modest inhibitory activity in the mCherry-GFP-LC3 assay.

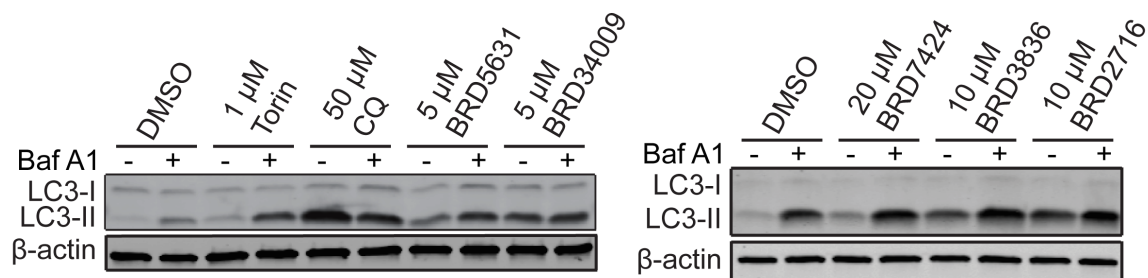


**Figure 2.6. Autophagy modulators enhance autophagic flux.** HeLa cells were treated with indicated compounds for 7 hours. For the last 4 hours, either DMSO or BafA1 (100 nM) was added, then protein samples were harvested for immunoblot analysis. The blot is representative of multiple experiments.

### 2.3.2 Autophagy modulators do not disrupt mTOR kinase activity

We then characterized BRD5631 and the other selected compounds more deeply in mechanistic assays for autophagy. Because inhibition of mTOR signaling is known to promote



autophagy, we determined whether the compounds affected phosphorylation of mTOR-regulated proteins, including p70 S6 kinase 1 (S6K1) (Thr389) (34) and the autophagy-initiating kinase ULK1 (Ser757) (18). Consistent with previous reports (21, 34), we confirmed that treatment with the mTOR kinase inhibitor torin1 and mTOR pathway modulator rottlerin led to decreased phosphorylation of S6K1 and ULK1 (Figure 2.7). In contrast, BRD5631 and other screening hits did not significantly affect S6K1 or ULK1 mTOR-dependent phosphorylation levels at 10  $\mu$ M, suggesting that they do not enhance autophagy by directly inhibiting mTOR or the mTOR signaling pathway.

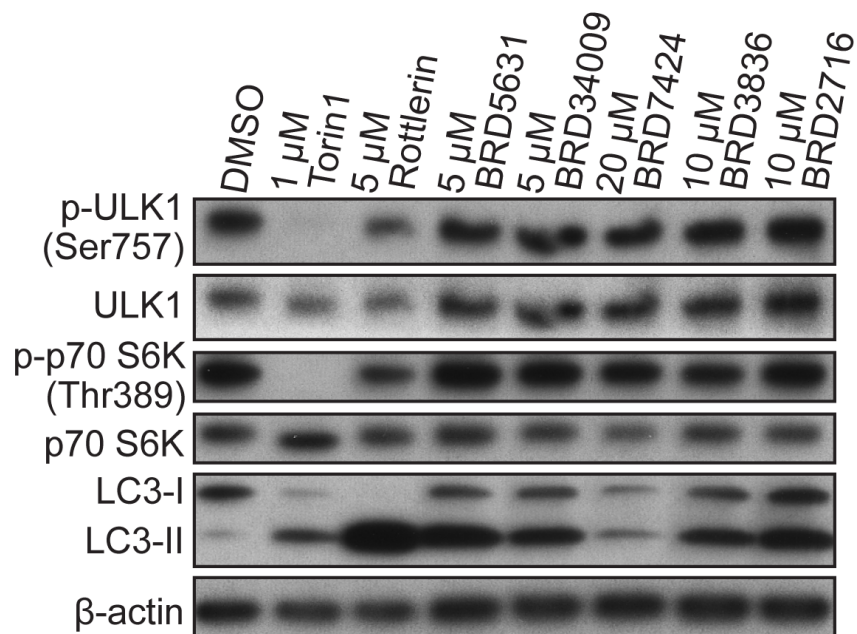


**Figure 2.7. Autophagy modulators do not disrupt mTOR kinase activity.** HeLa cells were treated with compounds for 4 hours, and then harvested for immunoblot analysis. The blot is representative of 3 independent experiments.

### 2.3.3 BRD5631 decreases the presence of aggregates in cells expressing poly-Q repeats (eGFP-HDQ74)

We assessed the ability of BRD5631 to promote clearance of an autophagic cargo using the well-established substrate, mutant huntingtin (eGFP-HDQ74) (35). Transient overexpression

of eGFP-HDQ74 in autophagy-deficient cells [*Atg5*<sup>-/-</sup> mouse embryonic fibroblasts (MEFs)] caused increased aggregate formation compared with their wild-type counterparts (*Atg5*<sup>+/+</sup> MEFs) due to its inability to be degraded by autophagy (36). Treatment with BRD5631 significantly reduced the number of eGFP-HDQ74-positive cells in *Atg5*<sup>+/+</sup> MEFs; this reduction was not observed in *Atg5*<sup>-/-</sup> MEFs, suggesting BRD5631 promotes clearance of mutant huntingtin in an autophagy-dependent manner (Figure 2.8A).

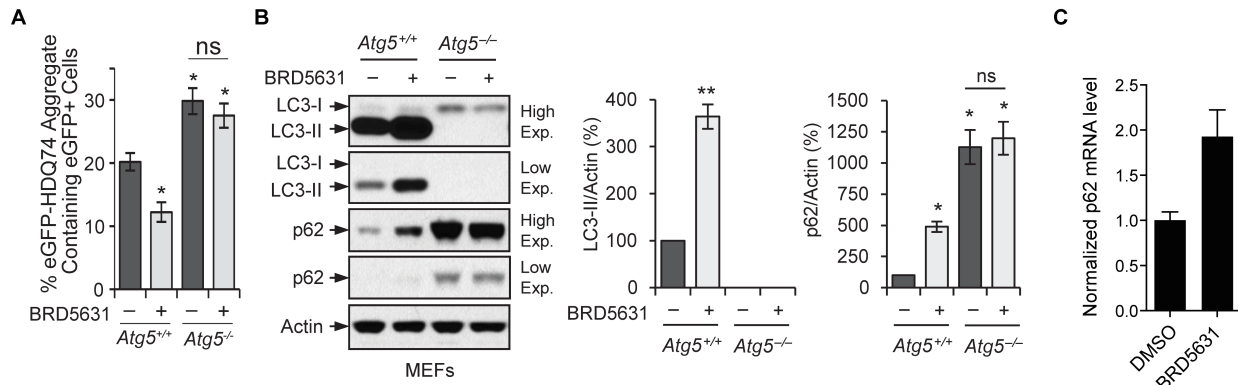


**Figure 2.8. BRD5631 decreases the presence of eGFP-HDQ74 containing-aggregates.** (A) *Atg5*<sup>+/+</sup> and *Atg5*<sup>-/-</sup> MEFs were transfected with eGFP-HDQ74 construct followed by treatment with DMSO or 10 $\mu$ M BRD5631 48 hours. Percentage of eGFP<sup>+</sup> cells with eGFP-HDQ74 aggregates was quantified by fluorescence microscopy. Data are presented as mean  $\pm$  SEM, n = 3. \**P* < 0.05, ns, not significant, compared to untreated *Atg5*<sup>+/+</sup> MEFs, unless indicated otherwise, unpaired Student *t* test. All data are representative of 3 independent experiments. (B) *Atg5*<sup>+/+</sup> and *Atg5*<sup>-/-</sup> MEFs, treated with DMSO or 10  $\mu$ M BRD5631 for 48 hours, were subjected to immunoblot analysis with anti-LC3, anti-p62, and anti-actin antibodies. Densitometric analysis shows LC3-II and p62 levels relative to actin (loading control). Data are presented as the mean  $\pm$  SD, n = 3 from one representative experiment. \**P* < 0.05; \*\**P* < 0.01; ns = not significant, compared to untreated *Atg5*<sup>+/+</sup> MEFs, unless indicated otherwise, unpaired Student *t* test. (C) *Atg5*<sup>+/+</sup> MEFs were treated with DMSO or 10  $\mu$ M BRD5631 for 48 hours and subjected to quantitative RT-PCR analysis to measure p62 mRNA levels relative to actin mRNA levels in each well. Results are normalized to DMSO. Data are presented as the mean  $\pm$  SD, n = 3 from a representative experiment.

We also measured changes in the level of another specific autophagy substrate, p62 (37), in response to BRD5631 in these cells. Under steady-state conditions, *Atg5*<sup>-/-</sup> MEFs displayed increased p62 levels compared with *Atg5*<sup>+/+</sup> MEFs. BRD5631 substantially increased LC3-II levels in *Atg5*<sup>+/+</sup> MEFs as expected; however, it increased p62 levels in *Atg5*<sup>+/+</sup> MEFs without any detectable effect in *Atg5*<sup>-/-</sup> MEFs (Figure 2.8B). Transcriptional up-regulation of p62

in response to autophagy activation has been previously reported (38), complicating interpretation of its levels as a readout for autophagic flux. We also observed that BRD5631 increased the transcript level of p62 in *Atg5*<sup>+/+</sup> MEFs (Figure 2.8C), suggesting a complex effect of BRD5631 on p62 levels in this cellular context.

#### **2.3.4 A subset of autophagy modulators suppress NPC1-induced cell death in a hiPSC-derived neuronal model of Niemann–Pick Type C1 disease**

It was recently shown that small-molecule enhancers of autophagy, such as CBZ, can rescue impairment of autophagic flux observed in NPC1, a lipid/lysosomal storage disease exhibiting accumulation of cholesterol in the late endosomal/lysosomal compartments and associated with degeneration of the cerebellum and liver in patients (9, 10). These enhancers also suppress cell death in NPC1 patient-specific human induced pluripotent stem cell (hiPSC)-derived neuronal and hepatic cells, which normally display cholesterol accumulation, impaired autophagic flux, and increased cell death in the absence of any external stressors relative to control cells (10). Using this system, we assessed the ability of the prioritized compounds to rescue the NPC1-associated loss of cell viability relative to the positive control (100  $\mu$ M CBZ). We found that BRD5631, BRD2716, and BRD34009 significantly reduced cell death in NPC1 hiPSC-derived neurons (Figure 2.9A). Interestingly, these compounds did not rescue increased cell death in NPC1 hiPSC-derived hepatic cultures (Figure S2.4). We further examined the impact of these compounds on autophagic flux by measuring p62 levels in NPC1 hiPSC-derived neurons, which display accumulation of this autophagy substrate relative to control cells (10) (Figure 2.9B). In contrast to the results obtained in MEFs, treatment with BRD5631, BRD2716, and BRD34009 reduced levels of endogenous p62 in NPC1 neuronal cells (Figure 2.9B). The correlation between the neuroprotective effects of BRD5631, BRD2716, and BRD34009 and clearance of autophagy substrates in NPC1 neuronal cells suggests a possible role for increased autophagic flux in rescuing cells from the disease phenotype.

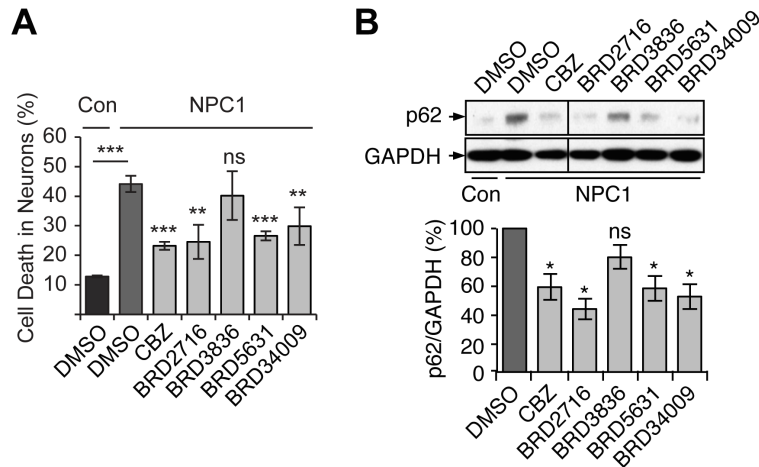


**Figure 2.9. A subset of autophagy modulators rescues impairments in NPC1 disease hiPSC-derived neurons.** (A) Control (WIBR3-derived) neurons were treated with DMSO, and NPC1 hiPSC (WIBR-IPS-NPC1-derived) neurons were treated with DMSO, DOS compounds (10  $\mu$ M each), or CBZ (100  $\mu$ M) for 3 days. Cell death was quantified using TUNEL assay and apoptotic nuclear morphology. Data are presented as the mean  $\pm$  SD and are representative of two independent experiments, each run in triplicate. (B) Cell populations treated as described in A were subjected to immunoblot analysis. All samples were run in the same gel and blotted at the same time. The line denotes where one intervening lane was excised. Densitometric analysis shows p62 levels relative to GAPDH in NPC1 hiPSC-derived neurons. The control condition was set to 100%, and data represent the mean  $\pm$  SEM of samples from the same experiment in A. \* $P < 0.05$ , \*\* $P < 0.01$ , \*\*\* $P < 0.001$ , ns, not significant, compared to DMSO-treated NPC1 cells, unless indicated otherwise, unpaired Student  $t$  test.

### 2.3.5 A subset of autophagy modulators enhances bacterial clearance in an autophagy-dependent manner

Several bacterial pathogens are selectively targeted by autophagy for degradation (bacterial xenophagy), including *Salmonella*, *Shigella*, Mtb, and group A *Streptococcus* (39). Furthermore, compromised antibacterial autophagy has been implicated by studies of disease-associated genes (ATG16L1, IRGM), potentially contributing to inflammation via an increased microbial burden within the intestinal epithelium (40). To determine if BRD5631 and other hits can promote antibacterial autophagy, we first measured their ability to inhibit bacterial replication using a bioluminescent strain of *Salmonella* infecting mammalian epithelial cells (HeLa). Three of five prioritized autophagy modulators (BRD5631, BRD34009, BRD2716)

inhibited *Salmonella* replication over time, beginning as early as 3-hour post-infection (p.i.), to similar or greater levels than an autophagy modulator reported to have anti-*Salmonella* activity, TFP (41) (Figures 2.10A and S2.5 A and B). Traditional CFU assays confirmed the results of the luminescence assay (Figure S2.5C). None of the prioritized small molecules displayed general bactericidal activity in the absence of host cells or cytotoxicity to host cells at the concentration used for the clearance assay (Figure S2.5 D and E).

To assess the dependence of replication inhibition on autophagy, we tested the antibacterial activity of hits on a clonal ATG16L1-deficient HeLa cell line generated using the clustered regularly interspaced short palindromic repeats (CRISPR)-Cas9 system (42) (Figure S2.5F). ATG16L1 forms a complex with ATG5-ATG12 conjugates to promote conjugation of LC3 to phosphatidylethanolamine and elongation of autophagosomal membranes (43). As expected, ATG16L1-deficient cells displayed significantly greater levels of bacterial replication than the parental line (Figure S2.5G), and an antibiotic that directly targets bacteria [chloramphenicol (CP)] was able to suppress bacterial replication in both cell lines. When we treated the ATG16L1-deficient cells with BRD5631 and other hits, no reduction in bacterial replication was observed (Figures 2.10A and S2.5A). Although the interpretation may be complicated by the increased rate of replication in the knockout cells, these data suggest that autophagy is required for the effect of BRD5631 on bacterial clearance.

To determine whether compounds that inhibit replication of intracellular *Salmonella* affect its association with the antibacterial autophagy machinery, we measured the colocalization of dsRed-expressing *Salmonella* with both LC3 and NDP52, an adaptor protein that targets galectin-8- or ubiquitin-coated *Salmonella* to autophagy (39). As reported previously, treatment with TFP enhanced the maximal colocalization of *Salmonella* and LC3 and NDP52 observed at 1-hour p.i., which was maintained at later time points (4-hour p.i.) when the colocalization events subsided in vehicle control-treated cells (Figure 2.10B). BRD5631 was

able to moderately enhance colocalization events at 1-hour p.i. and later time points to a higher level than TFP (Figure 2.10B).

The CD risk allele ATG16L1 T300A has been linked to impaired colocalization of *Salmonella* and LC3 in genetically modified HeLa cells (44). To determine if BRD5631 is able to overcome defects in colocalization of *Salmonella* and LC3 in the presence of this risk allele, we performed the colocalization assay in ATG16L1-deficient HeLa cells reconstituted with wild type ATG16L1 or ATG16L1 T300A (Figure S2.5H). As reported, LC3 recruitment was diminished in the absence of ATG16L1. Reintroducing ATG16L1 T300A partially rescued the colocalization ratio, but significantly less than the ratio in cells reconstituted with wild-type ATG16L1 (Figure 2.10C). TFP and BRD5631, as well as the autophagy-inducing peptide Tat-beclin 1, moderately enhanced the colocalization of LC3 and *Salmonella* in ATG16L1 T300A cells (Figure 2.10C). Similarly, BRD5631 and TFP inhibited bacterial replication in the presence of ATG16L1 T300A (Figure 2.10D).

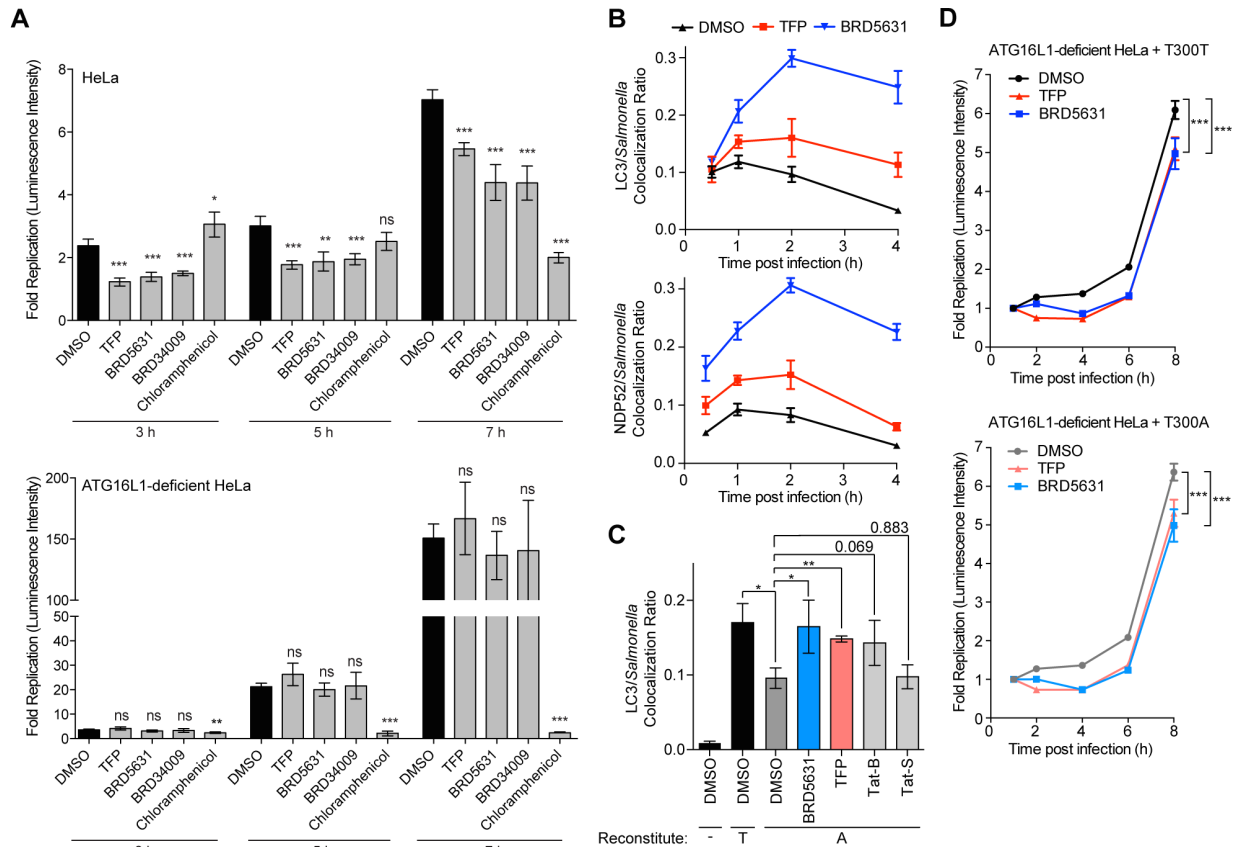


**Figure 2.10. Autophagy modulators clear invasive bacteria.** (A) *Salmonella* survival in cells was assessed in the bioluminescent bacterial replication assay. Luminescence intensity in live cells was measured at each indicated time point, and fold replication values were calculated for each well as raw luminescence intensity divided by the intensity at 1 hour p.i. Data are presented as mean  $\pm$  SD,  $n = 4$  from a representative experiment. (B) HeLa cells were pretreated with compound for 3 hours and infected with *Salmonella*. Cells were then fixed and subjected to immunostaining at indicated time points. Colocalization ratios were calculated to compare *Salmonella* colocalized with LC3 or NDP52 to total *Salmonella*. Data are presented as mean  $\pm$  SD,  $n = 4$  from a representative experiment. (C) ATG16L1-deficient HeLa cells were reconstituted with ATG16L1 T300T (T) or T300A (A), seeded on coverslips, pretreated, infected, and fixed and stained at 1 hour p.i. Tat-B represents Tat-beclin peptide and Tat-S, scrambled Tat-beclin peptide. Data are presented as mean  $\pm$  SD of three independent experiments. At least 100 bacteria per coverslip and triplicated coverslips in each experiment were scored. (D) ATG16L1-deficient HeLa cells were reconstituted as described in C and infected, treated, and imaged as described in A. In A–D, all compounds were treated at 10  $\mu$ M. \* $P < 0.05$ , \*\* $P < 0.01$ , \*\*\* $P < 0.001$ , ns, not significant, unpaired Student  $t$  test.

### 2.3.6 A subset of autophagy modulators suppresses IL-1 $\beta$ secretion in an autophagy-dependent manner

Previous studies have demonstrated a role for autophagy in the regulation of IL-1 $\beta$  levels. Although activation of autophagy by rapamycin has been shown to induce pro-IL-1 $\beta$  degradation and decreased IL-1 $\beta$  secretion in macrophages (14), the effect of mTOR-independent modulation of autophagy on cytokine production has not been systematically explored. To determine whether the mTOR-independent autophagy modulators discovered in our screen could regulate IL-1 $\beta$  release in response to microbial TLR4 and NOD2 ligands, we tested BRD5631 and other hits in IFN- $\gamma$ -primed macrophages stimulated with lipopolysaccharide (LPS) and muramyl dipeptide (MDP). LPS-MDP stimulated robust IL-1 $\beta$  secretion from immortalized bone marrow-derived macrophages (Figure 2.11A). The anti-inflammatory glucocorticoid dexamethasone (Dex) and the caspase1 inhibitor VX-765, compounds that target transcriptional and posttranslational steps in IL-1 $\beta$  production, respectively, significantly reduced IL-1 $\beta$  release (Figure 2.11A). All tested DOS-derived autophagy modulators reduced IL-1 $\beta$  secretion at 10  $\mu$ M (Figure 2.11A). Furthermore, the effect of these compounds on IL-1 $\beta$  secretion was dose-dependent and not associated with cytotoxicity (Figure S2.6 A and B).

To determine whether the observed reduction in IL-1 $\beta$  release was autophagy-mediated, we assayed their IL-1 $\beta$ -repressive activity in immortalized bone marrow-derived macrophages (iBMDM) in which *Atg5* had been deleted by CRISPR. Consistent with *Atg5* deletion, these cells show reduced levels of ATG5-ATG12 conjugates and LC3-II (Figure S2.6C). IL-1 $\beta$  secretion following LPS-MDP stimulation was significantly higher in the *Atg5* CRISPR line compared with parental controls, consistent with previous reports for other autophagy-deficient cell models (45) (Figure S2.6D). All four autophagy modulators suppressed IL-1 $\beta$  release in the parental cell line with little to no effect in the *Atg5* CRISPR cell line, suggesting that activities for these compounds are autophagy-mediated (Figure 2.11A).



The CD risk allele ATG16L1 T300A has also been linked to increased levels of IL-1 $\beta$  in patients (46). To determine whether DOS-derived compounds are able to reduce IL-1 $\beta$  levels in the presence of this disease allele, we evaluated the activity of the compounds in ATG16L1 T300A cells derived from knock-in mice. Consistent with previous observations (45), splenic CD11b<sup>+</sup> macrophages from ATG16L1 T300A mice demonstrated increased IL-1 $\beta$  release compared with wild-type controls (Figure 2.11B). Interestingly, BRD5631 significantly reduced the elevated IL-1 $\beta$  levels observed in ATG16L1 T300A cells (Figure 2.11B).

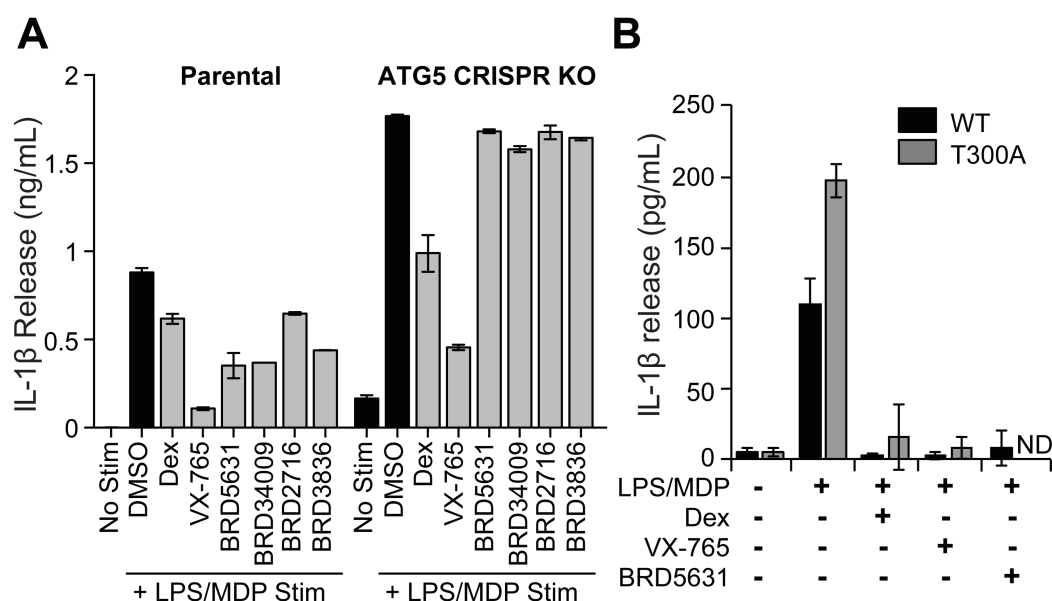


**Figure 2.11. Autophagy modulators suppress IL-1 $\beta$  secretion.** (A) IL-1 $\beta$  secretion was measured in immortalized murine bone marrow-derived macrophages primed with IFN- $\gamma$  (100 ng/mL) for 16 hours and then stimulated with LPS (10 ng/mL)-MDP (10  $\mu$ g/mL) for 24 hours, both in the presence of Dex (5  $\mu$ M), VX-765 (20  $\mu$ M), or DOS compounds (each 10  $\mu$ M). Secreted IL-1 $\beta$  was detected by ELISA. Data are presented as mean  $\pm$  SD,  $n = 3$  from a representative experiment of three independent experiments. (B) IL-1 $\beta$  secretion was measured in murine splenic CD11b<sup>+</sup> macrophages (ATG16L1 WT or T300A) primed with IFN- $\gamma$  (100 ng/mL) for 6 hours and then treated with IFN- $\gamma$  (100 ng/mL)-LPS (2 ng/mL)-MDP (10  $\mu$ g/mL) for 24 hours, both in the presence of Dex, VX-765, or BRD5631. Secreted IL-1 $\beta$  was detected by ELISA. Data are presented as mean  $\pm$  SD,  $n = 4$  mice. ND, not detected.

## 2.4 Conclusion and discussion

Here we present the identification of novel autophagy modulators, our strategies undertaken to prioritize a short list of hits, and the characterization of prioritized hits in functional

assays. In the HTS, 59,541 compounds were tested using a phenotypic-based assay. Numbers of GFP-LC3 punctae induced by compound treatment were measured as a surrogate for autophagy modulation. The hit rate of the primary screen was high (about 3%). A high hit rate is not uncommon, given autophagy is associated with cellular stress and in some occasions, cell death, which small molecules in screening libraries can often induce by altering physicochemical status in cells (47). To further annotate a large number of hits emerging from the HTS, two assays that are compatible with high-throughput format were adapted. The toxicity of hits to HeLa cells was evaluated using CellTiter-Glo reagent. To distinguish if small-molecule hits were putative activators or disruptors of later steps of autophagy, a microscopy-based mCherry-GFP-LC3 assay was used. Although mCherry-GFP-LC3 assay was a powerful assay that enables the assessment of autophagic flux in a high-throughput manner, it had a caveat that a longer treatment time was required. Therefore, it was important to keep in mind the difference in treatment times between GFP-LC3 and mCherry-GFP-LC3 assays, and be aware that compounds may elicit additional effects, either off-target effects or downstream effects of on-target effects, with a longer treatment time. Results of these assays, along with preliminary observations of SAR facilitated us to generate a short list of hits for deeper functional characterizations.

Several compounds discovered in our screen for autophagy enhancers contain a biphenyl or diphenyl alkyne group and a basic amine. Although basic amines are thought to bias compounds for accumulation in acidic cellular compartments such as lysosomes (48), our data suggest that these molecules do not reduce cell viability, disrupt lysosomal protease function, or perturb accumulation of LysoTracker Red, making them distinct from known lysosomotropic molecules. It is certainly possible that the compounds accumulate at higher concentrations within acidic compartments and exert a specific function on a lysosomal protein or signal to regulate autophagy. Indeed, an analogous model has been proposed to underlie the activity of

functional inhibitors of acid sphingomyelinase (ASM), which cause extrusion and consequent inactivation of ASM from the inner lysosomal membrane (49). Whether small molecules that operate through such a mechanism could be exploited in a therapeutic context remains unclear, but it is worth noting that similar structural moieties are present within previously reported FDA-approved enhancers of autophagy [e.g., calcium channel modulators (niguldipine) and D2 receptor modulators (TFP)] (50), arguing that such agents can be tolerated by humans. Further studies are needed to investigate how BRD5631 promotes autophagy in cells, and which regulatory pathways are involved in this process.

Human genetic studies have linked autophagy to several diseases, and depending on the context, impairment of autophagy can lead to distinct phenotypes in specific cell types and organ systems. For example, CD-associated genetic variants in ATG16L1 have implicated autophagy defects as contributing to compromised antibacterial activity in epithelial cells, elevated IL-1 $\beta$  secretion from monocytes and macrophages, reduced Paneth cell function, and impaired antigen presentation in dendritic cells (40). These observations, as well as examples from other diseases, such as Niemann–Pick disease, Mtb infection,  $\alpha$ 1-antitrypsin deficiency, and neurodegenerative disorders, suggest that small-molecule modulation of canonical and/or selective autophagy in disease-relevant cell types could be therapeutically beneficial (11, 51).

Though several small-molecule enhancers of autophagy have been described, the mechanisms of action necessary to impact these disease-related immune pathways are not well understood. Modulating the mTOR signaling pathway appears to affect disease phenotypes in several contexts, including promoting the autophagic clearance of bacteria (13) and suppress IL-1 $\beta$  secretion by targeting pro-IL-1 $\beta$  for degradation (14). Nevertheless, mTOR signaling is also critical for nutrient sensing, cell growth and other fundamental processes. For several reasons, it may be beneficial to avoid perturbation of this critical cellular pathway in treating disease; for example, its inhibition has also been linked to infection when used in therapeutics

(52). These evidences suggest the importance of discovering novel, mTOR-independent modulators of autophagy. To this end, we have identified a set of novel DOS-derived small molecules that promote autophagy independently of mTOR, and that modulate a number of cell type-specific disease phenotypes.

Importantly, BRD5631 appears to modulate several disease-associated phenotypes, including decreasing numbers of aggregate-expressing cells, reducing apoptosis of neurons in NPC1 models (at 10-fold lower concentration than CBZ), enhancing bacterial clearance, and decreasing IL-1 $\beta$  secretion. As such, studying BRD5631 and its MoA may reveal therapeutically beneficial mechanisms for modulating autophagy in the context of human disease. For example, in CD patients, the risk allele ATG16L1 T300A has been linked to elevated IL-1 $\beta$  levels (46). Furthermore, the ATG16L1 T300A knock-in mouse model recapitulates many of the autophagy-relevant phenotypes observed in CD patients, including the overproduction of IL-1 $\beta$  in response to microbial ligands, providing a valuable system to test the impact of our compounds in the presence of a CD risk allele (45). We demonstrated that BRD5631 robustly suppressed the elevated IL-1 $\beta$  observed in ATG16L1 T300A macrophages from knock-in mice, revealing this molecule can modulate relevant phenotypes in the context of a human disease allele. Given BRD5631 itself is not well-tolerated *in vivo* (data not shown), the successful development of analogs that separate toxicity from autophagy enhancement would be a critical step to determine whether BRD5631 modulates autophagy in a therapeutically relevant manner.

The evaluation of autophagy enhancement as a therapeutic strategy will ultimately require careful investigation of its complex relationship to cell death and cell survival in different physiological contexts. For example, autophagy has been proposed to promote cell survival in the context of cancer and cell death in the context of hypoxia–ischemia. Small-molecule probes that modulate autophagy will be critical for studying the pathway in different disease-relevant contexts and for understanding how it can be targeted to yield new medicines that are both safe and effective.

## 2.5 Materials and methods

**Cell lines and reagents.** HeLa cell lines were cultured in Iscove's Modified Dulbecco's Medium (IMDM) supplemented with 10% FBS (Corning), 1X GlutaMAX, 55  $\mu$ M  $\beta$ -mercaptoethanol, 2.5 mM NaOH, and 100 U/mL penicillin/streptomycin. *Atg5<sup>+/+</sup>* and *Atg5<sup>-/-</sup>* MEFs (gift from Noboru Mizushima)(53) were maintained in Dulbecco's modified Eagle's medium (DMEM) supplemented with 10% FBS, 100 U/mL penicillin/streptomycin, 2 mM L-glutamine, and 1% non-essential amino acids in a 37°C, 5% CO<sub>2</sub> humidified incubator. Human embryonic stem cells (hESCs) (WIBR3 cells) and Niemann-Pick type C1 disease patient-specific hiPSCs (WIBR-IPS-NPC1 cells) were cultured as described previously (10). Briefly, hESCs and hiPSCs were maintained on MEF feeder layers in hESC medium [DMEM/F12 supplemented with 15% fetal bovine serum (FBS, HyClone), 5% KnockOut Serum Replacement, 1 mM glutamine, 100 U/mL penicillin/streptomycin, 1% nonessential amino acids (Invitrogen), 0.1 mM  $\beta$ -mercaptoethanol (Sigma), and 4 ng/mL FGF2 (R&D Systems)]. Cell lines were passaged every 5 to 7 days with 1.5 mg/mL collagenase type IV. Reagents used for cell culture were from Life Technologies unless otherwise stated. EGFP-HDQ74 construct (mutant huntingtin exon 1 with 74 polyglutamine repeats) was a gift from David Rubinsztein and was used as previously described (54). Reagents were obtained from the following suppliers: PI-103 (Calbiochem), Torin1 (Tocris Bioscience), BafA1 (LC Laboratories), CQ, CBZ, pepA, rottlerin, TFP, and CP (Sigma-Aldrich), E64d (Santa Cruz Biotechnology), dexamethasone (Cayman Chemical), VX-765 (Selleck Chemicals). DOS compounds were obtained from the Broad Institute Compound Management Group in 8-point twofold dilution series from a top concentration of 10  $\mu$ M and were evaluated for  $\geq$  90% purity by high-performance liquid chromatography-mass spectrometry (HPLC-MS).

**Primary screen for modulators of autophagy.** HeLa cells stably expressing GFP-LC3 were plated in 384-well plates (Aurora Biotechnologies, 1022-11330) at 5,000 cells per well in 50  $\mu$ L IMDM. The following day, 100 nL of compounds were pin-transferred into plates using a CyBi-

Well Vario (CyBIO) so the final concentrations were 10  $\mu$ M and incubated with cells for 4 hours at 37°C. Cells were then fixed in 3.7% paraformaldehyde (PFA) for 15 minutes at room temperature, washed, and DNA stained with 2  $\mu$ g/mL Hoechst 33342 (Sigma, B2261). High-throughput imaging at 20X was performed on an *ImageXpress* Micro automated microscope (Molecular Devices) and the number of GFP punctae per cell was quantified using the *MetaXpress* high-content image analysis software (Transfluo module).

**Dual tagged mCherry-GFP-LC3 reporter assay.** HeLa cells stably expressing mCherry-GFP-tagged LC3 were seeded overnight in 384-well plates (Corning, 3712) at 2,000 cells per well in 50  $\mu$ L IMDM. 400 representative DOS hits along with in-plate controls (PI-103, CQ, and BafA1) were pin-transferred into plates in 8-point dose and incubated at 37°C for 24 hours. Cells were then fixed, DNA stained, and imaged as above. *CellProfiler* automated image analysis software was used to quantify the total area of autophagosomes (mCherry<sup>+</sup>/GFP<sup>+</sup>; yellow punctae) and autolysosomes (mCherry<sup>+</sup>/GFP<sup>-</sup>; red punctae) per cell (55).

**Assessment of prevalence.** For primary GFP-LC3 assay and dual-tagged mCherry-GFP-LC3 reporter assays, significance was assessed by computing an empirical test statistic, termed *prevalence*, which summarizes the observed shift in mass under the test hypothesis compared to the distribution of null hypothesis. Specifically, it was computed as the area under the curve of the test distribution beyond the critical value corresponding to 95% confidence of the null distribution. The null distribution was estimated from the observed number of autophagic vesicles per cell in DMSO-treated wells.

**Immunoblotting.** *HeLa cells and iBMDMs.* Cells were washed with phosphate buffered saline (PBS) and lysed for 30 minutes in lysis buffer [100 mM Tris-HCl pH 7.6, 1% NP-40, 100 mM NaCl, and Complete EDTA-free Protease Inhibiter Cocktail (Roche)] on ice. Following SDS-PAGE (TGX Any kD gels, Bio-Rad), proteins were transferred onto PVDF membranes (Immobilon-FL or Immobilon-P, Millipore) and blocked in Odyssey blocking buffer (LI-COR P/N 927) for 1 hour at room temperature. Membranes were subjected to overnight primary antibody

incubation at 4°C and 1 hour secondary antibody incubation at room temperature. Blots in Figures 2.6 and S2.5H were imaged on the LI-COR infrared imaging system. Blots of phospho-ULK1 and ULK1 in Figure 2.7 were visualized with SuperSignal West Femto Chemiluminescent Substrate (Thermo Scientific). All other blots in Figure 2.7 and Figure S2.6C were visualized with SuperSignal West Pico Chemiluminescent Substrate (Thermo Scientific). All antibodies and dilutions used are summarized in Table S2.2.

*hESC/hiPSC-derived neuronal cells and MEFs.* Cell pellets were lysed on ice in lysis buffer [10 mM Tris-HCl pH 7.4, 2% sodium dodecyl sulfate, 1 mM DTT, 10% glycerol, 120 mg/mL urea, Complete EDTA-free Protease Inhibitor Cocktail (Roche, 11873580001)] for 30 minutes, boiled for 10 minutes at 100°C and subjected to SDS-PAGE and immunoblot analysis as previously described (36). Blots were incubated with primary antibodies at 4°C overnight. Immunoblots were then probed with secondary antibodies for 1 hour at room temperature, and visualized using Amersham ECL Western Blotting Detection Reagent (GE Healthcare, RPN2106). All antibodies and dilutions used are summarized in Table S2.2.

**CellTiter-Glo assay.** HeLa cells were seeded in 384-well plates at 2,000 cells per well in IMDM supplemented with 10% FBS. The following day, 100 nL compounds were pin-transferred into plates using a CyBi-Well Vario (CyBIO) and incubated with cells for 72 hours at 37°C. 25 µL of CellTiter-Glo reagent (Promega) was added to each well and incubated for 30 minutes at room temperature. Plates were analyzed by measuring luminescence with the Synergy H4 plate reader (BioTek).

**DQ-BSA assay.** HeLa cells were plated overnight in 384-well plates (Corning, 3712) at 2,500 cells per well in 50 µL IMDM. The following day, cells were incubated with 10 µg/mL DQ-BSA (Life Technologies, D12051) for 1 hour. Afterward, DQ-BSA was washed away, and cells were subsequently treated with compound for 6 hours. In the last 30 minutes, nuclei were stained with 2 µg/mL Hoechst 33342. Images of live cells were taken by *ImageXpress* Micro microscope

using DAPI and Texas Red filters. MetaXpress (Transflour module) was used to quantify number and intensity of DQ-BSA punctae.

**LysoTracker assay.** HeLa cells were seeded overnight in 384-well plates (Corning, 3712) at 2,500 cells per well in 50  $\mu$ L IMDM. The following day, compounds were pin-transferred into plates and incubated at 37°C for 4 hours. Subsequently, 10  $\mu$ L of IMDM containing LysoTracker Red dye (Life Technologies, L7528) and Hoechst 33342 was added to bring the LysoTracker Red dye and Hoechst 33342 to final concentrations of 100 nM and 2  $\mu$ g/mL, respectively. After staining for 1 hour, the media in each well was replaced with PBS and imaging was performed with an *ImageXpress* Micro automated microscope using the DAPI and TRITC filters.

MetaXpress (Transflour module) was used to quantify the number of LysoTracker Red punctae per cell and average intensity of LysoTracker Red per cell.

**Quantification of mutant huntingtin aggregates.** The percentage of eGFP<sup>+</sup> cells with eGFP-HDQ74 aggregates was assessed as described previously (36). Briefly, *Atg5*<sup>+/+</sup> and *Atg5*<sup>-/-</sup> MEFs were transfected with 2.5  $\mu$ g eGFP-HDQ74 construct using FuGENE HD transfection reagent (Promega, E2311) according to the manufacturer's protocol followed by treatment with 10  $\mu$ M BRD5361 for 48 hours, after which the transfected cells were assessed for eGFP-HDQ74 aggregates by fluorescence microscopy.

**Differentiation of hESCs/hiPSCs into neuronal and hepatic-like cells.** Neurons were generated from neural precursors, which were derived from hESCs and hiPSCs using an embryoid body-based protocol as described previously (56). Differentiation of hESCs and hiPSCs into hepatic-like cells was induced as previously described (57). Generation and maintenance of NPC1 hiPSC-derived neuronal and hepatic-like cultures, which expressed the neuronal (Tuj1 and MAP2) and hepatic (HNF4 $\alpha$  and AFP) markers, respectively, were carried out as described previously (10).

**Analysis of cell death in hESC/hiPSC-derived neuronal-like cultures.** Analysis of cell death in neurons was assessed by DAPI staining and TUNEL labeling (Roche Diagnostics,



11684795910). The TUNEL labeling assay was performed according to manufacturer's instructions. Fluorescein<sup>+</sup> nuclei were counted and analyses of DAPI-stained apoptotic nuclear morphology in neuronal cultures were performed as described elsewhere (10).

**Analysis of cell death in hESC/hiPSC-derived hepatic-like cultures.** Analysis of apoptotic cells in hepatic cultures was performed with FITC Annexin V Apoptosis Detection Kit I (BD Biosciences, 556547) using FACS according to the manufacturer's protocol, as previously described (10).

**Quantitative RT-PCR.** Cells were seeded in 96-well plates and subjected to compound treatment. Cells were then washed once with PBS, and mRNA samples were harvested from cells using Dynabeads mRNA DIRECT Kit (Invitrogen, 61012) and converted to cDNA using the High Capacity cDNA Reverse Transcription Kit (Life Technologies, 4368813) following manufacturers' instructions. RT-PCR was performed on a CFX384 Real-Time PCR Detection System (Bio-Rad) with TaqMan Fast 2x Master Mix (Life Technologies, 4444557). The following TaqMan probes (Life Technologies) were used: Sqstm1 Mm00448091 and ActB Mm00607939. Reaction conditions consisted of 40 cycles of PCR with 60°C annealing temperatures. Relative mRNA levels are acquired by examining the threshold cycle ( $C_T$ ) values using the equations: Normalized p62 mRNA level =  $2^{-\Delta\Delta C_T}$ .  $\Delta\Delta C_T = (C_T \text{ p62} - C_T \text{ actin})_{\text{BRD5631-treated}} - (C_T \text{ p62} - C_T \text{ actin})_{\text{DMSO-treated}}$ .

**ATG16L1 CRISPR methods.** The second exon of *ATG16L1* was targeted in HeLa cells using the px330 plasmid CRISPR system as described (42). Briefly, a 20-nucleotide guide sequence complementary to exon 2 of *ATG16L1* (CCCTGTCCTT CCGCTGCATT) was cloned into px330 as described. The Cas9 vector containing *ATG16L1*-specific sgRNA sequence was then used to transfect HeLa cells using FuGENE (Roche) according to the manufacturer's instructions. After 48-72 hours post transfection, cells were plated in limiting dilution in 96-well plates to isolate single cell clones. DNA was isolated from clonal populations using DNeasy (Qiagen) and *ATG16L1* exon 2 was PCR-amplified and sequenced to identify clones with frameshift mutations

in all loci. ATG16L1 loss was also confirmed at the protein level. Western blotting for LC3 shift confirmed the absence of LC3-II conversion in these cells.

**Atg5 CRISPR method.** The second exon of *Atg5* was targeted in iBMDMs using the pXPR\_001 plasmid CRISPR system as described (58). Briefly, a guide sequence complementary to exon 2 of *Atg5* (CACCGAAGATGTGCTTCGAGATGTG) was cloned into pXPR\_001 plasmid, and co-transfected into HEK293T cell with pCMV-dR8.91 and VSV-G plasmids for lentivirus production. iBMDMs were transduced with lentivirus for 48 hours, and then selected with puromycin. After 7-10 days of selection, ATG5 loss in iBMDM populations were confirmed by western blotting for LC3 shift and loss of ATG5-ATG12 complex, and used in experiments immediately once confirmed.

**Bioluminescent bacterial replication assay.** Bioluminescent bacterial replication assays were performed as previously described (41). Briefly, HeLa cells were seeded overnight in 96-well plates (Corning, 3904) at 10,000 cells per well in 100  $\mu$ L antibiotic-free IMDM. The following day, an overnight bacterial culture of *S. enterica* serovar Typhimurium expressing the *Photobacterium luminescens lux* operon (Perkin Elmer, Xen26) was diluted 1:30 in LB media containing 30  $\mu$ g/mL kanamycin and cultured with shaking at 37°C for 4 hours. The bacterial culture was then diluted 1:40 in antibiotic-free IMDM and incubated with HeLa cells for 30 minutes at 37°C. Following infection, the bacterial suspension was removed and replaced with IMDM containing 20  $\mu$ g/mL gentamicin. After 10 minutes at room temperature, the cells were washed a second time without the 10-minute incubation, then the media was replaced with IMDM containing compounds and 20  $\mu$ g/mL gentamicin. Plates were then incubated at 37°C and analyzed at indicated time points post infection by measuring luminescence with the Synergy H4 plate reader (BioTek).

**Gentamicin protection assay.** HeLa cells were plated at 10,000 cells per well in 100  $\mu$ L antibiotic-free IMDM. The following day, cells were infected for 30 minutes with 1:40 diluted *S. Typhimurium* Xen26 (overnight culture diluted 1:30 and grown for an additional 4 hours) in

antibiotic-free IMDM media. Cells were washed with media containing 20 µg/mL gentamicin and incubated with media containing the indicated compound and 20 µg/mL gentamicin for 20 hours. Cells were then washed, lysed with 1% Triton X-100 in PBS, diluted, and plated on LB supplemented with 50 µg/mL kanamycin. CFUs were counted after a 20-hour incubation at 37°C.

**Compound toxicity to *Salmonella*.** *S. enterica* serotype Typhimurium Xen26 (overnight culture diluted 1:30 and grown for an additional 4 hours) was diluted 1:4000 into antibiotic-free IMDM media and 50 µL of this solution was added to each well of a 96-well plate (Corning, 3904). Bacteria solutions were treated with 50 µL of each compound (20 µM) or gentamicin (20 µg/mL) in IMDM media (final concentrations of 10 µM and 10 µg/mL, respectively). After 12 hours at 37°C, plates were analyzed by measuring luminescence with the Synergy H4 plate reader (BioTek) to determine bactericidal activity of compounds in the absence of mammalian cells.

**LC3 or NDP52/*Salmonella* colocalization assay.** HeLa cells were seeded overnight in 96-well plates (Corning, 3904) at 12,500 cells per well, or on coverslips in 24-well plates at 50,000 cells per well in antibiotic-free IMDM. The following day, the medium was replaced with antibiotic-free IMDM containing compounds. The culture of *S. enterica* serotype Typhimurium strain SL1344 expressing DsRed (Clontech) was prepared as previously described (41). After the 3-hour compound pretreatment, antibiotic-free IMDM containing 1:20 diluted bacterial culture was added to each well (25 µL for 96-well plates or 50 µL for 24-well plates). Cells were infected for 20 minutes at 37°C. Cells were washed three times with IMDM containing 50 µg/mL gentamicin and subsequently incubated in IMDM containing 20 µg/mL gentamicin and compounds. At indicated post-infection time points, the medium was aspirated and cells were fixed in methanol at -20°C for 2.5 minutes. Cells were then incubated with primary antibodies (rabbit anti-LC3B, mouse anti-NDP52, and goat anti-*Salmonella* CSA1) diluted in 10% donkey serum (Jackson ImmunoResearch) in PBS for 1 hour at room temperature. Cells were then washed and incubated with secondary antibodies (Alexa Fluor 488-conjugated donkey anti-rabbit IgG, Cy5-

conjugated donkey anti-mouse IgG, and Alexa Fluor 546-conjugated donkey anti-goat IgG) and 2 µg/mL Hoechst 33342 in 10% donkey serum in PBS at room temperature for 1 hour. Imaging of cells in 96-well plates was performed with *ImageXpress* Micro automated microscope, with nine 40x images taken per well and with DAPI, GFP, TRITC, and Cy5 filters. *CellProfiler* was used to quantify the number of LC3<sup>+</sup> bacteria and NDP52<sup>+</sup> bacteria (55). Coverslips were scored under wide-field fluorescence illumination with a 64X lens and a 1.6X Optovar (Zeiss Axio Observer.D1; Carl Zeiss MicroImaging). The number of LC3<sup>+</sup> bacteria was scored in randomly chosen fields, with at least 100 bacteria examined on each coverslip, and triplicate coverslips examined in each independent experiment.

**IL-1β secretion assay.** *Immortalized bone marrow-derived macrophages (iBMDMs).* To generate an iBMDM line, BMDMs were infected with a J2 retrovirus (carrying the v-myc and v-raf oncogenes) and cultured at 37°C in DMEM containing 10% FBS and 100 U/mL penicillin/streptomycin for two weeks with 5 ng/ml M-CSF followed by two weeks without M-CSF. On day 1 of the assay, 100,000 iBMDMs per well were plated in 96-well plates (Corning, 3904). The following day, cells were treated with compound and 100 ng/mL IFNγ for 16 hours followed by a 24-hour stimulation with 10 ng/mL LPS, 10 µg/mL MDP, and compound. The amount of IL-1β released into cell supernatants was then measured by ELISA (BD Biosciences, 559603).

*Splenic CD11b<sup>+</sup> cells.* CD11b<sup>+</sup> cells were isolated by positive selection using CD11b microbeads (Miltenyi) and spleens derived from C57BL/6 *Atg16l1<sup>wt/wt</sup>* and *Atg16l1<sup>T300A/T300A</sup>* mice. Freshly isolated splenic CD11b<sup>+</sup> cells were plated at 100,000 cells per well in 96-well plates (Corning, 3904) and cultured at 37°C in RPMI containing 10% FBS and 100 U/mL penicillin/streptomycin. Cells were treated for 6 hours with 100 ng/mL IFNγ followed by a 24-hour stimulation with 2 ng/mL LPS, 10 µg/mL MDP, and 100 ng/mL IFNγ. IFNγ and LPS-MDP-IFN treatments were performed in the presence of compound and the amount of IL-1β released was measured as above.

**SYTOX Green assay.** Following the removal of supernatant for the IL-1 $\beta$  ELISA, cells remaining in the 96-well plate were washed with phosphate-free buffer and then 50  $\mu$ L of SYTOX Green solution in phosphate-free buffer (100 nM) (Life Technologies, S7020) was added to each well. After 30 minutes, the staining solution was removed, the cells were washed twice with phosphate-free buffer, and total fluorescence was measured with the Synergy H4 plate reader [Excitation/Emission (nm) 504/523].

**Mice.** T300A knock-in mice were generated and maintained as previously described (45). Animals were housed in a pathogen-free facility, and all procedures were performed in accordance with the institutional animal care and use committee at Massachusetts General Hospital.

**Statistical analysis.** For GFP-LC3 punctae formation assays, dose curves and EC<sub>50</sub> values were determined using the log (agonist) vs. normalized response – variable slope model in Prism 6 (GraphPad). The chemical moieties enrichment analysis was performed in MATLAB R2013b (MathWorks). *P* values of Student's t-test were determined using Prism 6 (GraphPad). \**P* < 0.05; \*\**P* < 0.01; \*\*\**P* < 0.001; ns, non-significant.

## 2.6 References

1. S.-Y. Kuo *et al.*, Small-molecule enhancers of autophagy modulate cellular disease phenotypes suggested by human genetics. *Proceedings of the National Academy of Sciences* **112**, E4281-E4287 (2015).
2. Y. Cheng, X. Ren, W. N. Hait, J. M. Yang, Therapeutic targeting of autophagy in disease: biology and pharmacology. *Pharmacological reviews* **65**, 1162-1197 (2013).
3. S. Y. Shaw *et al.*, Selective modulation of autophagy, innate immunity, and adaptive immunity by small molecules. *ACS chemical biology* **8**, 2724-2733 (2013).
4. J. J. Kim *et al.*, Host cell autophagy activated by antibiotics is required for their effective antimycobacterial drug action. *Cell host & microbe* **11**, 457-468 (2012).
5. V. Sundaramurthy *et al.*, Integration of chemical and RNAi multiparametric profiles identifies triggers of intracellular mycobacterial killing. *Cell host & microbe* **13**, 129-142 (2013).
6. S. Shoji-Kawata *et al.*, Identification of a candidate therapeutic autophagy-inducing peptide. *Nature* **494**, 201-206 (2013).
7. S. Chauhan *et al.*, Pharmaceutical screen identifies novel target processes for activation of autophagy with a broad translational potential. *Nat Commun* **6**, 8620 (2015).
8. T. Hidvegi *et al.*, An autophagy-enhancing drug promotes degradation of mutant alpha1-antitrypsin Z and reduces hepatic fibrosis. *Science* **329**, 229-232 (2010).
9. S. Sarkar, Regulation of autophagy by mTOR-dependent and mTOR-independent pathways: autophagy dysfunction in neurodegenerative diseases and therapeutic application of autophagy enhancers. *Biochemical Society transactions* **41**, 1103-1130 (2013).
10. D. Maetzel *et al.*, Genetic and chemical correction of cholesterol accumulation and impaired autophagy in hepatic and neural cells derived from Niemann-Pick Type C patient-specific iPS cells. *Stem cell reports* **2**, 866-880 (2014).
11. S. Sarkar *et al.*, Impaired autophagy in the lipid-storage disorder Niemann-Pick type C1 disease. *Cell reports* **5**, 1302-1315 (2013).
12. H. C. Chiu *et al.*, Eradication of intracellular *Salmonella enterica* serovar Typhimurium with a small-molecule, host cell-directed agent. *Antimicrobial agents and chemotherapy* **53**, 5236-5244 (2009).
13. I. Tattoli *et al.*, Amino acid starvation induced by invasive bacterial pathogens triggers an innate host defense program. *Cell host & microbe* **11**, 563-575 (2012).
14. J. Harris *et al.*, Autophagy controls IL-1beta secretion by targeting pro-IL-1beta for degradation. *The Journal of biological chemistry* **286**, 9587-9597 (2011).

15. J. Hemelaar, V. S. Lelyveld, B. M. Kessler, H. L. Ploegh, A Single Protease, Apg4B, Is Specific for the Autophagy-related Ubiquitin-like Proteins GATE-16, MAP1-LC3, GABARAP, and Apg8L. *Journal of Biological Chemistry* **278**, 51841-51850 (2003).
16. T. G. Nguyen *et al.*, Development of Fluorescent Substrates and Assays for the Key Autophagy-Related Cysteine Protease Enzyme, ATG4B. *ASSAY and Drug Development Technologies* **12**, 176-189 (2014).
17. L. Vezenkov *et al.*, Development of fluorescent peptide substrates and assays for the key autophagy-initiating cysteine protease enzyme, ATG4B. *Bioorg Med Chem* **23**, 3237-3247 (2015).
18. J. Kim, M. Kundu, B. Viollet, K. L. Guan, AMPK and mTOR regulate autophagy through direct phosphorylation of Ulk1. *Nature cell biology* **13**, 132-141 (2011).
19. L. H. Rosenberg *et al.*, Development of an HTS-Compatible Assay for the Discovery of Ulk1 Inhibitors. *J Biomol Screen* **20**, 913-920 (2015).
20. Y. Kabeya *et al.*, LC3, a mammalian homologue of yeast Apg8p, is localized in autophagosome membranes after processing. *The EMBO Journal* **19**, 5720-5728 (2000).
21. A. D. Balgi *et al.*, Screen for chemical modulators of autophagy reveals novel therapeutic inhibitors of mTORC1 signaling. *PloS one* **4**, e7124 (2009).
22. U. Chandrachud *et al.*, Unbiased Cell-based Screening in a Neuronal Cell Model of Batten Disease Highlights an Interaction between Ca<sup>2+</sup> Homeostasis, Autophagy, and CLN3 Protein Function. *The Journal of biological chemistry* **290**, 14361-14380 (2015).
23. L. Zhang *et al.*, Small molecule regulators of autophagy identified by an image-based high-throughput screen. *Proceedings of the National Academy of Sciences of the United States of America* **104**, 19023-19028 (2007).
24. N. Mizushima, T. Yoshimori, B. Levine, Methods in mammalian autophagy research. *Cell* **140**, 313-326 (2010).
25. M. E. Fitzgerald *et al.*, Build/couple/pair strategy for the synthesis of stereochemically diverse macrolactams via head-to-tail cyclization. *ACS combinatorial science* **14**, 89-96 (2012).
26. B. Gerard *et al.*, Synthesis of a stereochemically diverse library of medium-sized lactams and sultams via S(N)Ar cycloetherification. *ACS combinatorial science* **13**, 365-374 (2011).
27. L. A. Marcaurelle *et al.*, An aldol-based build/couple/pair strategy for the synthesis of medium- and large-sized rings: discovery of macrocyclic histone deacetylase inhibitors. *Journal of the American Chemical Society* **132**, 16962-16976 (2010).
28. G. Marino, M. Niso-Santano, E. H. Baehrecke, G. Kroemer, Self-consumption: the interplay of autophagy and apoptosis. *Nature reviews. Molecular cell biology* **15**, 81-94 (2014).

29. S. Kimura, T. Noda, T. Yoshimori, Dissection of the Autophagosome Maturation Process by a Novel Reporter Protein, Tandem Fluorescent-Tagged LC3. *Autophagy* **3**, 452-460 (2007).
30. R. Ashoor, R. Yafawi, B. Jessen, S. Lu, The contribution of lysosomotropism to autophagy perturbation. *PloS one* **8**, e82481 (2013).
31. S. Nadanaciva *et al.*, A high content screening assay for identifying lysosomotropic compounds. *Toxicology in vitro : an international journal published in association with BIBRA* **25**, 715-723 (2011).
32. C. L. Vázquez, M. I. Colombo, Chapter 6 Assays to Assess Autophagy Induction and Fusion of Autophagic Vacuoles with a Degradative Compartment, Using Monodansylcadaverine (MDC) and DQ - BSA. **452**, 85-95 (2009).
33. B. Lemieux, M. D. Percival, J. P. Falgoutyret, Quantitation of the lysosomotropic character of cationic amphiphilic drugs using the fluorescent basic amine Red DND-99. *Analytical biochemistry* **327**, 247-251 (2004).
34. C. C. Thoreen *et al.*, An ATP-competitive mammalian target of rapamycin inhibitor reveals rapamycin-resistant functions of mTORC1. *The Journal of biological chemistry* **284**, 8023-8032 (2009).
35. B. Ravikumar *et al.*, Inhibition of mTOR induces autophagy and reduces toxicity of polyglutamine expansions in fly and mouse models of Huntington disease. *Nature genetics* **36**, 585-595 (2004).
36. S. Sarkar, B. Ravikumar, D. C. Rubinsztein, Chapter 5 Autophagic Clearance of Aggregate - Prone Proteins Associated with Neurodegeneration. **453**, 83-110 (2009).
37. G. Bjorkoy *et al.*, p62/SQSTM1 forms protein aggregates degraded by autophagy and has a protective effect on huntingtin-induced cell death. *The Journal of cell biology* **171**, 603-614 (2005).
38. M. H. Sahani, E. Itakura, N. Mizushima, Expression of the autophagy substrate SQSTM1/p62 is restored during prolonged starvation depending on transcriptional upregulation and autophagy-derived amino acids. *Autophagy* **10**, 431-441 (2014).
39. J. Huang, J. H. Brumell, Bacteria-autophagy interplay: a battle for survival. *Nature reviews. Microbiology* **12**, 101-114 (2014).
40. P. Kuballa, W. M. Nolte, A. B. Castoreno, R. J. Xavier, Autophagy and the immune system. *Annual review of immunology* **30**, 611-646 (2012).
41. K. L. Conway *et al.*, Atg16l1 is required for autophagy in intestinal epithelial cells and protection of mice from Salmonella infection. *Gastroenterology* **145**, 1347-1357 (2013).
42. L. Cong *et al.*, Multiplex genome engineering using CRISPR/Cas systems. *Science* **339**, 819-823 (2013).



43. N. Fujita *et al.*, The Atg16L complex specifies the site of LC3 lipidation for membrane biogenesis in autophagy. *Molecular biology of the cell* **19**, 2092-2100 (2008).
44. P. Kuballa, A. Huett, J. D. Rioux, M. J. Daly, R. J. Xavier, Impaired autophagy of an intracellular pathogen induced by a Crohn's disease associated ATG16L1 variant. *PLoS one* **3**, e3391 (2008).
45. K. G. Lassen *et al.*, Atg16L1 T300A variant decreases selective autophagy resulting in altered cytokine signaling and decreased antibacterial defense. *Proceedings of the National Academy of Sciences of the United States of America* **111**, 7741-7746 (2014).
46. T. S. Plantinga *et al.*, Crohn's disease-associated ATG16L1 polymorphism modulates pro-inflammatory cytokine responses selectively upon activation of NOD2. *Gut* **60**, 1229-1235 (2011).
47. H. Vakifahmetoglu-Norberg, H. G. Xia, J. Yuan, Pharmacologic agents targeting autophagy. *J Clin Invest* **125**, 5-13 (2015).
48. A. M. Kaufmann, J. P. Krise, Lysosomal sequestration of amine-containing drugs: analysis and therapeutic implications. *Journal of pharmaceutical sciences* **96**, 729-746 (2007).
49. J. Kornhuber *et al.*, Identification of novel functional inhibitors of acid sphingomyelinase. *PLoS one* **6**, e23852 (2011).
50. W. H. Halliwell, Cationic Amphiphilic Drug-Induced Phospholipidosis. *Toxicologic Pathology* **25**, 53-60 (1997).
51. D. C. Rubinsztein, P. Codogno, B. Levine, Autophagy modulation as a potential therapeutic target for diverse diseases. *Nature reviews. Drug discovery* **11**, 709-730 (2012).
52. R. J. Motzer *et al.*, Efficacy of everolimus in advanced renal cell carcinoma: a double-blind, randomised, placebo-controlled phase III trial. *The Lancet* **372**, 449-456.
53. A. Kuma *et al.*, The role of autophagy during the early neonatal starvation period. *Nature* **432**, 1032-1036 (2004).
54. Y. Narain, A. Wytttenbach, J. Rankin, R. A. Furlong, D. C. Rubinsztein, A molecular investigation of true dominance in Huntington's disease. *Journal of Medical Genetics* **36**, 739-746 (1999).
55. A. E. Carpenter *et al.*, CellProfiler: image analysis software for identifying and quantifying cell phenotypes. *Genome biology* **7**, R100 (2006).
56. M. C. Marchetto *et al.*, A model for neural development and treatment of Rett syndrome using human induced pluripotent stem cells. *Cell* **143**, 527-539 (2010).
57. K. Si-Tayeb *et al.*, Highly efficient generation of human hepatocyte-like cells from induced pluripotent stem cells. *Hepatology* **51**, 297-305 (2010).

58. O. Shalem *et al.*, Genome-Scale CRISPR-Cas9 Knockout Screening in Human Cells. *Science* **343**, 84-87 (2014).

*Page left intentionally blank*

# Chapter III

## Discovery of a Small-Molecule Probe for V-ATPase Function

Adapted from L. N. Aldrich *et al.*, Discovery of a Small-Molecule Probe for V-ATPase Function.  
*J Am Chem Soc* **137**, 5563-5568 (2015) (1)

## Collaborator Contributions

- **Dr. Adam Castoreno** conducted the primary screen with my assistance and conducted the toxicity assay.
- **Dr. Leslie Aldrich** synthesized DOS compounds.
- **Dr. Gautam Goel** and **Dr. Vlado Dančik** analyzed data of the primary screen and the autophagy flux assay.
- **Dr. Leslie Aldrich** assisted in assays measuring lysosomal functions.
- **Dr. Matthew Rees** and **Dr. Brinton Seashore-Ludlow** assisted in the analysis of cancer cell profiling.

### 3.1 Introduction

Studies of human genetics and physiology have implicated autophagy in several inflammatory, neurodegenerative, infectious, and autoimmune diseases, revealing the importance of cellular homeostasis in human disease and motivating the discovery of small-molecule probes to investigate the different stages of this complex pathway (2-4). Lysosomes are the site of degradation and recycling in eukaryotic cells for macromolecules, organelles, and pathogens engulfed through autophagy, endocytosis, and phagocytosis. Degradation within the lysosome is facilitated by lysosomal hydrolases, including proteases, peptidases, phosphatases, nucleases, glycosidases, and lipases, and products are released by diffusion or carrier-mediated transporters for reuse by cells (5). In some cell types, lysosomes can also deliver cargo to pathogen recognition receptors (PRRs), or preserve degraded cargo for antigen presentation (6). The acidic pH in the lysosomal lumen (pH = 4.5–5.0), which is required for optimal hydrolase activity, is generated and maintained by the V-ATPase, a protein complex on lysosomal membranes that hydrolyzes ATP to drive protons into lysosomes (7). Mutations in various subunits of the V-ATPase complex have been linked to osteopetrosis (8, 9), X-linked myopathy (10), distal renal tubular acidosis, sensorineural deafness (11, 12), and pulmonary tuberculosis (13), and the complex has been studied as a potential dependency of certain cancer cells (7, 14, 15).

Beyond its degradative function, recent studies have identified the lysosome as a critical component of various signaling pathways. For example, amino acids in the lysosomal lumen promote the recruitment of the mTOR to the lysosomal membrane and the activation of mTOR signaling in a V-ATPase- and Ragulator-dependent manner (16, 17), leading to enhancement of cell growth and protein synthesis and inhibition of autophagy (18). mTOR also regulates TFEB, a transcription factor that promotes expression of genes required for the biogenesis of lysosomes and activation of the endolysosomal system and autophagic catabolism (19, 20). Lysosomes and lysosomal proteins, such as NPC1 and NPC2, additionally maintain cholesterol

homeostasis by controlling cholesterol efflux from the lysosomal lumen (21, 22). The lysosome is also involved in exocytosis to promote intercellular signaling and plasma membrane repair through fusion with the plasma membrane to restore membrane integrity (23).

The study of lysosomes has been greatly enabled by the discovery of small-molecule probes that perturb lysosomal function through distinct mechanisms, including direct inhibition of lysosomal proteases, inhibition of the V-ATPase, extrusion and degradation of enzymes from the lysosomal membrane, or perturbation of lysosomal pH through protonation and accumulation in lysosomes (24, 25). Many of these modulators are derived from natural sources, including the protease inhibitors leupeptin, pepA, and E64d, as well as several classes of V-ATPase modulators, including the plecomacrolides, BafA1 and concanamycin A; the macrolides, archazolid A and palmerolide A; and the benzolactone enamides, apicularen A and salicylihalamide A (26, 27). Additional small molecules that perturb the lysosome may serve as useful tools to study its role in cellular physiology and human disease biology.

DOS aims to synthesize candidate probes and therapeutics having novel mechanisms of action not easily found in other sources of synthetic compounds. The short and modular synthetic pathways that result from the build/couple/pair (BCP) strategy, which mimics the strategy used in nature to synthesize natural products, ensure ease of chemical optimization of starting points found using screening. This chemistry has yielded compounds enriched for  $sp^3$ -hybridized skeletal atoms and often results in all possible stereoisomers to maximize diversity of scaffold shape (28-31).

Here we report the discovery of a novel small-molecule inhibitor of lysosomal acidification (BRD1240) through high-content screening of a DOS-derived compound collection. We identified BRD1240 on the basis of its ability to increase numbers of autophagosomes, as measured by GFP-LC3 punctae accumulation. Among screening hits, BRD1240 displayed a particularly striking dependence of activity on stereochemistry, suggesting a potentially selective interaction with a protein target. Subsequent experiments revealed that BRD1240 blocks the

maturation of autophagosomes to autolysosomes, likely due to its ability to interfere with lysosomal acidification.

To study the MoA of BRD1240, we measured the sensitivity of 83 cancer cell lines to BRD1240 and compared the resulting sensitivity profile to those of 480 other small molecules spanning a range of protein targets; the profile of BRD1240 correlated most strongly with that of BafA1, a potent, specific inhibitor of the V-ATPase. Biochemical assays confirmed that BRD1240 can suppress V-ATPase function, though with kinetics different than that of BafA1, suggesting it may operate through a different molecular mode of action. BRD1240 may serve as a probe to study how lysosomal acidification is regulated by the multi- subunit molecular machine, V-ATPase, and how it affects cellular physiology.

### **3.2 BRD1240 increases autophagosome number by inhibiting autophagosomal turnover**

We performed a HTS of 59,541 stereochemically and skeletally diverse compounds derived from DOS for compounds that modulate autophagosome number. The primary HTS was conducted in HeLa cells stably expressing a GFP-LC3 fusion protein (Figure 3.1). LC3 normally displays a diffuse cytosolic pattern (LC3-I), but upon induction of autophagy, LC3 is cleaved and conjugated to phosphatidylethanolamine (LC3-II), and accumulates on autophagosome membranes. As such, the number of autophagosomes can be estimated by counting the number of GFP-LC3 “punctae per cell” by microscopy (32). Hits were selected on the basis of their ability to elicit statistically significant changes in the number of punctae/cell compared with the observed number in DMSO-treated wells. Significance was assessed by computing the area under the curve (AUC) of the test distribution in compound-treated wells beyond the critical value corresponding to 95% confidence of the null distribution estimated from the observed number of “punctae per cell” in DMSO-treated wells.



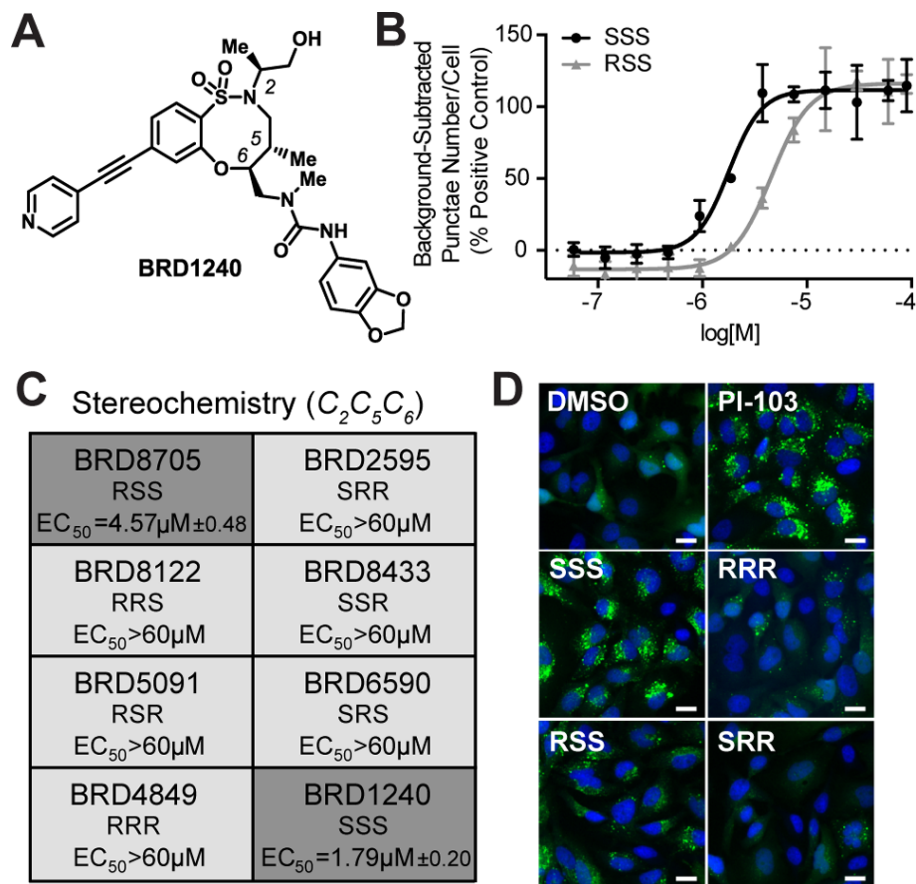


**Figure 3.1. BRD1240 increases the GFP-LC3 punctae number, and this activity is dependent on stereochemistry.** (A) Chemical structure of BRD1240. (B) Dose–response curves of BRD1240 (SSS) and BRD8705 (RSS) in the GFP-LC3 punctae formation assay. The positive control for increased punctae number is PI-103, a dual PI3K/ mTOR inhibitor. Values are presented as the average  $\pm$  SD of three independent experiments, each run in duplicate. (C) Dose–response data ( $EC_{50}$ ) for all stereoisomers in the GFP-LC3 punctae formation assay. Values are presented as average  $\pm$  SEM. (D) Representative images from the GFP-LC3 punctae formation assay following treatment with DMSO; PI-103 (5  $\mu M$ ); BRD1240 and its enantiomer, BRD4849 (RRR); and BRD8705 (RSS) and its enantiomer, BRD2595 (SRR) (all 20  $\mu M$ ). Blue (Hoechst 33342), green (eGFP). Scalar bars represent 10  $\mu m$ .

Among confirmed hits, BRD1240 was particularly potent and displayed a striking SAR with respect to the stereochemistry within the ring (Figure 3.1). Only two of the eight stereoisomers were active, the SSS and RSS diastereomers, with the sole difference being the configuration of the extra-annular methyl group; all other stereoisomers were inactive (Figures 3.1C and D and S3.1). The dependence of BRD1240 activity on its stereochemistry suggests a small-molecule–protein interaction that is highly dependent on the three-dimensional structure

of the molecule. Notably, the enantiomer of BRD1240 (BRD4849), which has the same physicochemical properties as BRD1240, does not cause an increase in GFP-LC3 punctae number, supporting a hypothesis that BRD1240 does not simply perturb lysosomal function by accumulating nonspecifically within the organelle as has been observed for other small molecules (25).

The number of GFP-LC3 punctae in the cell can be increased by either activation of autophagy or inhibition of autophagy at a late step in the process, such as by disrupting lysosomal function. To test BRD1240 for these activities, we performed an assay for autophagosome formation and maturation (flux) that relies on visualizing an LC3 protein tagged with both mCherry and eGFP. The assay exploits the differential sensitivities of mCherry and eGFP to the acidic lysosomal environment to infer autophagic flux. The eGFP signal is attenuated in autolysosomes, while the mCherry signal remains stable (33); as a result, autophagosomes (eGFP<sup>+</sup>/mCherry<sup>+</sup>: yellow puncta) and autolysosomes (eGFP<sup>-</sup>/mCherry<sup>+</sup>: red puncta) can be distinguished and counted by high-throughput imaging. This assay was optimized using a known activator of autophagy, PI-103 (dual inhibitor of mTOR and PI3K), and a known inhibitor of lysosomal acidification, BafA1 (V-ATPase inhibitor). As expected, PI-103 robustly increased the number of autolysosomes (red puncta), while BafA1 increased the number of autophagosomes (yellow puncta) by blocking autophagic flux (Figure 3.2A). Similar to BafA1, BRD1240 and its active diastereomer (BRD8705) robustly inhibited autolysosome formation, causing a significant accumulation of autophagosomes (Figures 3.2A and S3.2A). These results suggest that BRD1240 blocks autophagosomal turnover. In further support of this hypothesis, we found that treatment with BRD1240, when cotreated with the lysosomal protease inhibitors, E64d and pepA, caused no additional increase in LC3-II/LC3-I ratio by Western blot (Figure 3.2B).

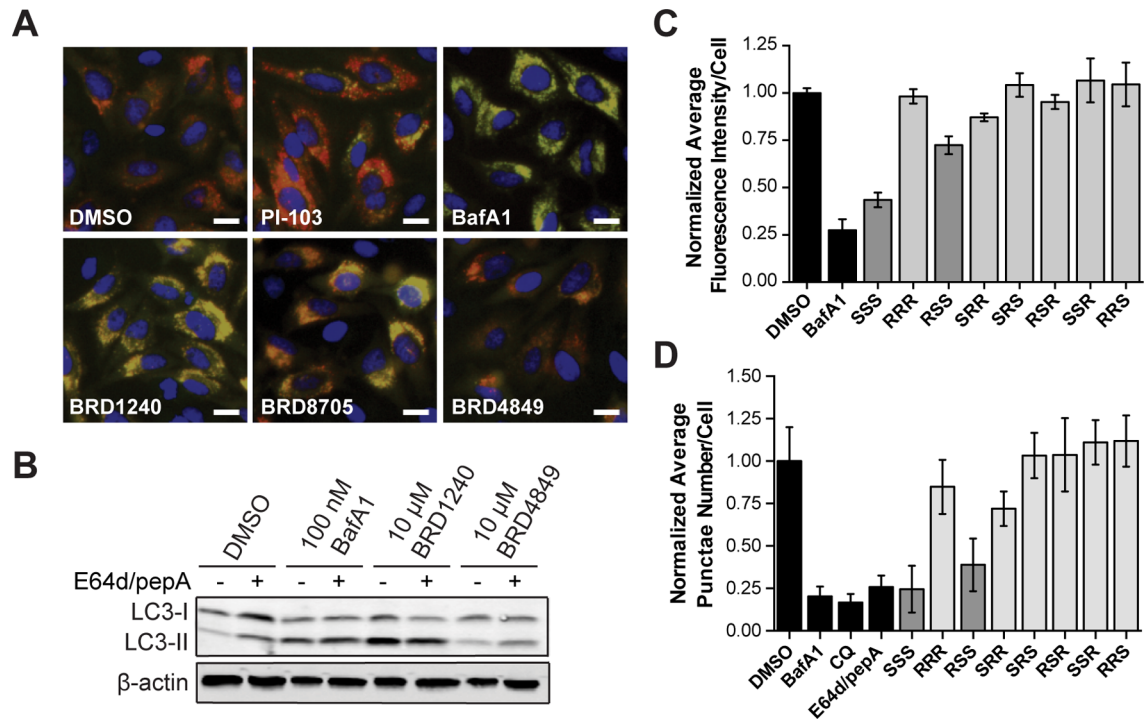


**Figure 3.2. BRD1240 blocks the later stages of autophagy.** (A) Representative images from the mCherry-eGFP-LC3 assay following treatment with DMSO, PI-103 (5  $\mu$ M), BafA1 (100 nM), BRD1240 (10  $\mu$ M), BRD8705 (10  $\mu$ M), and BRD4849 (10  $\mu$ M). Blue (Hoechst 33342), red (mCherry), green (eGFP). Scalar bars represent 10  $\mu$ m. (B) Western blot for LC3-I to LC3-II shift in HeLa cells treated with BafA1, BRD1240, and BRD4849 with or without 10  $\mu$ g/mL E64d/pepA. (C) Normalized average fluorescence intensity of punctae per cell for BafA1 (100 nM), BRD1240 (SSS) (10  $\mu$ M), and all seven stereoisomers (10  $\mu$ M) in HeLa cells in the LysoTracker displacement assay. (D) Normalized average punctae number per cell for BafA1 (200 nM), chloroquine (CQ) (50  $\mu$ M), E64d/pepA (10  $\mu$ g/mL), BRD1240 (20  $\mu$ M), and all seven stereoisomers (20  $\mu$ M) in HeLa cells in the DQ-BSA assay. In parts C and D data are presented as the average  $\pm$  SD of three independent experiments, each run in duplicate.

### 3.3 BRD1240 modulates lysosomal function

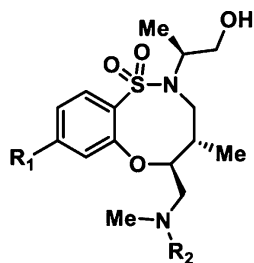
To determine whether BRD1240 disrupts autophagic flux by perturbing lysosomal function, we first tested its effects on cellular staining with a pH-sensitive cationic fluorescent dye (LysoTracker Red), which accumulates in acidic cellular compartments (34). The fluorescent signal was greatly diminished after BRD1240 and BRD8705 treatment, suggesting that the compounds may inhibit lysosomal acidification (Figures 3.2C and S3.2B). In contrast, none of the inactive stereoisomers was capable of diminishing the fluorescent LysoTracker signal. We then tested whether BRD1240 affected the ability of lysosomal proteases, which

require an acidic environment for optimal activity, to process a fluorogenic substrate (DQ-BSA) (35). As expected, treatment with compounds that inhibit lysosomal proteases directly (E64d/pepA) or indirectly by increasing lysosomal pH (BafA1 and CQ) significantly decreased both DQ-BSA punctae number and intensity (Figures 3.2D and S3.2C). We found that treatment with BRD1240 and BRD8705 for 6 hours also robustly decreased DQ-BSA punctae number and intensity, whereas the inactive stereoisomers had no activity in the assay. These data implicate the lysosome as a potential site of action of BRD1240.

### **3.4 BRD1240 has notable structure-activity relationships**

To understand better the structural elements that, in addition to the stereochemistry of the ring, are required for the activity of BRD1240, we tested analogues of BRD1240 in both the GFP-LC3 and LysoTracker assays (Tables 3.1 and S3.1). Movement of the nitrogen of the pyridine from the 4-position to the 3-position, or replacement of the pyridine with a phenyl ring, resulted in a complete loss of activity, confirming the importance of the nitrogen heteroatom at this position. It is possible that this nitrogen participates in a critical hydrogen bonding interaction with a protein target of BRD1240. Changes to the urea moiety were slightly more tolerated. Complete removal of the piperonyl urea ablated activity as did replacement of the urea with various amides; however, exchange of the piperonyl urea moiety with a *meta*-methoxy urea moiety yielded an active analogue. These observations suggest that an electron-rich phenyl urea is optimal for activity, but subtle changes at this position may be acceptable. More drastic changes to either position resulted in completely inactive analogues. Importantly, the SAR trends observed in the GFP-LC3 assay are paralleled in the LysoTracker assay, strengthening the hypothesis that BRD1240's effects on autophagosome number are linked to its ability to perturb lysosomal function.

**Table 3.1 BRD1240 analogues reveal SAR in GFP-LC3<sup>a</sup> and LysoTracker assays<sup>b</sup>**



Compound	R <sub>1</sub>	R <sub>2</sub>	GFP-LC3 (20 μM)	LysoTracker (20 μM)
BRD1240			267 ±11	46 ±11
BRD2852		“	125 ±23	103 ±5
BRD0237		“	113 ±10	110 ±7
BRD6840		“	107 ±17	116 ±8
BRD7020		“	139 ±5	118 ±8
BRD1609			259 ±14	46 ±4
BRD1295	“		148 ±22	99 ±16
BRD7039	“		181 ±14	120 ±11
BRD5960	“		114 ±14	126 ±10
BRD73146	“		136 ±14	116 ±12
BRD9117	“		136 ±18	130 ±14
DMSO	-	-	100 ±10	100 ±3

<sup>a</sup>GFP-LC3 punctae formation data are presented as the average of three independent experiments run in duplicate and are reported as relative average percent intensity ± SEM at 20 μM. <sup>b</sup>LysoTracker displacement data are presented as the average of two independent experiments run in duplicate and are reported as relative average percent intensity ± SEM at 20 μM.

### **3.5 BRD1240 kills a similar subset of cancer cells as the V-ATPase inhibitor, Bafilomycin A1**

Profiling the sensitivity of cancer cell lines to small molecules has emerged as a powerful tool for gaining insights into their MoAs (36). Compounds with similar MoAs have been shown to elicit a similar pattern of responses across panels of cancer cell lines (36-38). We measured the sensitivity of 83 cancer cell lines to BRD1240 and its inactive enantiomer, BRD4849, and compared it to the patterns of sensitivity measured for 479 other small molecules spanning a diverse range of known MoAs gathered as part of the NCI's Cancer Target Discovery and Development Network (39). We found that the patterns of sensitivity elicited by BRD1240 and BafA1 were highly similar, while such correlation was not observed between the inactive stereoisomer BRD4849 and BafA1 (Figure 3.3B,C). Furthermore, among the 481 compounds tested in these 83 cancer cell lines in the project, the correlation between BRD1240 and BafA1 is the strongest (Figure 3.3D). These data suggest that BRD1240 and BafA1 may share a common MoA, and that BRD1240 may inhibit lysosomal acidification by directly suppressing the activity of V-ATPase.

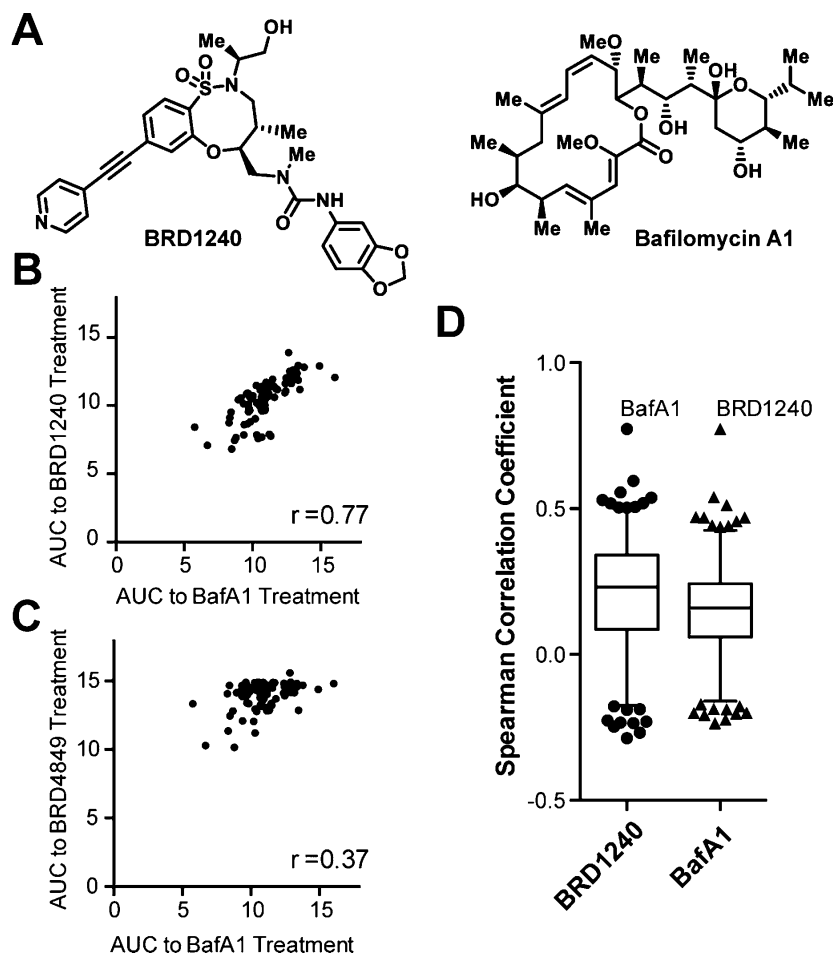


**Figure 3.3. Comparison of 481 compounds in 83 cancer cell lines reveals a significant correlation between BRD1240, but not inactive stereoisomer BRD4849, and BafA1, a potent V-ATPase inhibitor.** (A) Chemical structures of BRD1240 and BafA1. (B, C) Scatter plots presenting the AUC for each cell line in response to compound treatments.  $r$  values indicate the Spearman correlation coefficient calculated on the basis of each data plot. (D) Box and whisker plot showing the Spearman correlation coefficient between sensitivities of BRD1240 or BafA1 and the other 480 compounds tested in 83 cancer cell lines.

### 3.6 BRD1240 suppresses V-ATPase function in biochemical assays using membrane fractions

To determine whether BRD1240 perturbs lysosomal acidification by modulating V-ATPase activity, we tested its activity in a previously described *in vitro* V-ATPase activity assay using cellular membrane fractions (17) (Figure 3.4A). Both BRD1240 and BafA1 suppressed lysosomal acidification in this assay. Interestingly, the activity of BRD1240 was

dependent on pretreating the system with the compound for 1 hour, while BafA1 performed identically regardless of whether a pretreatment step was included (Figure 3.4B,C). Our results suggest that BRD1240 perturbs lysosomal acidification by suppressing V-ATPase function, but potentially by a mode of action different than that of BafA1. Additional work will be required to identify the specific protein target of BRD1240, and whether this target is among the multiple subunits of the V-ATPase complex or its accessory regulatory factors.

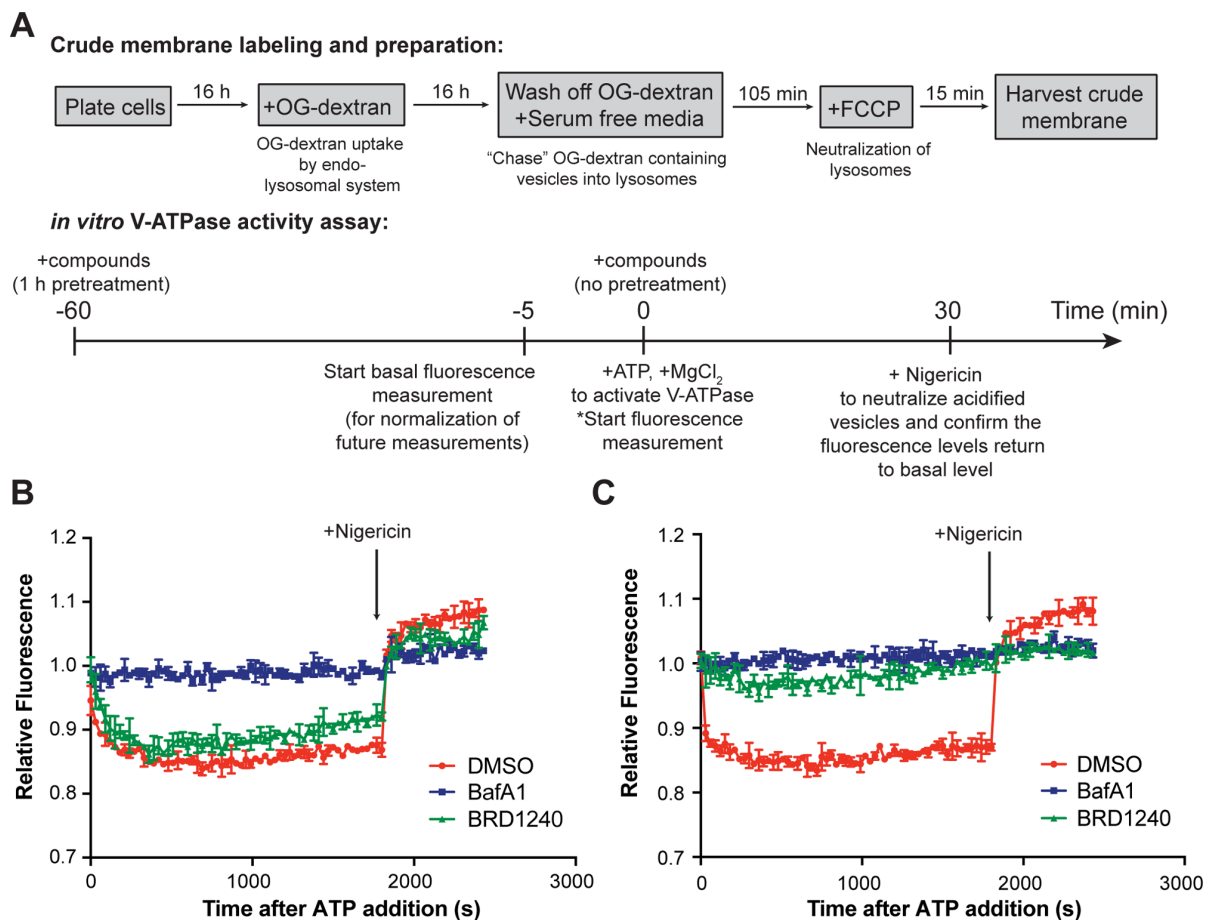


**Figure 3.4. BafA1 and BRD1240 deacidify lysosomes in an *in vitro* V-ATPase activity assay.** (A) Scheme of the assay protocol. (B) Performances of DMSO, BafA1 (100 nM), and BRD1240 (10  $\mu$ M) in the *in vitro* V-ATPase assay over 30 minutes after ATP addition and after introduction of 10  $\mu$ g/mL nigericin when no pretreatment was applied. Higher relative fluorescence values are indicative of higher pH. (C) Performances of these compounds in the assay when 1 hour pretreatment was applied. In parts B and C, representative results from three independent experiments are shown. Values are presented as the average  $\pm$  SD of two technical replicates.



### 3.7 Conclusion

Small-molecule probes have been critical to understanding the dynamic and multifunctional role of the lysosome in cellular physiology. We have identified BRD1240 as a novel small-molecule inhibitor of lysosomal acidification potentially operating via suppression of V-ATPase function. BRD1240 was derived from DOS, and its activity displays striking dependence on the stereochemistry of the ring. It promotes cell death in numerous cancer cell lines with a sensitivity profile that correlates significantly to that of the naturally occurring V-ATPase inhibitor, BafA1. These results highlight the power of DOS and HTS to yield novel, potent, and selective probes to study cellular pathways of biological and medical interest.

### 3.8 Experimental methods

**Cell lines and reagents.** HeLa, eGFP-LC3 HeLa and mCherry-eGFP-LC3 HeLa cell lines were cultured in IMDM and supplemented with 10% FBS (Corning), 1X GlutaMAX, 55  $\mu$ M  $\beta$ -mercaptoethanol, 2.5 mM NaOH and 100 U/mL penicillin/streptomycin. HEK-293T cells were cultured in DMEM with 10% FBS, 2 mM GlutaMAX and 100 U/mL penicillin/streptomycin. All cell culture reagents were purchased from Life Technologies, unless otherwise stated. PI-103 was purchased from Calbiochem. BafA1 was purchased from LC Laboratories. CQ and pepA were purchased from Sigma-Aldrich. E64d was purchased from Santa Cruz Biotechnology.

**GFP-LC3 punctae formation assay.** HeLa cells stably expressing eGFP-LC3 were plated in 384-well plates (Corning, 3712) at 2,500 cells per well in 50  $\mu$ L of IMDM. The following day, 100 nL of compounds were pin-transferred into plates using a CyBi-Well Vario (CyBio) and incubated with cells for 4 hours at 37°C. Cells were then fixed in 3.7% PFA for 15 minutes at room temperature, washed, and DNA stained with 2  $\mu$ g/mL Hoechst 33342 (Sigma B2261). High-throughput imaging at 20X was performed on an ImageXpress Micro automated microscope (Molecular Devices) using the DAPI and GFP filters. Four sites were imaged for each well with about 250-300 cells per site. The number of GFP punctae per cell was quantified using the MetaXpress high-content image analysis software (Transflour module).

For the primary screen, significant differences were assessed by computing an empirical test statistic, termed prevalence, which compares the observed distribution of punctae per cell in compound- treated cells (test hypothesis) to that of DMSO-treated cells (null hypothesis). Specifically, it is computed as the AUC of the test distribution beyond the critical value corresponding to 95% confidence of the null distribution. Prevalence is useful for assessing significance when comparing two populations that do not follow a normal distribution pattern, which is the case for punctae per cell in the GFP-LC3 assay. The concentration of the positive control (5  $\mu$ M PI-103) was selected through dose-response studies identifying the lowest concentration in the range at which PI-103 reproducibly demonstrates maximal activity (typically

5-20  $\mu\text{M}$ ) without apparent significant toxicity (Figure S3.1A and data not shown). Plates in which 5  $\mu\text{M}$  PI-103 induced a prevalence score  $\geq 0.5$  were considered well performing and included for further analysis. Z' scores were calculated for overall assay performance using prevalence scores from 32 wells of negative control (DMSO) and 32 wells of positive control (PI-103) on each plate and were typically between 0.6-0.8 for all plates screened.

To quantify the effect of hit compounds on autophagosome number in dose-response (Figure 3.1), we computed the average number of GFP punctae per cell following compound treatment (2 wells per dose point), and subtracted the average number observed for DMSO-treated cells (16 wells). These values were normalized to the background-subtracted average number of punctae per cell observed for the positive control 20  $\mu\text{M}$  PI-103 (16 wells), and plotted in Figure 3.1.

**mCherry-eGFP-LC3 assay.** HeLa cells stably expressing mCherry-eGFP-tagged LC3 were seeded overnight in 384-well plates (Corning, 3712) at 2,000 cells per well in 50  $\mu\text{L}$  of IMDM. Compounds along with in-plate controls (PI-103, CQ, and BafA1) were pin-transferred into plates and incubated at 37°C for 24 hours. Cells were then fixed in 3.7% PFA for 15 minutes at room temperature, washed, and DNA stained with 2  $\mu\text{g}/\text{mL}$  Hoechst 33342 (Sigma B2261). High-throughput imaging at 20X was performed on an ImageXpress Micro automated microscope (Molecular Devices) using the DAPI, Texas Red, and GFP filters. Four sites were imaged for each well with about 250-300 cells per site.

**Immunoblotting.** Cells were washed with PBS and lysed for 30 minutes on ice in the lysis buffer [100 mM Tris-HCl (pH=7.6), 100 mM NaCl, 1% NP-40, and Complete Mini protease inhibitor cocktail (Roche)]. Following SDS-PAGE (Mini-PROTEAN TGX Any kD gels, Bio-Rad), proteins were transferred onto PVDF membranes (Immobilon-FL, Millipore) and blocked in the Odyssey blocking buffer (LI-COR P/N 927) for 1 hour at room temperature. Membranes were subjected to overnight primary antibody incubation at 4°C and 1 hour secondary antibody incubation at room temperature, and subsequently imaged on the LI-COR infrared imaging

system. The following antibodies were used: 1:1,000  $\alpha$ -LC3B (L7543), 1:5,000  $\alpha$ -actin (A1978), from Sigma, and 1:20,000 IRDye 680LT Goat  $\alpha$ -Rabbit IgG(H+L) (P/N 926-68021) and 1:5,000 IRDye 800CW Goat  $\alpha$ -mouse IgG(H+L) (P/N 926-32210) from LI-COR Biosciences.

**LysoTracker displacement assay.** HeLa cells were seeded overnight in 384-well plates (Corning, 3712) at 2,500 cells per well in 50  $\mu$ L of IMDM. The following day, compounds were pin-transferred into plates and incubated at 37°C for 4 hours. Subsequently, 10  $\mu$ L of IMDM containing LysoTracker Red dye (Life Technologies, L7528) and Hoechst 33342 was added to bring the LysoTracker dye and Hoechst 33342 to final concentrations of 100 nM and 2  $\mu$ g/mL, respectively. After staining for 1 hour, the media in each well was replaced with PBS and the plate was immediately imaged on an ImageXpress Micro automated microscope using the DAPI and Texas Red filters. Four sites were imaged for each well with about 200-250 cells per site. MetaXpress (Transfluor module) was used to quantify the number of LysoTracker punctae per cell and average intensity of LysoTracker Red per cell.

**DQ-BSA assay.** HeLa cells were seeded overnight in 384-well plates (Corning, 3712) at 2,500 cells per well in 50  $\mu$ L of IMDM. The following day, the media was replaced with 50  $\mu$ L of IMDM containing 10  $\mu$ g/mL DQ-BSA Red dye (Life Technologies, D12051), and the cells were incubated at 37°C for 1 hour. The media was aspirated, the cells were washed with IMDM, and fresh IMDM was added. Compounds were pin-transferred into plates and incubated at 37°C for 6 hours. During the final 1 hour, 10  $\mu$ L of IMDM containing Hoechst 33342 (final concentration of 2  $\mu$ g/mL) was added. After staining for 1 hour, the media in each well was replaced with PBS and the plate was immediately imaged on an ImageXpress Micro automated microscope using the DAPI and Texas Red filters. Four sites were imaged for each well with about 200-250 cells per site. MetaXpress (Transfluor module) was used to quantify the number of DQ-BSA Red punctae per cell.

**Sensitivity profiling of 83 cancer cell lines.** Cancer cell-line sensitivity data were gathered as previously described (37, 39). Briefly, cells were plated at 500 cells per well in 1536-well plates,

allowed to adhere overnight, and treated for 72 hours with each compound at 16 different concentrations. ATP levels were measured using CellTiterGlo (Promega) as a measure of viability, and the area under the dose response curve (AUC) was determined as a metric for sensitivity. To identify compounds having similar activity as BRD1240, we computed correlation coefficients between the profiles of sensitivity measurements gathered for BRD1240 and each of 480 compounds. Spearman correlation was initially selected over Pearson correlation since it is less affected by single (or a few) extreme outlier cell line measurements and better equipped to capture the correlation across the whole cell line collection. Similar results were obtained with Pearson correlations (data not shown).

***In vitro* V-ATPase activity assay.** This assay was performed as previously described (17). Briefly, HEK293 cells from a confluent 15-cm dish were incubated overnight with 35 µg/mL Dx-OG514 (Life Technologies D-7176). The following day, cells were washed with PBS once and incubated with serum-free DMEM for 2 hours. 15 minutes prior to lysis, FCCP (Sigma) was added into the medium to a final concentration of 1 µM. Cells were scraped, pelleted and resuspended in 750 µL fractionation buffer [50 mM KCl, 90 mM K-Gluconate, 1 mM EGTA, 50 mM Sucrose, 5 mM Glucose, 20 mM HEPES (all from Sigma), Complete Mini protease inhibitor cocktail (Roche), pH=7.4] supplemented with 1 µM FCCP. Cells were broken by spraying for 7-10 times through a 25G needle, and subsequently spun down at 10,000 rpm for 15 seconds at 4°C. Afterward, the supernatant was collected and centrifuged at max speed for 20 minutes, yielding a pellet containing the organelle fraction. The pellet was resuspended in pre-warmed fractionation buffer supplemented with 1% BSA (Sigma), split into 12 aliquots, and transferred into a black 96-well plate (Corning, 3904). If compound pretreatment was applied, membranes were incubated with compounds at 37°C for 1 hour. Baseline fluorescence was measured at 530 nm upon 511 nm excitation in a Synergy H4 microplate reader (BioTek) at 30-second intervals for 5 minutes. To activate the V-ATPase, 5 mM ATP (Sigma, A1852) and 5 mM MgCl<sub>2</sub> were introduced to each well, and fluorescence reading was continued for another 25

minutes. Active V-ATPases caused lysosomal reacidification and therefore caused a decrease in fluorescence emission of OG-514 over time. At the end of the measurement, 1 µg/mL nigericin (Sigma) was added to each well to ensure the observation of rapid dissipation of the lysosomal proton gradient.

**Statistical analysis.** Dose-response curves and EC<sub>50</sub> values from the GFP-LC3 punctae formation assay were generated using the least squares fit function (four parameters), with the constraint that “top value” had to be larger than 100, in Prism 6 software (GraphPad). Spearman correlation coefficients computed to identify compounds having similar activity as BRD1240 against 83 cancer cell lines were determined using MATLAB R2013b (MathWorks).

### 3.9 Reference

1. L. N. Aldrich *et al.*, Discovery of a Small-Molecule Probe for V-ATPase Function. *J Am Chem Soc* **137**, 5563-5568 (2015).
2. V. Deretic, T. Saitoh, S. Akira, Autophagy in infection, inflammation and immunity. *Nature reviews. Immunology* **13**, 722-737 (2013).
3. W. E. Hochfeld, S. Lee, D. C. Rubinsztein, Therapeutic induction of autophagy to modulate neurodegenerative disease progression. *Acta pharmacologica Sinica* **34**, 600-604 (2013).
4. B. Levine, N. Mizushima, H. W. Virgin, Autophagy in immunity and inflammation. *Nature* **469**, 323-335 (2011).
5. E.-L. Eskelinen, Y. Tanaka, P. Saftig, At the acidic edge: emerging functions for lysosomal membrane proteins. *Trends in Cell Biology* **13**, 137-145 (2003).
6. C. Watts, The endosome-lysosome pathway and information generation in the immune system. *Biochimica et biophysica acta* **1824**, 14-21 (2012).
7. V. Marshansky, J. L. Rubinstein, G. Gruber, Eukaryotic V-ATPase: novel structural findings and functional insights. *Biochimica et biophysica acta* **1837**, 857-879 (2014).
8. A. Bhargava *et al.*, Osteopetrosis mutation R444L causes endoplasmic reticulum retention and misprocessing of vacuolar H<sup>+</sup>-ATPase a3 subunit. *The Journal of biological chemistry* **287**, 26829-26839 (2012).
9. N. Ochotny *et al.*, The V-ATPase a3 subunit mutation R740S is dominant negative and results in osteopetrosis in mice. *Journal of bone and mineral research : the official journal of the American Society for Bone and Mineral Research* **26**, 1484-1493 (2011).
10. N. Ramachandran *et al.*, VMA21 deficiency prevents vacuolar ATPase assembly and causes autophagic vacuolar myopathy. *Acta neuropathologica* **125**, 439-457 (2013).
11. D. Batlle, S. K. Haque, Genetic causes and mechanisms of distal renal tubular acidosis. *Nephrology, dialysis, transplantation : official publication of the European Dialysis and Transplant Association - European Renal Association* **27**, 3691-3704 (2012).
12. D. G. Fuster, J. Zhang, X. S. Xie, O. W. Moe, The vacuolar-ATPase B1 subunit in distal tubular acidosis: novel mutations and mechanisms for dysfunction. *Kidney international* **73**, 1151-1158 (2008).
13. R. Capparelli, D. Palumbo, M. Iannaccone, D. Iannelli, Human V-ATPase gene can protect or predispose the host to pulmonary tuberculosis. *Genes and immunity* **10**, 641-646 (2009).
14. K. Cotter *et al.*, Activity of Plasma Membrane V-ATPases is Critical for the Invasion of MDA-MB231 Breast Cancer Cells. *The Journal of biological chemistry*, (2014).

15. J. Zhou *et al.*, Immunity to the Vacuolar ATPase Complex Accessory Unit ATP6S1 in Patients with Malignant Melanoma. *Cancer immunology research* **3**, 59-67 (2015).
16. Y. Sancak *et al.*, Ragulator-Rag complex targets mTORC1 to the lysosomal surface and is necessary for its activation by amino acids. *Cell* **141**, 290-303 (2010).
17. R. Zoncu *et al.*, mTORC1 senses lysosomal amino acids through an inside-out mechanism that requires the vacuolar H(+)-ATPase. *Science* **334**, 678-683 (2011).
18. M. Laplante, D. M. Sabatini, mTOR signaling in growth control and disease. *Cell* **149**, 274-293 (2012).
19. C. Settembre *et al.*, TFEB links autophagy to lysosomal biogenesis. *Science* **332**, 1429-1433 (2011).
20. C. Settembre *et al.*, A lysosome-to-nucleus signalling mechanism senses and regulates the lysosome via mTOR and TFEB. *The EMBO journal* **31**, 1095-1108 (2012).
21. J. C. Cruz, S. Sugii, C. Yu, T. Y. Chang, Role of Niemann-Pick Type C1 Protein in Intracellular Trafficking of Low Density Lipoprotein-derived Cholesterol. *Journal of Biological Chemistry* **275**, 4013-4021 (2000).
22. R. E. Infante *et al.*, NPC2 facilitates bidirectional transfer of cholesterol between NPC1 and lipid bilayers, a step in cholesterol egress from lysosomes. *Proceedings of the National Academy of Sciences of the United States of America* **105**, 15287-15292 (2008).
23. P. Saftig, J. Klumperman, Lysosome biogenesis and lysosomal membrane proteins: trafficking meets function. *Nature reviews. Molecular cell biology* **10**, 623-635 (2009).
24. J. Kornhuber *et al.*, Identification of novel functional inhibitors of acid sphingomyelinase. *PloS one* **6**, e23852 (2011).
25. Y. P. Yang *et al.*, Application and interpretation of current autophagy inhibitors and activators. *Acta pharmacologica Sinica* **34**, 625-635 (2013).
26. T. Diyabalanage, C. D. Amsler, J. B. McClintock, B. J. Baker, Palmerolide A, a Cytotoxic Macrolide from the Antarctic Tunicate *Synoicum adareanum*. *Journal of the American Chemical Society* **128**, 5630-5631 (2006).
27. M. Huss, H. Wieczorek, Inhibitors of V-ATPases: old and new players. *The Journal of experimental biology* **212**, 341-346 (2009).
28. M. E. Fitzgerald *et al.*, Build/couple/pair strategy for the synthesis of stereochemically diverse macrolactams via head-to-tail cyclization. *ACS combinatorial science* **14**, 89-96 (2012).
29. B. Gerard *et al.*, Synthesis of a stereochemically diverse library of medium-sized lactams and sultams via S(N)Ar cycloetherification. *ACS combinatorial science* **13**, 365-374 (2011).



30. L. A. Marcaurelle *et al.*, An Aldol-Based Build/Couple/Pair Strategy for the Synthesis of Medium- and Large-Sized Rings: Discovery of Macrocyclic Histone Deacetylase Inhibitors. *Journal of the American Chemical Society* **132**, 16962-16976 (2010).
31. T. E. Nielsen, S. L. Schreiber, Towards the optimal screening collection: a synthesis strategy. *Angewandte Chemie* **47**, 48-56 (2008).
32. N. Mizushima, A. Yamamoto, M. Matsui, T. Yoshimori, Y. Ohsumi, In Vivo Analysis of Autophagy in Response to Nutrient Starvation Using Transgenic Mice Expressing a Fluorescent Autophagosome Marker. *Molecular Biology of the Cell* **15**, 1101-1111 (2004).
33. S. Kimura, T. Noda, T. Yoshimori, Dissection of the Autophagosome Maturation Process by a Novel Reporter Protein, Tandem Fluorescent-Tagged LC3. *Autophagy* **3**, 452-460 (2007).
34. B. Lemieux, M. D. Percival, J. P. Falgueyret, Quantitation of the lysosomotropic character of cationic amphiphilic drugs using the fluorescent basic amine Red DND-99. *Analytical biochemistry* **327**, 247-251 (2004).
35. C. L. Vázquez, M. I. Colombo, Chapter 6 Assays to Assess Autophagy Induction and Fusion of Autophagic Vacuoles with a Degradative Compartment, Using Monodansylcadaverine (MDC) and DQ - BSA. **452**, 85-95 (2009).
36. R. H. Shoemaker, The NCI60 human tumour cell line anticancer drug screen. *Nat Rev Cancer* **6**, 813-823 (2006).
37. D. J. Adams *et al.*, NAMPT Is the Cellular Target of STF-31-Like Small-Molecule Probes. *ACS Chemical Biology* **9**, 2247-2254 (2014).
38. M. R. Boyd *et al.*, Discovery of a Novel Antitumor Benzolactone Enamide Class That Selectively Inhibits Mammalian Vacuolar-Type (H<sup>+</sup>)-ATPases. *Journal of Pharmacology and Experimental Therapeutics* **297**, 114-120 (2001).
39. A. Basu *et al.*, An interactive resource to identify cancer genetic and lineage dependencies targeted by small molecules. *Cell* **154**, 1151-1161 (2013).

# **Chapter IV**

**Identification of Small-Molecule Modulators of Caspase-3  
Processing of ATG16L1 T300A**

## **Collaborator Contributions**

- **Dr. Geraldine Paulus** assisted in the initial assay development of AlphaLISA assay.
- **Kate Hartland, Corrie Aghia** and **Jean Santos** assisted in the generation of automation pipeline and in data management of HTS.
- **Dr. Josh Bittker** and **Dr. Benjamin Chittick** analyzed the HTS data.
- **Dr. Ryan Michael** assisted in the hit prioritization of the primary screen.

## 4.1 Introduction

Due to the progress in genome-wide association studies (GWAS), more and more risk alleles of human diseases have been identified. These risk alleles have provided good starting points for dissecting relationships between genes or particular variants of genes and the pathogenesis of diseases. Moreover, experiments can be designed to develop specific modulators of risk alleles once mechanisms underlying risk alleles are elucidated.

A coding polymorphism in the autophagic core protein ATG16L1 (rs2241880, T300A) is associated with an increased risk of developing CD (1, 2). In cell and animal models, the T300A risk variant has been linked with phenotypes that underlie the pathogenesis of CD, including elevated inflammatory cytokine secretion (3, 4), defective antibacterial autophagy in epithelial cells and dendritic cells (5-7), as well as morphological and functional defects in Paneth cells (8). In tissue samples from patients carrying the T300A risk allele, altered gut microbiota compositions were observed (9, 10), and abnormal Paneth cell phenotypes were also confirmed (11).

Mechanistic studies have revealed that ATG16L1 T300A is more susceptible to cleavage by caspase-3, which can be activated upon cellular stresses, including starvation and pathogen invasion (8, 12). The accelerated degradation of ATG16L1 T300A suggests how the polymorphism can lead to impaired selective autophagy in the context of CD. These findings have suggested possible therapeutic strategies to stabilize ATG16L1 T300A upon caspase-3 cleavage and have motivated us to find small-molecule inhibitors of ATG16L1 T300A processing. Considering the importance of caspase-3 in cellular processes, such as apoptosis, we aim to identify small molecules that disrupt the protein–protein interaction of ATG16L1 and caspase-3, which should enhance the stability of ATG16L1 without interfering caspase-3 activity. A similar approach was taken to study amyloid precursor protein (APP) processing by secretases, and a set of small molecules was successfully identified that protected APP from secretase cleavage without disrupting secretase activity (13).

To identify small molecules that specifically inhibit caspase-3 processing, an *in vitro* caspase-3 cleavage assay with ATG16L1 T300A as the substrate is suitable. The amount of remaining full-length ATG16L1 can be used as a surrogate for the level of ATG16L1 cleaved by caspase-3. Theoretically, in full-length protein molecules, the distance between N- and C-termini of protein is small enough so the presence of full-length proteins can yield signals in assays using technologies that measure proximity. AlphaLISA is one of such technologies that, in this case, uses donor beads and acceptor beads binding peptide tags on the C- and N-termini of the protein, respectively. Excitation of the donor bead triggers the release of singlet oxygen, which in turn stimulates the emission of light from the acceptor beads binding the other end of protein. Cleavage of ATG16L1 T300A will result in the separation of N- and C-termini of proteins and consequently a decrease in the signal. (Figure 4.1)

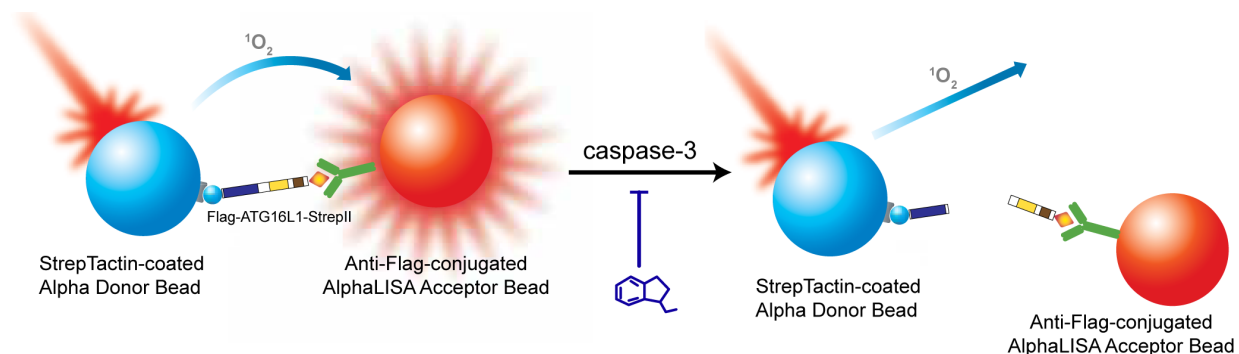


**Figure 4.1. Principle of measuring ATG16L1 processing by caspase-3 using AlphaLISA technology.** Level of full-length ATG16L1 with N-terminal FLAG-tag and C-terminal StrepII-tag can be measured with AlphaLISA acceptor beads conjugated with anti-FLAG antibodies and donor beads coated with *StrepTactin*. Cleavage of ATG16L1 by caspase-3 results in a decrease in AlphaLISA signal as the N- and C-terminus of the protein are not in proximity anymore. Small molecules that suppress the cleavage of ATG16L1 can rescue the decrease in AlphaLISA signal.

Ideally, ATG16L1 T300A with peptide tags on both ends can be produced in *E. coli* or other protein expression systems. However, the purification of full-length ATG16L1 in prokaryotic systems was reported to be challenging by Parkhouse et al. (14) and our colleagues (data not shown). Given the amount of time needed for optimizing systems other than *E. coli* to produce large quantity of ATG16L1, I propose using lysates from ATG16L1 deficient HeLa cells

stably reconstituted with dual-tagged ATG16L1 T300A. Active caspase-3 will be added directly to cell lysates and the amount of full-length ATG16L1 T300A in lysates after caspase-3 cleavage will be measured by the AlphaLISA system.

Here, I present my efforts toward the identification of small-molecule probes that suppress ATG16L1 T300A degradation by caspase-3. An assay using cell lysates containing ATG16L1 T300A and recombinant active caspase-3 was developed and 20,876 small molecules were tested. The activities of 3 small molecules were confirmed in-dose. One small molecule, BRD5064, was particularly potent. Plans of future studies for dissecting the mechanism of BRD5064 and for studying its functions in cellular systems are included in the end of this chapter.

## **4.2 Validation of a knockout-reconstitution system expressing ATG16L1 T300A in HeLa cells**

First, I validated that ATG16L1 variants with peptide tags on the N-terminus (FLAG) and C-terminus (StrepII) were functionally adequate as compared to endogenous ATG16L1 variants. ATG16L1 deficient HeLa cells were stably reconstituted with FLAG- and StrepII-tagged wild type, T300A or D299E ATG16L1 variants (hereafter, dual-tagged-WT, T300A or D299E HeLa cells, respectively). D299E is a variant insensitive to caspase-3 cleavage caused by the mutation at the caspase-3 recognition site (15). Reconstitution with any of ATG16L1 variants could rescue the basal autophagic flux, as indicated by the presence of LC3-I to LC3-II conversion (Figure 4.2). Dual-tagged ATG16L1 variants also retained their characteristics in sensitivity to caspase-3 in cells or in lysates. When intracellular caspase-3 was activated by staurosporine (STA) treatment (16), dual-tagged-T300A were more susceptible to caspase-3 cleavage as indicated by a decrease in the level of full-length protein and a concurrent increase in the level of N-terminal fragment, while dual-tagged WT ATG16L1 is less susceptible and

dual-tagged D299E ATG16L1 is insensitive (Figure 4.3A). Similar results were observed with lysates of HeLa cells expressing dual-tagged ATG16L1 variants treated with active human caspase-3 (Figure 4.3B). Altogether, these evidences supported that dual-tagged-ATG16L1 performed as endogenous ATG16L1, and thus I could use lysates from these reconstituted HeLa cell lines for the screening assay.

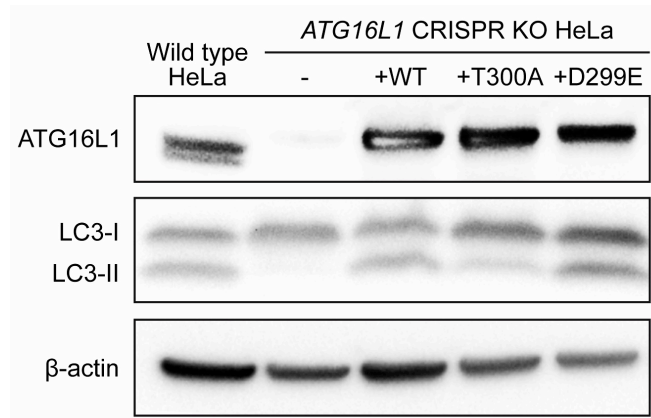


**Figure 4.2. Reconstitution of dual-tagged ATG16L1 variants rescued autophagy flux in ATG16L1 CRISPR knockout cells.** Lysates of HeLa cell lines were harvested for immunoblotting.

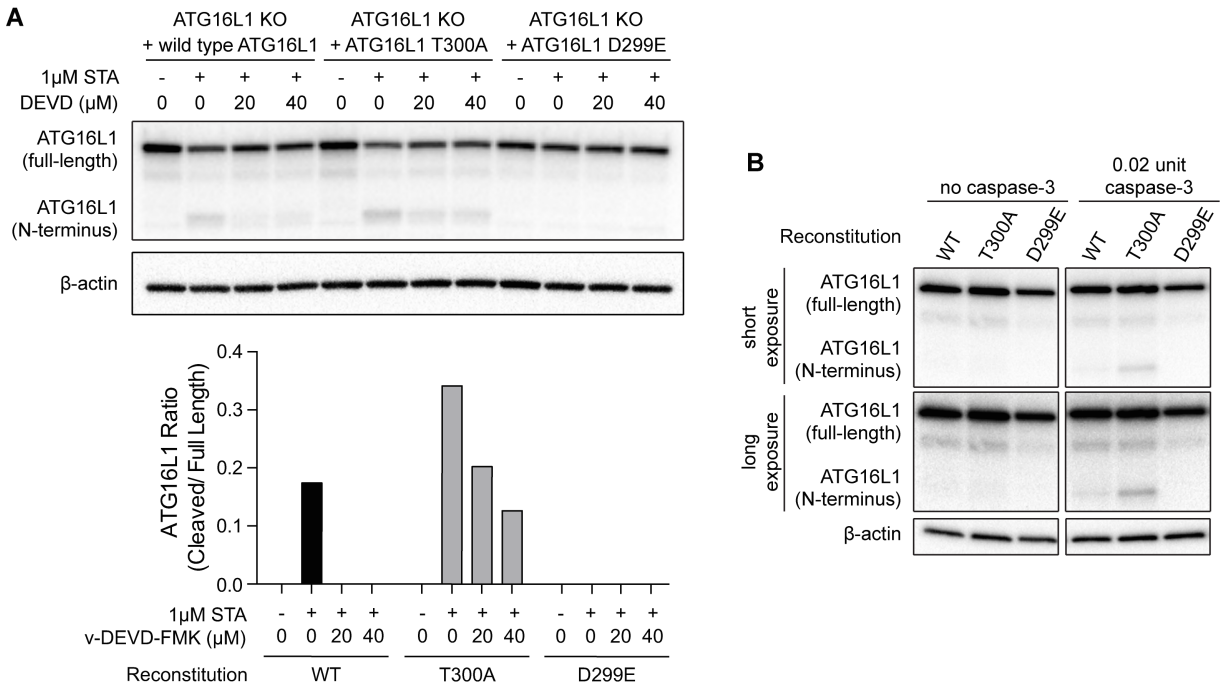


**Figure 4.3. Dual-tagged ATG16L1 T300A is more susceptible to caspase-3 cleavage.** (A) HeLa cells were pretreated with DMSO or z-DEVD-FMK for 1 hour and further treated with DMSO or 1 $\mu$ M STA for 3.5 hours. Cell lysates were then harvested for immunoblotting. (B) Lysates of HeLa cell lines were incubated with or without active human caspase-3 in lysis buffer supplemented with 10 mM DTT at 25°C for 45 minutes and the subjected for immunoblotting.

### 4.3 Development of the AlphaLISA assay for assessing the level of full-length ATG16L1 protein

When incubated with AlphaLISA donor beads and acceptor beads binding StrepII- and FLAG-tags, respectively, full-length T300A ATG16L1 in lysates of dual-tagged-T300A HeLa cells could elicit a robust and dose-dependent increase in the AlphaLISA signal (Figure 4.4). Lysate concentrations of up to 100,000 cells per well were tested (Figure S4.1A); however, I was not able to observe a “hook point”, a drop of AlphaLISA signal commonly observed when the binding capacity of beads is saturated. The lack of hook point might indicate that a higher concentration of ATG16L1 protein was necessary to saturate the bead binding capacity, or the dimeric nature of ATG16L1 (17) could also play a role in this observation. To ensure a robust



detection but also to avoid artifacts from using high concentrations of cell lysates, lysates of 15,000 cells per well were used for subsequent experiments.

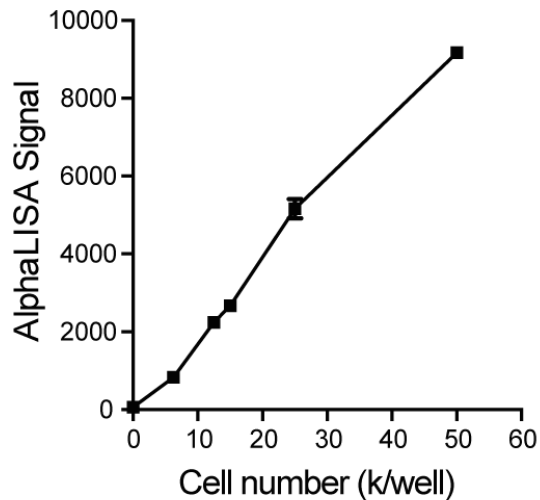


**Figure 4.4. Measurement of level of full-length ATG16L1 T300A in the AlphaLISA assay.** Cell lysates of HeLa cells stably expressing dual-tagged ATG16L1 T300A were plated at various concentrations. Levels of full-length ATG16L1 were measured by AlphaLISA. Data are presented as mean  $\pm$  SD,  $n = 2$ . All data are representative of multiple independent experiments.

The caspase-3 cleavage assay with lysates from dual-tagged-T300A HeLa cells was developed and AlphaLISA technology was implemented to measure levels of full-length dual-tagged ATG16L1 in the 384-well plate format. Incubating lysates with active human caspase-3 resulted in a decrease in AlphaLISA signal, which could be rescued when caspase-3 activity was suppressed by its inhibitor, z-DEVD-FMK (Figure 4.5A). Consistent with previous study (8) and results obtained in the immunoblotting-based assay (Figure 4.3B), dual-tagged wild type ATG16L1 was more resistant than dual-tagged-ATG16L1 T300A, and dual-tagged ATG16L1 D299E was completely insensitive to caspase-3 processing in the same assay (Figure 4.5B). These results indicated that the caspase-3 cleavage reaction with dual-tagged-ATG16L1 variants could be performed in a miniaturized format in 384-well plates, and AlphaLISA technology could be utilized to measure the level of full-length dual-tagged-ATG16L1 in the condition of the miniaturized caspase-3 cleavage assay. Therefore, the caspase-3 cleavage

assay with AlphaLISA technology was suitable for screening for small molecules that protect ATG16L1 T300A from caspase-3 processing.

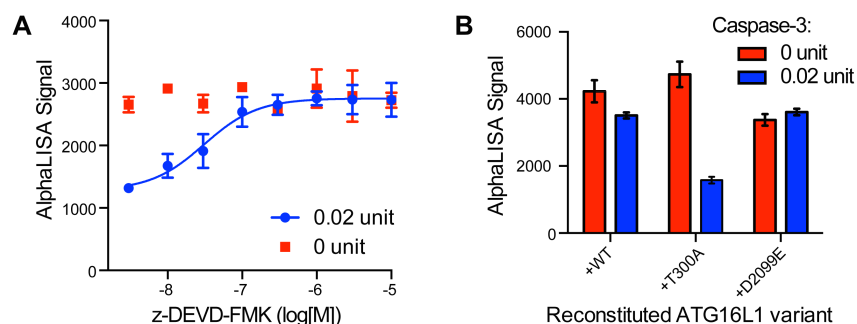


**Figure 4.5 Measurement of ATG16L1 processing by caspase-3 in the AlphaLISA assay.** (A) Cell lysates were incubated with z-DEVD-FMK in-dose and then incubated with caspase-3 (0.02 unit) or vehicle control. (B) HeLa cells stably expressing dual-tagged WT ATG16L1, T300A or D299E were incubated with caspase-3 (0.02 unit) or vehicle control. In both parts, levels of full-length ATG16L1 were measured by AlphaLISA. Data are presented as mean  $\pm$  SD,  $n = 3$ . All data are representative of multiple independent experiments.

I then tested the robustness of the system for high-throughput small-molecule screen. A key component was to understand the kinetics of the reaction, so I could ensure that effects of small molecules were measured when the caspase-3 cleavage reaction was within the linear range. The enzymatic reaction curve of caspase-3 cleavage at 25°C indicated that the reaction was still within the linear range and had reached about 50% cleavage, providing a good dynamic range at 20 minutes after initiation (Figure 4.6A). The stability of reagents was also an important factor in the robustness of the system for HTS, as reagents were usually needed to be prepared in advance and the operation time of each HTS experiment was longer due to larger numbers of samples. In this regard, I tested the stability of the substrate, dual-tagged ATG16L1 T300A, and the enzyme, caspase-3 under the screening conditions to account for any artifact that might be introduced by the non-specific degradation of components in the assay. Results indicated that both the substrate and the enzyme were stable for up to 60 minutes, longer than the estimated operation time needed for the assay (Figure 4.6B and C). Overall, these data indicated that the system was compatible with high-throughput small-molecule screen, as we

were able to robustly capture the time point optimal for testing activities of small molecules, and the stability of the substrate and the enzyme was proven adequate during the time period needed for the operation of our HTS assays.

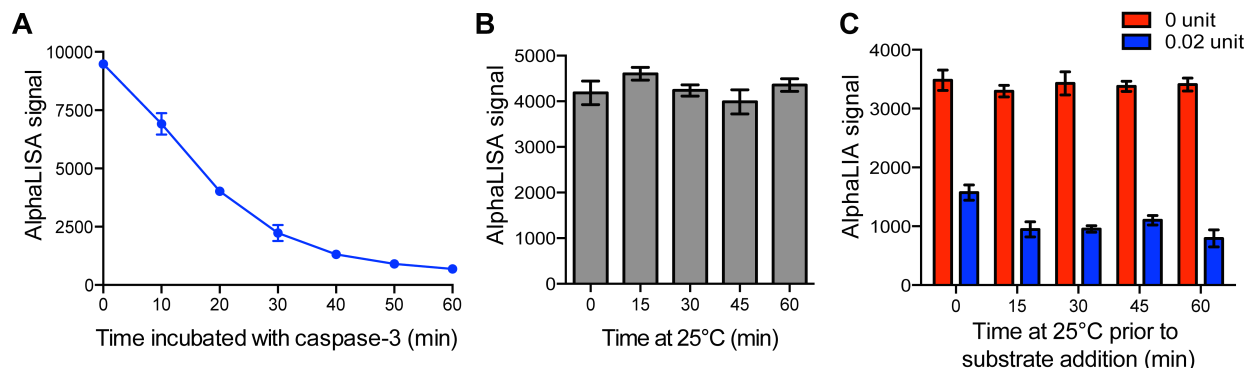


**Figure 4.6. Kinetics of ATG16L1 processing by caspase-3 and the stability of reagents.** (A) Cell lysates of HeLa cells stably expressing dual-tagged ATG16L1 T300A were incubated with caspase-3 (0.02 unit) for various periods of time. (B) Cell lysates were incubate at 25°C for various periods of time. (C) Caspase-3 (0.02 unit) or vehicle control was incubated at 25°C for various periods of time and then incubated with cell lysates. In all parts, levels of full length ATG16L1 were measured by AlphaLISA. Data are presented as mean  $\pm$  SD,  $n = 3$ . All data are representative of multiple independent experiments.

#### 4.4 Primary screening of 20,876 compounds and confirmation of hits in dose in the AlphaLISA assay

20,876 commercially available small molecules were tested in the AlphaLISA assay in duplicates with automated systems. These small molecules were selected to compose a collection of maximized diversity in chemical structures among commercially available small molecules. The primary screen was divided into 5 batches, and caspase-3 incubation time was optimized for each batch to ensure that 50% cleavage was achieved in DMSO-treated lysates and the enzymatic reaction was within linear range (Supplementary Methods). In two out of five batches, two plates with positive controls in-dose were included, one at the beginning and the other at the end of each experiment, for quality control. Data from these positive control plates suggested that the reproducibility within a batch or across separate batches was acceptable

(Figure 4.7). When we examined the data, positional effects that affected AlphaLISA signal levels were observed, resulting in higher signals at the center of each plate. In two out of five batches, artifacts that were likely caused by clogging of tubing systems in the liquid dispensing instruments were observed (Supplementary Methods). All of these effects were taken into account during data processing. Although positional effects and artifacts could be removed to some extents, these effects still resulted in some noises and high signal outliers with low reproducibility across duplicates (Figure S4.2).

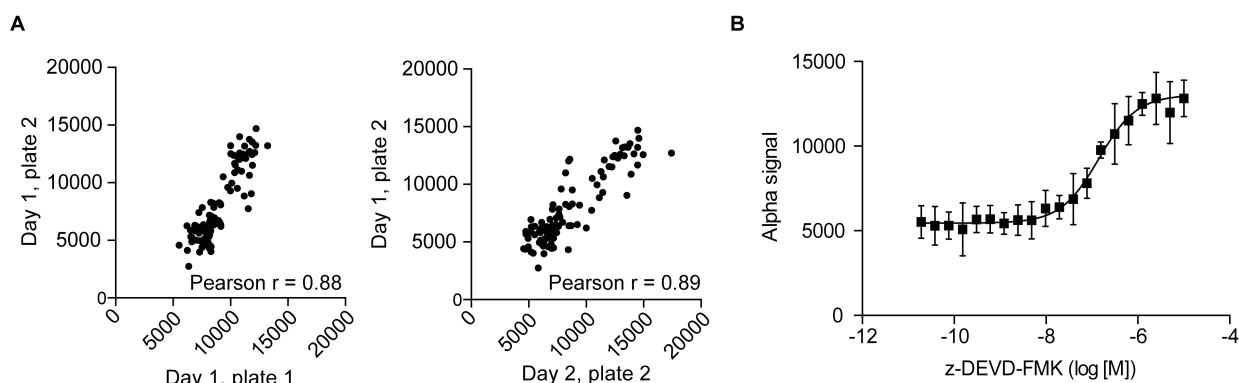


**Figure 4.7. Performance of the positive control, z-DEVD-FMK, in the primary screen.** Plates containing 5 replicates of z-DEVD-FMK in-dose were tested in two separate batches in the primary screen. (A) Performance of z-DEVD-FMK on two plates tested on the same day and on two plates tested on separate days were examined and plotted. (B) Dose curve of z-DEVD-FMK on one representative plate were plotted. Data are presented as mean  $\pm$  SD,  $n = 5$ .

Considering the presence of outliers, two strategies were applied for hit calling. The first approach was based on Bayesian statistics and considered both the potency and the reproducibility of compounds (18). We prioritized 119 compounds that had  $p$  values smaller than 0.05 based on the Bayesian statistics, and had percent effects larger than 15%. In parallel, the other approach utilized the robust Z scores of each compound, which indicated its activity in inducing an increase in the signal compared to DMSO-treated wells. Only the average robust Z score of each compound, but not the reproducibility of Z scores among replicates, was taken into account. This case, compounds that only had one replicate showing high activity could also be prioritized. We prioritized 98 compounds that had average robust Z scores larger than 3.20

out of these 98 compounds also met the Bayesian criteria. Among these 197 compounds, 7 compounds might have characteristics of 'pan assay interference compounds' (PAINS), assessed computationally by published criteria (19).

All 197 compounds were retested in-dose in the AlphaLISA assay. The activity of one compound, BRD5064, was confirmed as it elicited a robust and dose-response effect (Figure 4.8). Two additional compounds showed weak effects (Figure S4.3). None of these compounds had characteristics of PAINS based on the computational analysis. Whether these compounds would have any pan assay interference characteristic in the *in vitro* or cellular systems of our interest would still need to be experimentally validated.

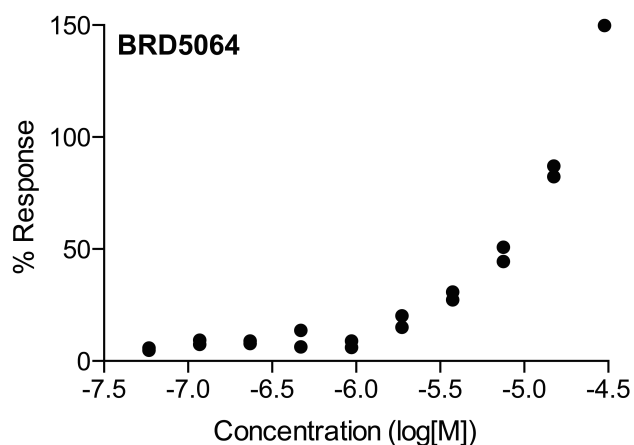


**Figure 4.8. BRD5064 elicited a dose-dependent rescue of signals in the AlphaLISA assay.** BRD5064 was tested in-dose in duplicate in the automated AlphaLISA assay. The values of % response were calculated as following: the average value of Alpha signal of in-plate neutral control wells was subtracted from the value of each well, and then the subtracted value was normalized to the average Alpha signal of in-plate positive control wells.

## 4.5 Conclusion and future directions

Here I present the development of a high-throughput assay for the identification of small molecules that protect the CD risk allele ATG16L1 T300A from caspase-3 cleavage, a mechanism underlying the functional consequence of ATG16L1 T300A. With this assay, 3 hits were identified among 20,876 compounds and one of them, BRD5064, was particularly potent.

Future experiments are needed to study if these small molecules protect ATG16L1 by specifically disrupting the interaction between ATG16L1 and caspase-3 or by broadly inhibit caspase-3 activity. To identify small-molecule hits that emerge from the screen as caspase-3 inhibitors, secondary assays will be implemented to measure effects of these hits on caspase-3 activity for processing substrates other than ATG16L1. Although small-molecule inhibitors of caspase-3 can be useful probes to study caspase-3 activation by CD-related cellular stresses, caspase-3 inhibitors emerging from our screen are not likely to have comparable selectivity and potency compared with previously published caspase-3 inhibitors, which have been optimized with medicinal chemistry efforts (20). For this reason, further experiments will not be conducted to investigate and optimize small-molecule caspase-3 inhibitors emerging from this screen.

It is possible that small-molecule hits identified in an *in vitro* assay with cell lysates will not perform similarly in living cells. Small-molecule hits may not be able to diffuse or be transported across the cell membrane, or may be metabolized by other enzymes in cells. To ensure small-molecule hits are active in cells before testing them in CD-relevant assays, these hits will be tested in cellular systems. The assay will rely on activating caspase-3 in cells carrying ATG16L1 T300A, and then measure the level of full-length ATG16L1 T300A by AlphaLISA or Western blot. If these hits are not active in cells, chemical optimization can be attempted to improve the solubility and stability of hits.

Hits will be selected based on their performance in secondary assays and will be tested in cellular assays in ATG16L1 T300A background to examine if they can alleviate CD phenotypes. Small molecules identified in my studies will not only be potential probes for CD therapeutics, but will also be made available to the research community as tools for studying the contribution of a common polymorphism, ATG16L1 T300A, in the context of a complex diseases that can be affected by various genetic and environmental factors.

## 4.6 Experiment methods

**Cell lines and reagents.** HeLa cell lines were cultured in IMDM supplemented with 10% FBS (Sigma Aldrich), 1X GlutaMAX, 55  $\mu$ M  $\beta$ -mercaptoethanol, 2.5 mM NaOH, and 100 U/mL penicillin/streptomycin (Invitrogen). HEK293T cells were cultured in Dulbecco's Modified Eagle Medium supplemented with 10% FBS and 1X GlutaMAX. Reagents are obtained from the following suppliers: active human caspase-3 full length protein (abcam), STA, z-DEVD-FKM, z-VAD-FMK and caspase-3/7 inhibitor I (ApeXBio), dithiothreitol (DTT), NSCI, Pefabloc SC, Aprotinin (Sigma-Aldrich).

**Lentivirus preparation.** HEK293T cells were seeded in 6-well tissue culture plates at 500,000 cells per well. The following day, FuGENE HD (Promega) was premixed with OPTI-MEM (Invitrogen) and the following plasmids: 1  $\mu$ g pCMV-dR8.91, 100 ng pCMV-VSV-G and 1  $\mu$ g dual-tagged ATG16L1 (isoform 1; wild type, T300A or D299E) inserted in modified lenti CSGW vector. Plasmid mixtures were added into each well followed by 18-hour incubation. Media were then removed and replaced with fresh growth media. 48 hours later, media containing lentivirus were harvested and sterile filtered. Aliquots of virus were stored at  $-80^{\circ}\text{C}$ .

**Lentiviral transduction.** ATG16L1 CRISPR KO HeLa cells (21) were seeded in 6-well tissue culture plates at 15,000 cells per well. The following day, lentivirus containing each dual-tagged ATG16L1 variant was added to cells. 48 hours later, media were removed and replaced with fresh IMDM containing 4  $\mu$ g/mL blasticidin (InvivoGen). Cells were passaged and cultured in IMDM containing 4  $\mu$ g/mL blasticidin.

**Immunoblotting.** Cells were washed with PBS and lysed for 30 minutes in standard lysis buffer [25 mM Tris-HCl pH 7.6, 0.5% NP-40, 150 mM NaCl, 1mM EDTA and Complete EDTA-free Protease Inhibiter Cocktail (Roche)] on ice. Following SDS-PAGE (TGX Any kD gels, Bio-Rad), proteins were transferred onto PVDF membranes (Immobilon-P, Millipore). For blotting for ATG16L1, membranes were blocked overnight at  $4^{\circ}\text{C}$  in 10% blotting-grade blocker (Bio-rad) in PBS. The next day, membranes were subjected to primary antibody (anti-ATG16L mAb, MBL,

M150-3, 1:1,000) incubation for 3 hours at room temperature and secondary antibody (HRP-linked anti-mouse IgG, Cell Signaling, #7076, 1:5,000) incubation for 1 hour at room temperature. Both primary and secondary antibodies were diluted in 1% blotting-grade blocker in PBS. For all other proteins, membranes were blocked in Odyssey blocking buffer (LI-COR, P/N 927) for 1 hour at room temperature. Membranes were then subjected to overnight primary antibody incubation (anti-LC3B, Sigma Aldrich, L7543, 1:1,000; anti- $\beta$ -actin, Cell Signaling, #4970, 1:5,000) at 4°C and 1 hour secondary antibody (HRP-linked anti-rabbit IgG, Cell Signaling, #7074, 1:5,000) incubation at room temperature. Primary antibodies were diluted in Odyssey blocking buffer. Secondary antibody was diluted in 0.5x Odyssey blocking buffer in PBS. Afterward, membranes visualized with SuperSignal West Pico Chemiluminescent Substrate (Thermo Scientific) supplemented with 10% SuperSignal West Femto Chemiluminescent Substrate (Thermo Scientific). Densitometry analyses on immunoblots were performed by Image Lab™ Software (Bio-rad).

**AlphaLISA assay.** Lysates of dual-tagged T300A HeLa cells were prepared at 3,000 cells per  $\mu$ L (if not indicated otherwise) in lysis buffer (25 mM Tris-HCl pH 7.6, 0.5% NP-40, 150 mM NaCl, 1 mM EDTA, 1 mM Pefabloc SC, 10  $\mu$ g/mL Aprotinin) supplemented with 10 mM DTT. If compound treatment was applied, compounds were mix with lysates to desired concentrations. Caspase-3 was diluted to 0.004 units per  $\mu$ L (if not indicated otherwise) in lysis buffer supplemented with 10 mM DTT, and then incubated at 25°C for 15 minutes. Strep-Tactin Alpha donor beads (PerkinElmer, AS106), anti-FLAG AlphaLISA acceptor beads (PerkinElmer, AL112) and z-DEVD-FMK were diluted in PBS supplemented with 0.1% BSA to the final concentration of 60  $\mu$ g/mL, 15  $\mu$ g/mL and 30  $\mu$ M, respectively. 5  $\mu$ L of lysates and 5  $\mu$ L caspase-3 were dispensed into each well of AlphaLISA plates (PerkinElmer, 6008350) and incubated for 20 minutes. 5  $\mu$ L beads were then distributed into each well, followed by an 1-hour incubation at room temperature. Plates were read on Wallac Envision plate reader (PerkinElmer) with “AlphaScreen” protocol.



**HTS.** Reagents containing lysate, caspase-3 and beads were prepared as described in the previous section. Assay plates were prepared by the Compound Management team of the Broad Institute. Positive control, neutral control and compounds were plated into AlphaLISA plates beforehand and stored at -20°C before experiments were conducted. For primary screen, compounds were tested at 10 µM. For confirmation screen, compounds were tested with 10-point dose with 2-fold dilution starting with 30 µM. 5 µL of lysates were dispensed into each well by combi followed by 15 minutes incubation at room temperature. 5 µL of caspase-3 were then dispensed into each well by combi and incubated at 25°C. The length of incubation time is experimentally optimized for each experiment. 5 µL of beads were then added into each well by combi, protected from light and incubated for 1 hour at room temperature. Plates were read on Wallac Envision plate reader with “HTS AlphaScreen” protocol.

**Statistical analysis.** Dose-response curves from the AlphaLISA assay were generated using the least squares fit function (four parameters) in Prism 6 software (GraphPad). Pearson correlation coefficients in Figure 4.7 were determined using the built-in analysis in Prism 6.

## 4.7 References

1. J. Hampe *et al.*, A genome-wide association scan of nonsynonymous SNPs identifies a susceptibility variant for Crohn disease in ATG16L1. *Nat Genet* **39**, 207-211 (2007).
2. J. D. Rioux *et al.*, Genome-wide association study identifies new susceptibility loci for Crohn disease and implicates autophagy in disease pathogenesis. *Nat Genet* **39**, 596-604 (2007).
3. T. S. Plantinga *et al.*, Crohn's disease-associated ATG16L1 polymorphism modulates pro-inflammatory cytokine responses selectively upon activation of NOD2. *Gut* **60**, 1229-1235 (2011).
4. M. Salem, O. H. Nielsen, K. Nys, S. Yazdanyar, J. B. Seidelin, Impact of T300A Variant of ATG16L1 on Antibacterial Response, Risk of Culture Positive Infections, and Clinical Course of Crohn's Disease. *Clin Transl Gastroenterol* **6**, e122 (2015).
5. R. Cooney *et al.*, NOD2 stimulation induces autophagy in dendritic cells influencing bacterial handling and antigen presentation. *Nat Med* **16**, 90-97 (2010).
6. C. R. Homer, A. L. Richmond, N. A. Rebert, J. P. Achkar, C. McDonald, ATG16L1 and NOD2 interact in an autophagy-dependent antibacterial pathway implicated in Crohn's disease pathogenesis. *Gastroenterology* **139**, 1630-1641, 1641 e1631-1632 (2010).
7. P. Kuballa, A. Huett, J. D. Rioux, M. J. Daly, R. J. Xavier, Impaired autophagy of an intracellular pathogen induced by a Crohn's disease associated ATG16L1 variant. *PLoS One* **3**, e3391 (2008).
8. K. G. Lassen *et al.*, Atg16L1 T300A variant decreases selective autophagy resulting in altered cytokine signaling and decreased antibacterial defense. *Proc Natl Acad Sci U S A* **111**, 7741-7746 (2014).
9. D. N. Frank *et al.*, Disease phenotype and genotype are associated with shifts in intestinal-associated microbiota in inflammatory bowel diseases. *Inflamm Bowel Dis* **17**, 179-184 (2011).
10. M. Sadaghian Sadabad *et al.*, The ATG16L1-T300A allele impairs clearance of pathosymbionts in the inflamed ileal mucosa of Crohn's disease patients. *Gut* **64**, 1546-1552 (2015).
11. K. Cadwell *et al.*, A key role for autophagy and the autophagy gene Atg16l1 in mouse and human intestinal Paneth cells. *Nature* **456**, 259-263 (2008).
12. A. Murthy *et al.*, A Crohn's disease variant in Atg16l1 enhances its degradation by caspase 3. *Nature* **506**, 456-462 (2014).
13. A. S. Espeseth *et al.*, Compounds that bind APP and inhibit Abeta processing in vitro suggest a novel approach to Alzheimer disease therapeutics. *The Journal of biological chemistry* **280**, 17792-17797 (2005).

14. R. Parkhouse, I. O. Ebong, C. V. Robinson, T. P. Monie, The N-terminal region of the human autophagy protein ATG16L1 contains a domain that folds into a helical structure consistent with formation of a coiled-coil. *PloS one* **8**, e76237 (2013).
15. H. R. Stennicke, M. Renatus, M. Meldal, G. S. Salvesen, Internally quenched fluorescent peptide substrates disclose the subsite preferences of human caspases 1, 3, 6, 7 and 8. *Biochemical Journal* **350**, 563-568 (2000).
16. E. López, I. Ferrer, Staurosporine- and H-7-induced cell death in SH-SY5Y neuroblastoma cells is associated with caspase-2 and caspase-3 activation, but not with activation of the FAS/FAS-L-caspase-8 signaling pathway. *Molecular Brain Research* **85**, 61-67 (2000).
17. N. Fujita *et al.*, Differential involvement of Atg16L1 in Crohn disease and canonical autophagy: analysis of the organization of the Atg16L1 complex in fibroblasts. *J Biol Chem* **284**, 32602-32609 (2009).
18. J. K. Kruschke, Bayesian estimation supersedes the *t* test. *Journal of Experimental Psychology: General* **142**, 573-603 (2013).
19. J. B. Baell, G. A. Holloway, New Substructure Filters for Removal of Pan Assay Interference Compounds (PAINS) from Screening Libraries and for Their Exclusion in Bioassays. *Journal of Medicinal Chemistry* **53**, 2719-2740 (2010).
20. M. Poreba *et al.*, Small Molecule Active Site Directed Tools for Studying Human Caspases. *Chem Rev* **115**, 12546-12629 (2015).
21. S.-Y. Kuo *et al.*, Small-molecule enhancers of autophagy modulate cellular disease phenotypes suggested by human genetics. *Proceedings of the National Academy of Sciences* **112**, E4281-E4287 (2015).

# **Chapter V**

## **Summary and Discussion**

## 5.1 Summary of research presented

This thesis presents efforts to discover small-molecule modulators of autophagy, and to utilize a subset of autophagy activators to study the effects of autophagy enhancements in the context of human diseases. In **Chapter II**, I describe our efforts to conduct a phenotypic-based screen for small-molecule modulators of autophagy. In collaboration with colleagues, we then developed assays to evaluate the toxicity of modulators emerging from the screen and their effects on autophagic flux. By systematically examining the chemical structures and potencies of 59,541 small molecules tested, we identified chemical moieties that enriched among hits in the primary screen and prioritized 5 representative hits containing combinations of different moieties. We confirmed that these prioritized small-molecule autophagy modulators do not act via disrupting lysosomal functions or via suppressing mTOR kinase activity. We tested prioritized hits in various disease-relevant cellular assays. These assays were selected since autophagy was known to facilitate the clearance of pathogenic agents (huntingtin aggregates and invasive *Salmonella*) or defective autophagy was suggested to underlie the pathogenesis of diseases (NPC1 and Crohn's disease). One small molecule, BRD5631, was able to alleviate disease phenotypes in all disease-relevant cellular assays tested. These observations suggest that the enhancement of autophagy can serve as a therapeutic strategy for human diseases related to autophagy. Future efforts are needed to elucidate the MoA of BRD5631, which will provide more insights in the roles of autophagy in disease models of our interests.

In **Chapter III**, I describe the characterization of BRD1240, a novel small-molecule disruptor of lysosomal functions. BRD1240 emerged as one of strongest hits of the primary screen. This indicated that the GFP-LC3 punctae formation based primary assay was capable of identifying both enhancers and inhibitors of autophagy flux, and highlighted the importance of implementing secondary assays to distinguish between enhancers and inhibitors of autophagic flux. The activity of BRD1240 was highly dependent on the stereochemistry of its core structure, which supported that the activity of BRD1240 was dependent on specific interactions between

the small molecule and its targets. We utilized an unbiased strategy of bioactivity profiling and identified that BRD1240 and a known V-ATPase inhibitor, BafA1, shared highly similar bioactivity profiles in killing cancer cell lines. Consequently, we hypothesized that BRD1240 disrupted lysosomal functions by suppressing the activity of V-ATPase. I then adapted an assay using lysosome-containing membrane fractions to validate that BRD1240 suppressed lysosomal acidification by disrupting V-ATPase function. Further studies are needed to identify the molecular target of BRD1240.

In cases that molecular mechanisms of disease pathogenesis are understood, target-based screening approach can be a powerful way to find small molecules that directly modulate disease-relevant biological targets. In **Chapter IV**, I present a disciplined plan to identify small molecules that directly target one common risk allele of CD, ATG16L1 T300A. Mechanistic studies have shown that ATG16L1 T300A is more susceptible to caspase-3 cleavage, which is accounted for compromised autophagy and selective autophagy underlying CD pathogenesis. I developed a biochemical assay using active recombinant caspase-3 and HeLa cell lysates containing ATG16L1 T300A. Applying the assay in a HTS, I identified small molecules that protect ATG16L1 T300A from caspase-3 cleavage. Future experiments are needed to study if these small molecules are pan inhibitors of caspase-3 activity, or can specifically disrupt the interaction between ATG16L1 T300A and caspase-3. It is also important to confirm that these small molecules can retain similar activity in cells and can therefore rescue phenotypes related to compromised autophagy in the context of CD.

## 5.2 Discussion and future directions

Small molecules emerging from our screens can serve not only as prototypes of pharmaceuticals, but also as probes for studying biological mechanisms. Small-molecule probes are widely used in life sciences researches, and in many cases can provide modulations that are challenging to be achieved by genetic tools. For instance, treatments with small-molecule probes can be easily applied conditionally or reversibly (1). In **Chapter II**, I present that probes such as BRD5631 and other autophagy enhancers can be utilized for studying autophagy enhancement in the context of various human diseases. Small-molecule probes enabled us to easily enhance autophagy in each cellular disease model, which is more challenging to achieve by genetically modifying each model. Additionally, in assays measuring the targeting and clearance of *Salmonella*, small-molecule probes enabled flexible treatment protocols such as variable pretreatment times before bacterial invasion. Further dissecting the MoA of these small molecules may reveal previously unidentified regulatory pathways of autophagy. Small-molecule probes emerging from targeted screens, such as probes targeting ATG16L1 T300A described in **Chapter IV**, can be used as chemical genetic tools to study functions of the risk allele in different contexts. Small-molecule probes, as well as the flexibility they can provide, are particularly valuable for studying complex diseases that are regulated by gene—gene and gene—environment interactions, such as CD (2). For example, gene—gene interaction of NOD2 and ATG16L1 risk alleles for the incidence of CD was observed in population-based studies (3). Modulation of ATG16L1 T300A in the cell or animal models carrying NOD2 risk allele could help to further dissect relationships between these risk alleles.

For small molecules emerging from phenotypic screens, such as BRD5631 and BRD1240, understanding the molecular targets of compounds of interests is critical for future medicinal chemistry efforts for probe optimization and drug discovery. Advanced technologies in genomics and proteomics have enabled a broad panel of experimental strategies that assist biologists to achieve more effective target identification processes. Depending on the prior

knowledge of the small molecules of interests, different methods should be applied. For BRD5631, efforts have already been initiated to examine its effects on transcription profiles of HeLa cells by RNA sequencing. The transcription profile elicited by BRD5631 cannot only provide insights on effects of the compound in an unbiased manner. Also, comparing transcription profiles induced by BRD5631 to a set of reference profiles for compounds with known mechanisms can be useful to reveal insights into MoA of BRD5631. On the contrary, BRD1240 has distinctive SAR based on its stereochemistry, which provides essential knowledge for derivatizing BRD1240 for affinity chromatography and mass spectrometry based methods [e.g. SILAC (4) or iTRAQ (5)]. Additionally, the inactive enantiomer of BRD1240 can serve as an optimal negative control in the experimental design of affinity chromatography. As BRD1240 is toxic to many cancer cell lines (6), resistance mutation selection is also a viable approach for target identification. Once mutated clones that are resistant to BRD1240 are generated, subsequent whole genome or exome sequencing can be applied to reveal the mutated molecular targets that underlie the resistance (7, 8).

Encouraged by the beneficial effects of autophagy modulation in contexts of diseases, many autophagy modulators are currently under investigations in clinical trials (9, 10). In the majority of trials, applications of chloroquine and hydroxychloroquine in cancer treatments are evaluated. A few other FDA approved drugs are utilized as autophagy inducers for neurodegenerative conditions, for example, Tamoxifen in amyotrophic lateral sclerosis and Rilmenidine in Huntington's disease (11, 12). Many other FDA-approved drugs and over-the-counter drugs are proven to stimulate autophagy and consequently elicit favorable effects in disease-related experimental systems (13). However, most of them have pleiotropic MoAs, and the concentration required to modulate autophagy in physiological conditions may not be safely achievable (14). These factors complicate the applications of currently available drugs as autophagy modulators for disease treatments. Furthermore, autophagy enhancement itself may have complicated effects in certain disease-relevant conditions. For instance, some invasive



bacteria, such as *Coxiella burnetii* and *Yersinia pseudotuberculosis*, can hijack autophagy machinery for growth by simultaneously inducing autophagy and blocking autophagosome fusion with the autolysosome (15-17). These bacteria can then use autophagosomes as a microenvironment for their growth. For *Salmonella*, a recent study has suggested that autophagy proteins can promote the repair of damaged SCV and thus affect particular populations of *Salmonella* (18). It is unclear what effects will be cast on the intracellular proliferation of these bacteria by autophagy enhancement, and if enhancing autophagy via different mechanisms will have different effects. Small molecules that modulate autophagy through a wide range of MoA are needed for future studies aiming to answer these questions, and can provide more candidate probes that can achieve efficacious and safe autophagy modulation for therapeutics.

### 5.3 References

1. C. J. O'Connor, L. Laraia, D. R. Spring, Chemical genetics. *Chem Soc Rev* **40**, 4332-4345 (2011).
2. J. Van Limbergen, G. Radford-Smith, J. Satsangi, Advances in IBD genetics. *Nat Rev Gastroenterol Hepatol* **11**, 372-385 (2014).
3. T. Okazaki *et al.*, Contributions of IBD5, IL23R, ATG16L1, and NOD2 to Crohn's disease risk in a population-based case-control study: evidence of gene-gene interactions. *Inflamm Bowel Dis* **14**, 1528-1541 (2008).
4. S. E. Ong *et al.*, Identifying the proteins to which small-molecule probes and drugs bind in cells. *Proc Natl Acad Sci U S A* **106**, 4617-4622 (2009).
5. I. P. Shadforth, T. P. Dunkley, K. S. Lilley, C. Bessant, i-Tracker: for quantitative proteomics using iTRAQ. *BMC Genomics* **6**, 145 (2005).
6. L. N. Aldrich *et al.*, Discovery of a Small-Molecule Probe for V-ATPase Function. *J Am Chem Soc* **137**, 5563-5568 (2015).
7. D. J. Adams *et al.*, NAMPT Is the Cellular Target of STF-31-Like Small-Molecule Probes. *ACS Chemical Biology* **9**, 2247-2254 (2014).
8. S. A. Wacker, B. R. Houghtaling, O. Elemento, T. M. Kapoor, Using transcriptome sequencing to identify mechanisms of drug action and resistance. *Nat Chem Biol* **8**, 235-237 (2012).
9. Y. Cheng, X. Ren, W. N. Hait, J. M. Yang, Therapeutic targeting of autophagy in disease: biology and pharmacology. *Pharmacol Rev* **65**, 1162-1197 (2013).
10. G. Kroemer, Autophagy: a druggable process that is deregulated in aging and human disease. *J Clin Invest* **125**, 1-4 (2015).
11. R. A. Frake, T. Ricketts, F. M. Menzies, D. C. Rubinsztein, Autophagy and neurodegeneration. *J Clin Invest* **125**, 65-74 (2015).
12. Taipei Medical University Shuang Ho Hospital. The Study of Tamoxifen Treatment in Patients With Motor Neuron Disease. In ClinicalTrials.gov [Internet]. Bethesda (MD): National Library of Medicine (US). 2000- [cited 2016 Apr 22]. Available from: <http://clinicaltrials.gov/show/NCT02166944> NLM Identifier: NCT02166944.
13. D. C. Rubinsztein, P. Codogno, B. Levine, Autophagy modulation as a potential therapeutic target for diverse diseases. *Nat Rev Drug Discov* **11**, 709-730 (2012).
14. H. Vakifahmetoglu-Norberg, H. G. Xia, J. Yuan, Pharmacologic agents targeting autophagy. *J Clin Invest* **125**, 5-13 (2015).
15. M. G. Gutierrez *et al.*, Autophagy induction favours the generation and maturation of the Coxiella-replicative vacuoles. *Cell Microbiol* **7**, 981-993 (2005).

16. K. Moreau *et al.*, Autophagosomes can support *Yersinia pseudotuberculosis* replication in macrophages. *Cell Microbiol* **12**, 1108-1123 (2010).
17. P. S. Romano, M. G. Gutierrez, W. Beron, M. Rabinovitch, M. I. Colombo, The autophagic pathway is actively modulated by phase II *Coxiella burnetii* to efficiently replicate in the host cell. *Cell Microbiol* **9**, 891-909 (2007).
18. S. Kreibich *et al.*, Autophagy Proteins Promote Repair of Endosomal Membranes Damaged by the Salmonella Type Three Secretion System 1. *Cell Host Microbe* **18**, 527-537 (2015).

# **Appendix A**

**Supplementary Materials for Chapter II**

## Supplementary Figures

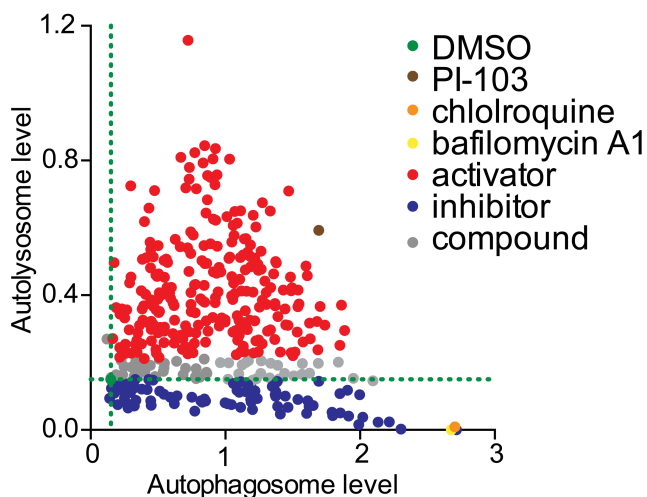
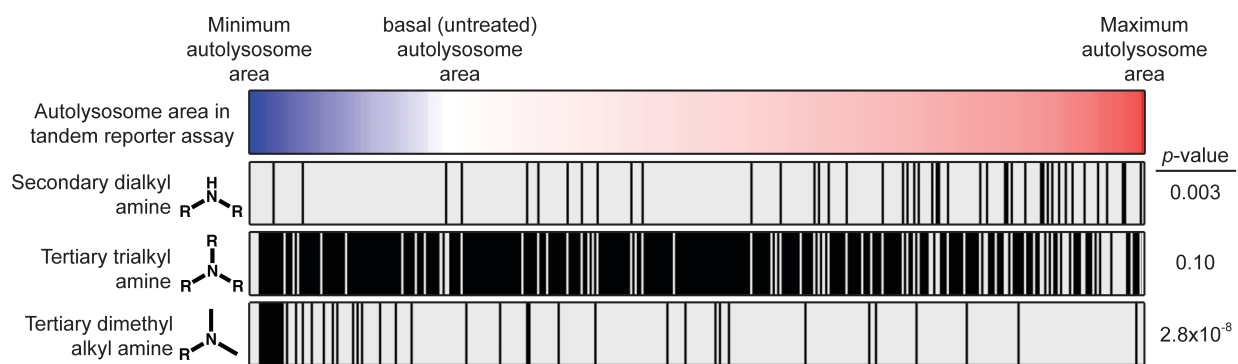


**Figure S2.1. DOS compounds have various effects on autophagic flux.** HeLa cells stably expressing mCherry-GFP-LC3 were treated with DOS compounds in 4-point dose (20, 10, 5, 2.5  $\mu$ M) for 24 hours. Cells were then fixed and stained with Hoechst 33342. Autophagosome and autolysosome punctae areas were quantified by fluorescence microscopy and automated image analysis. Prevalence values for autophagosomes and autolysosomes of each well were computed as described in Materials and Methods section. For each type of punctae induced by treatment of each compound, prevalence values of the lower three dose points were summed and plotted.

**Table S2.1. DOS compounds were classified into different categories and the hit rate of each category is calculated.**

Compound class	Compound #	Hit #	Hit rate
All compounds	59539	1987	3.3%
Compounds containing alkyl amine	22342	1770	7.9%
Compounds containing one the following lipophilic groups <b>and</b> alkyl amine:			
Diphenyl alkyne	152	92	60.5%
Biphenyl	736	193	26.2%
Compounds containing one the following lipophilic groups and <b>no</b> alkyl amine:			
Diphenyl alkyne	357	1	0.2%
Biphenyl	797	4	0.5%



Black lines represent compounds having indicated structural feature.

**Figure S2.2. Chemical moieties are enriched among hits that induce autolysosome formation.** 400 DOS compounds were ranked based on their activities in modulating autolysosome areas. Compounds with specific structural features are highlighted. The  $p$  values were calculated using hypergeometric distribution.

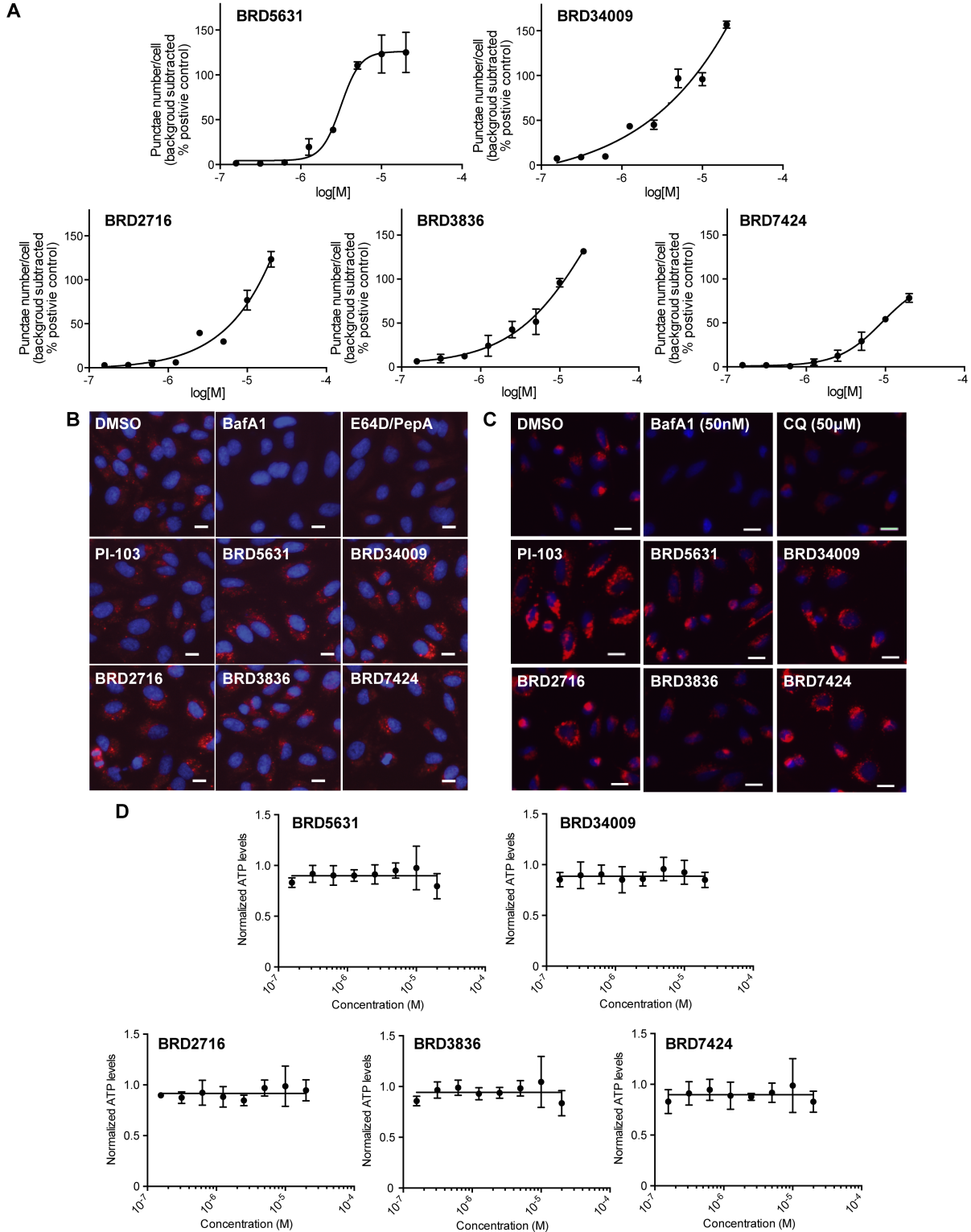


**Figure S2.3. DOS compounds induce autophagosome formation without perturbing lysosomal functions and without significant toxicity.** (A) HeLa cells stably expressing GFP-LC3 were treated with compounds in 8-point dose for 4 hours, after which cells were fixed and stained with Hoechst 33342 and punctae number was quantified by fluorescence microscopy and automated image analysis.

**Figure S2.3.** (Continued) Dose curves were generated using “log(agonist) vs. response – variable slope” model in Prism 6. Data points of dose curves are presented as the mean  $\pm$  SD,  $n = 3$  from a representative experiment. (B) HeLa cells were pulsed with DQ-BSA (10  $\mu\text{g}/\text{mL}$ ) for 1 hour followed by a 6-hour chase with the indicated compound. In the last 30 minutes, nuclei were stained with Hoechst 33342, and number and intensity of DQ-BSA punctae were quantified in live cells by fluorescence microscopy and automated image analysis. Representative images are shown. Scale bars represent 10  $\mu\text{m}$ . (C) HeLa cells were treated with compounds for 4 hours, then stained with LysoTracker Red dye (100 nM) and Hoechst 33342 for 1 hour. Number and intensity of LysoTracker Red punctae were quantified in live cells by fluorescence microscopy and automated image analysis. Representative images are shown. Scale bars represent 10  $\mu\text{m}$ . (D) HeLa cells were treated with compounds in 8-point dose for 72 hours, after which cell viability was assessed by measuring cellular ATP levels using CellTiter-Glo reagent. ATP levels were normalized to DMSO. Dose curves were generated using “log(agonist) vs. normalized response” model in Prism 6. Data are presented as the mean  $\pm$  SD,  $n = 2$  from three independent experiments.

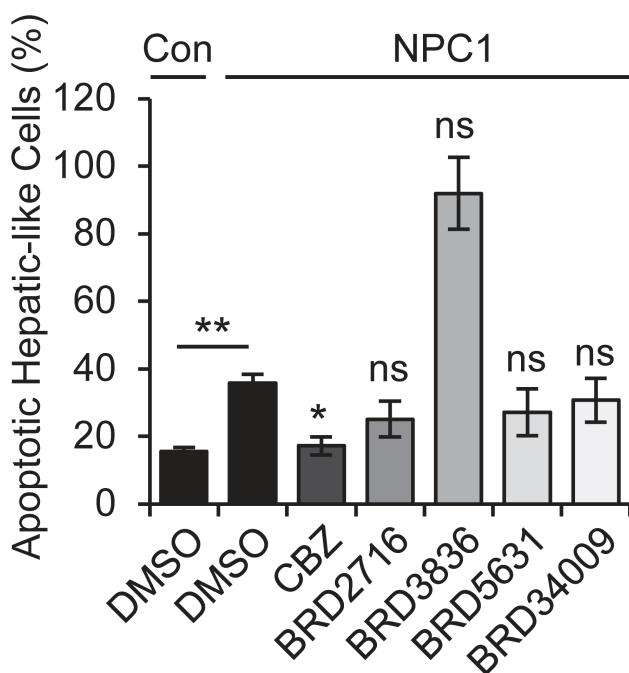


**Figure S2.4. DOS compounds do not significantly rescue cell death in hepatic-like cells.** Control (WIBR3-derived) hepatic-like cells were treated with DMSO (vehicle control), and NPC1 hiPSC (WIBR-IPS-NPC1)-derived hepatic-like cells were treated with DMSO, BRD2716, BRD3836, BRD5631, BRD34009 (10  $\mu\text{M}$  each), or CBZ (100  $\mu\text{M}$ , positive control) for 3 days. The FITC Annexin V Apoptosis Detection Kit I by FACS was used to quantify the percentage of apoptotic cells. Results are presented as mean  $\pm$  SD and are representative of two independent experiments performed in multiple replicates. \* $P < 0.05$ ; \*\* $P < 0.01$ ; ns = not significant, compared to DMSO-treated NPC1 cells unless indicated otherwise, unpaired Student  $t$  test.



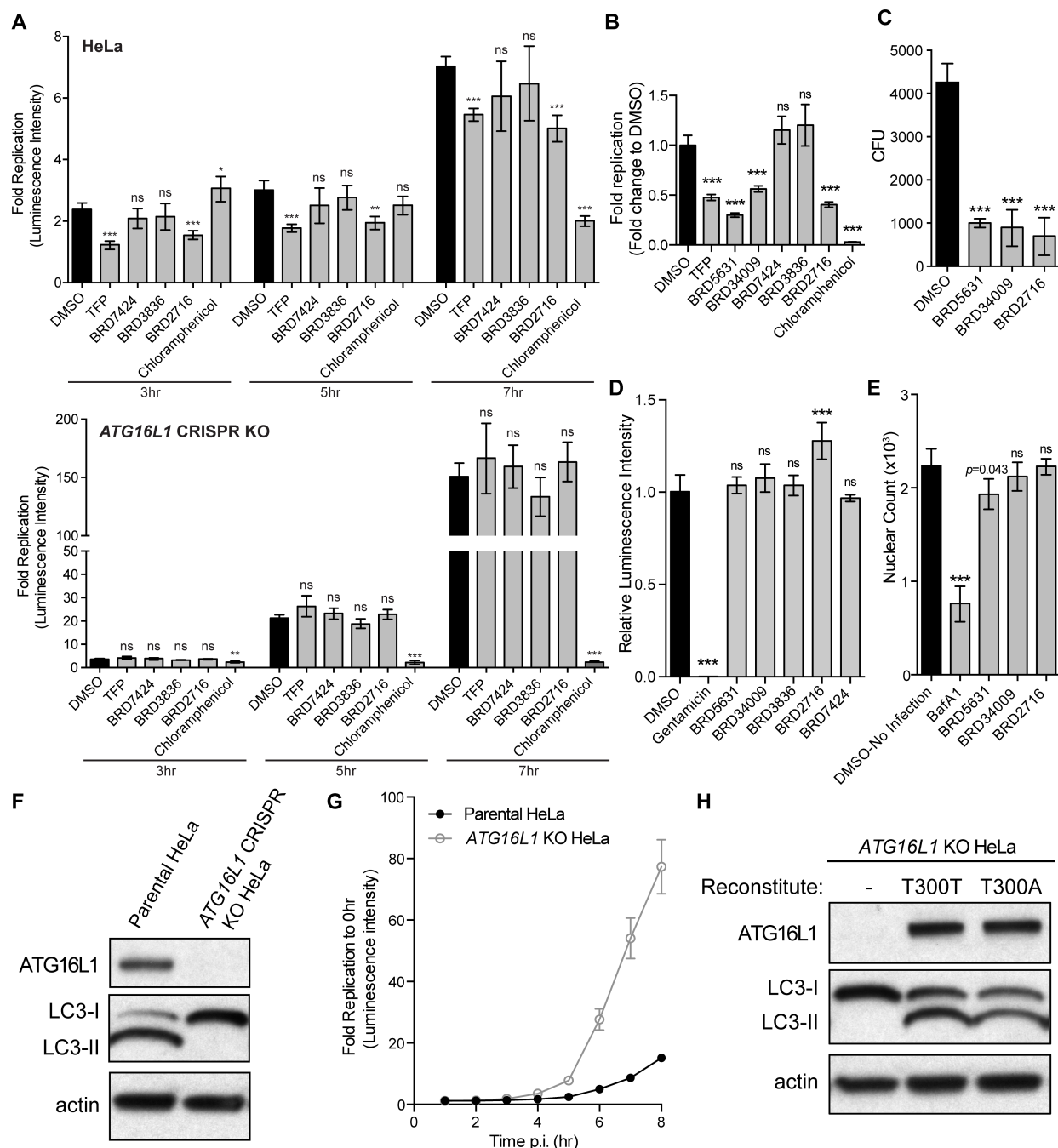


**Figure S2.5. A subset of DOS compounds promotes *Salmonella* clearance in an autophagy-dependent manner.** (A-B) *Salmonella* survival in cells was assessed in a bioluminescent bacterial replication assay. *Salmonella* luminescent units in live cells were measured at indicated time points in panel A, or at 20-hour p.i. in panel B. Fold replication value was calculated for each well as raw luminescence value at each time point divided by the value at 1-hour p.i. Data are presented as mean  $\pm$  SD,  $n=4$  from a representative experiment. (C) HeLa cells were infected and washed as above. Cells were then incubated with compounds for 20 hours before being lysed. Lysates were plated on LB plates containing kanamycin. Colonies were scored after an overnight incubation. Data are presented as mean  $\pm$  SD,  $n=4$  from a representative experiment.

**Figure S2.5.** (Continued) (D) Xen26 *Salmonella* were incubated with compounds (DMSO, BRD5631, BRD34009, BRD2716, BRD3836, BRD7424 at 10  $\mu$ M; gentamicin at 10  $\mu$ g/mL) in mammalian cell growth medium for 12 hours and luminescence intensity was measured. Data are presented as mean  $\pm$  SD, n =4 from a representative experiment. (E) HeLa cells were infected with DsRed *Salmonella* Typhimurium for 20 minutes. Cells were then washed and incubated with compounds (DMSO, BRD5631, BRD34009, or BRD2716 at 10  $\mu$ M; BafA1 at 200 nM). After 20 hours, cells were fixed and stained with Hoechst 33342 and the nuclei were counted by fluorescence microscopy. Data are presented as mean  $\pm$  SD, n = 4 from a representative experiment. (F) and (H) Cells were subject to immunoblot analysis with anti-ATG16L1, anti-LC3, and anti- $\beta$ -actin antibodies. (G) *Salmonella* survival in parental HeLa or ATG16L1 CRISPR KO cells was assessed in a bioluminescent bacterial replication assay. *Salmonella* luminescent units in live cells were measured at indicated time points. Fold replication value was calculated as described above. Data are presented as mean  $\pm$  SD, n = 4 from a representative experiment. Unpaired Student *t* test was conducted to compare each compound to DMSO at each time point. \**P* < 0.05; \*\**P* < 0.01; \*\*\**P* < 0.001; ns = not significant.

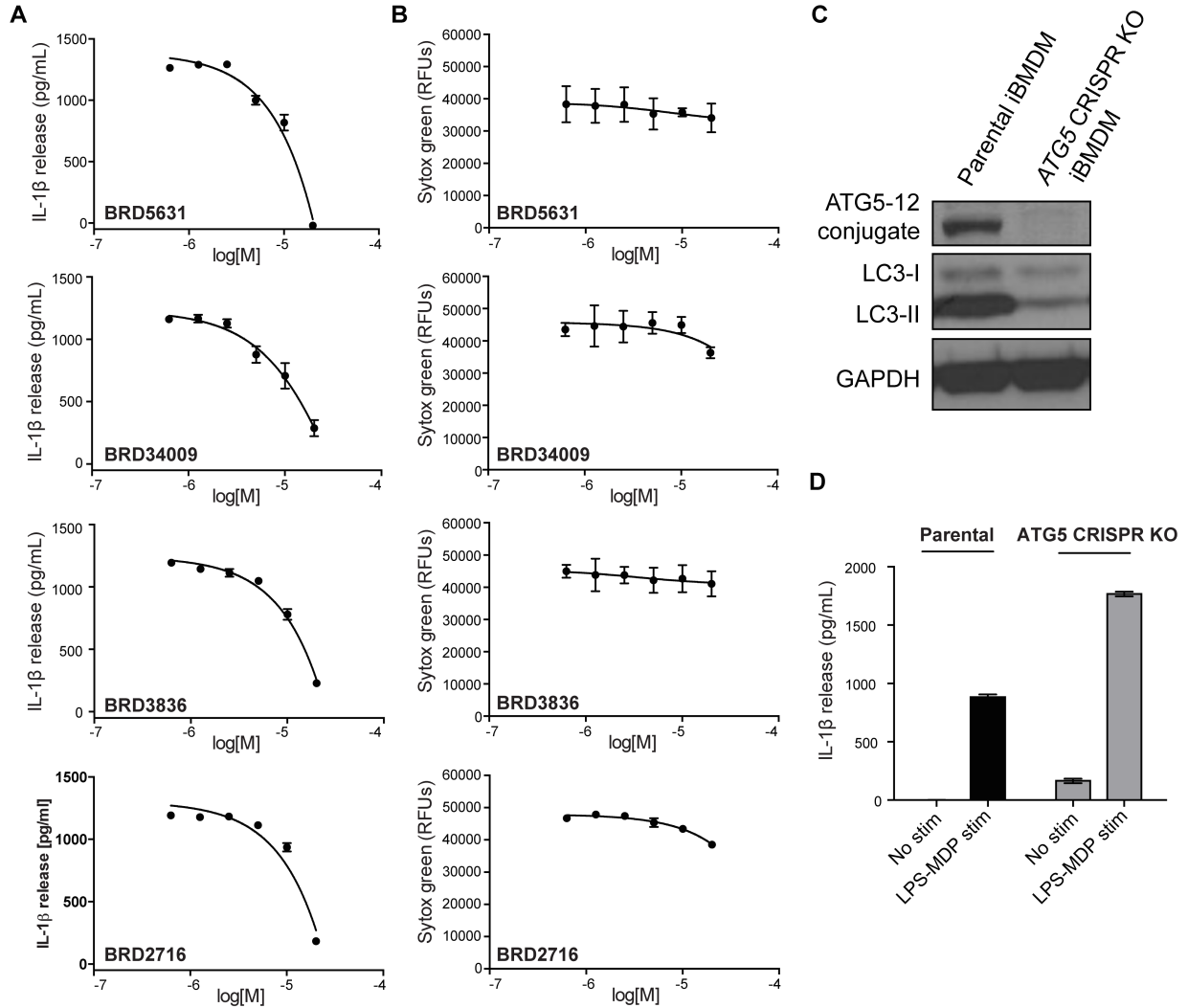


**Figure S2.6. Autophagy modulators suppress IL-1 $\beta$  secretion in an autophagy-dependent manner.** (A) IL-1 $\beta$  secretion was measured in murine iBMDMs primed with IFN $\gamma$  (100 ng/mL) for 16 hours and then stimulated with LPS (10 ng/mL)-MDP (10  $\mu$ g/mL) for 24 hours, both in the presence of compounds. The amount of IL-1 $\beta$  released into supernatants was assessed by ELISA. Data are presented as mean  $\pm$  SD, n = 3 from a representative experiment. Dose curves were generated using “log(inhibitor) vs. response” model in Prism 6. (B) iBMDMs were primed, stimulated, and treated with compound as indicated above. After supernatants were removed, cell viability in each well was assessed using SYTOX Green Nucleic Acid Stain following the manufacturer’s protocol. Data are presented as mean  $\pm$  SD, n = 3 from the same representative experiment in panel A. Dose curves were generated using “log(inhibitor) vs. response” model in Prism 6. (C) Wild type and *Atg5* CRISPR KO iBMDMs were subject to immunoblot analysis with anti-ATG5, anti-LC3 and anti-GAPDH antibodies. (D) Wild type and *Atg5* CRISPR KO iBMDMs were primed with IFN $\gamma$  (100 ng/mL) for 16 hours and stimulated with LPS (10 ng/mL)-MDP (10  $\mu$ g/mL) for 24 hours. The amount of IL-1 $\beta$  released into supernatants was measured by ELISA. Data are presented as mean  $\pm$  SD, n = 3 from a representative experiment.

**Table S2.2.** Antibodies used for immunoblotting.

<b>Antibody</b>	<b>Cell type</b>	<b>Vendor</b>	<b>Category number</b>	<b>Dilution</b>
<b>Primary</b>				
ATG16L1	HeLa	Cell Signaling	8089	1:1,000
ATG5	iBMDM	Novus Biologicals	NB110-53818	1:1,000
GAPDH	iBMDM	Cell Signaling	5174	1:5,000
GAPDH	ihESC-derived neuronal cells	Santa Cruz Biotechnology	sc-47724	1:5,000
LC3B	HeLa and iBMDM	Sigma Aldrich	L7543	1:1,000
LC3B	MEF	Novus Biologicals	NB100-2220	1:4,000
p62	ihESC-derived neuronal cells	BD Biosciences	610832	1:1,000
p62	MEF	Progen Biotechnik	GP62-C	1:1,000
p70 S6K1	HeLa	Cell Signaling	2708	1:1,000
phospho-p70 S6K1	HeLa	Cell Signaling	9205	1:1,000
phospho-ULK1	HeLa	Cell Signaling	6888	1:500
ULK1	HeLa	Cell Signaling	8054	1:500
$\beta$ actin	HeLa	Sigma Aldrich	A1978	1:5,000
$\beta$ actin	MEF	Sigma Aldrich	A2066	1:4,000
<b>Secondary</b>				
Guinea pig IgG (H+L)-HRP	MEF	Abcam	ab50210	1:10,000
Mouse IgG (H+L)-HRP	ihESC derived neuronal cells	EMD Biosciences	401253	1:10,000
Mouse IgG (H+L)-IRDye 800CW	HeLa	LI-COR Biosciences	926-32210	1:5,000
Mouse Immunoglobulins-HRP	HeLa (in Fig. 2D)	Dako	P0447	1:5,000
Rabbit IgG (H+L)-HRP	MEF	EMD Biosciences	401393	1:10,000
Rabbit IgG (H+L)-IRDye 680LT	HeLa	LI-COR Biosciences	926-68021	1:20,000
Rabbit Immunoglobulins-HRP	HeLa, iBMDM	Dako	P0448	1:5,000

*Page left intentionally blank*

# **Appendix B**

**Supplementary Materials for Chapter III**

## Supplementary Figures

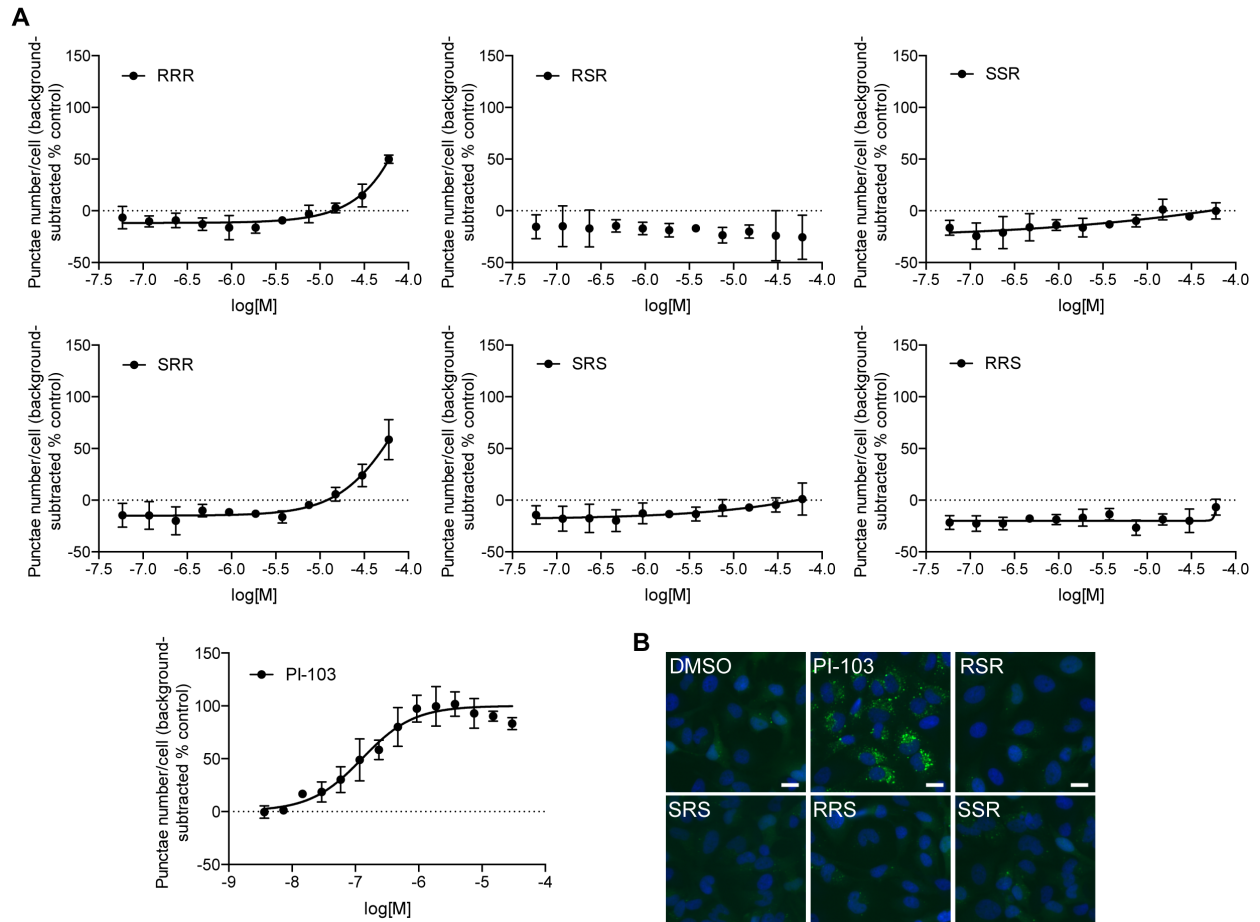
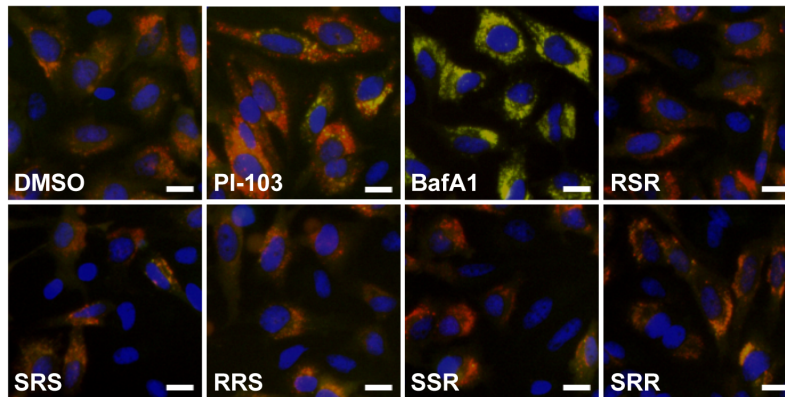
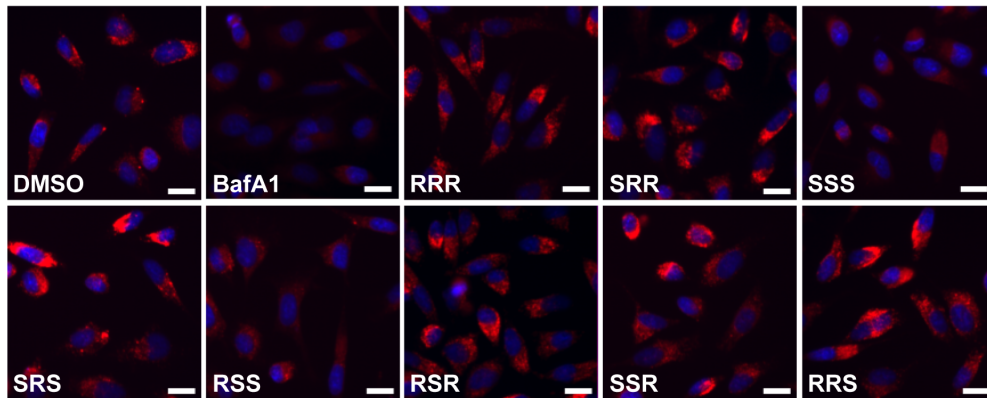


**Figure S3.1.** (A) Dose-response curves of BRD5091 (RSR), BRD6590 (SRS), BRD8122 (RRS), BRD8433 (SSR), BRD4849 (RRR) and BRD2595 (SRR), and PI-103 in the GFP-LC3 punctae formation assay. Values are presented as average  $\pm$  SD, generated from three independent experiments run in duplicates. (B) Representative images from the GFP-LC3 punctae formation assay following treatment with DMSO, PI-103 (5  $\mu$ M), RSR, SRS, RRS, and SSR (all 20  $\mu$ M). Blue (Hoechst 33342), Green (eGFP). Scalar bars represent 10  $\mu$ m.

A



B



C

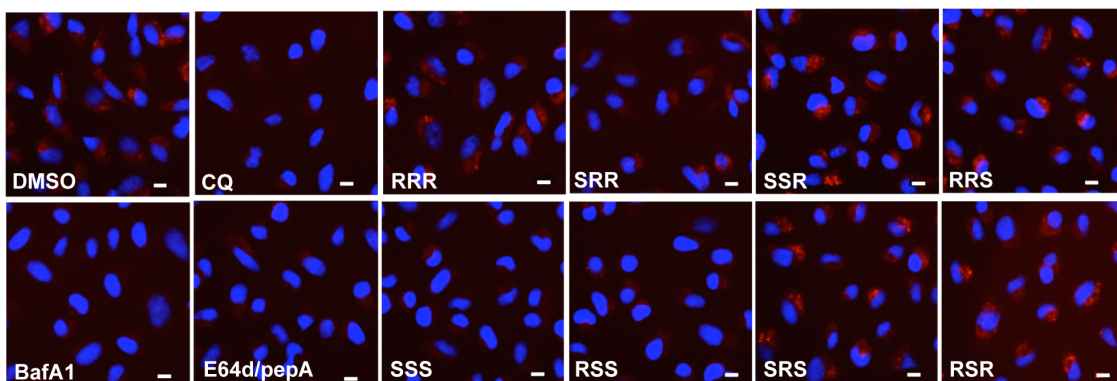


**Figure S3.2.** (A) Representative images from the tandem reporter-LC3 assay following treatment with DMSO, PI-103 (5  $\mu$ M), BafA1 (100 nM), RSR, SRS, RRS, SSR and SRR (all 10  $\mu$ M). Blue (Hoechst 33342), Red (mCherry), Green (eGFP). Scalar bars represent 10  $\mu$ m. (B) Representative images from the LysoTracker displacement assay following treatment with BafA1 (100 nM), BRD1240 (SSS) and its stereoisomers (all 10  $\mu$ M). Blue (Hoechst 33342), Red (LysoTracker). Scalar bars represent 10  $\mu$ m. (C) Representative images from the DQ-BSA assay following treatment with DMSO, chloroquine (CQ, 50  $\mu$ M), BafA1 (100 nM), E64d/pepA (10  $\mu$ g/mL each), BRD1240 (SSS), and all seven stereoisomers (all 10  $\mu$ M). Blue (Hoechst 33342), Red (DQ-BSA). Scalar bars represent 10  $\mu$ m.



**Table S3.1.** Representative images from the GFP-LC3 punctae formation assay and LysoTracker assay following treatment with DMSO, BRD1240, and all analogs (20  $\mu$ M). Blue (Hoechst 33342), Green (eGFP), Red (LysoTracker). Scalar bars represent 20 $\mu$ m (GFP-LC3) and 10 $\mu$ m (LysoTracker).

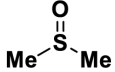
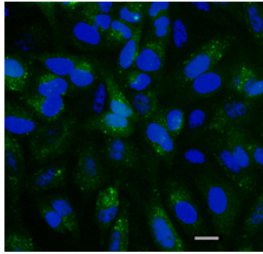
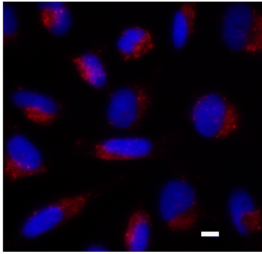
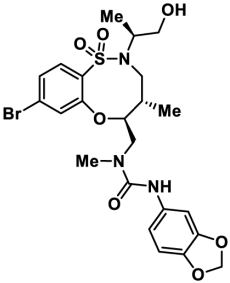
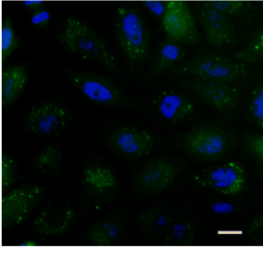
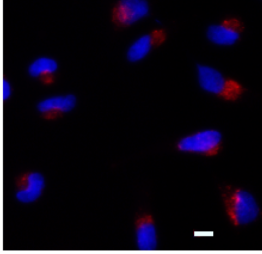
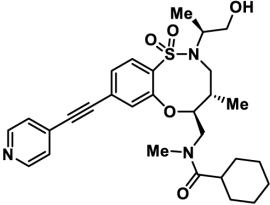
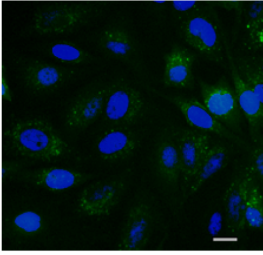
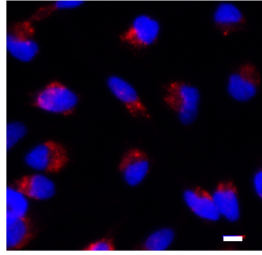
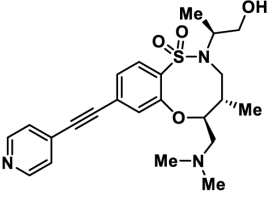
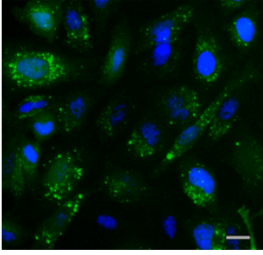
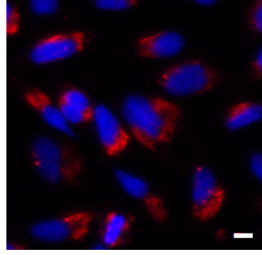
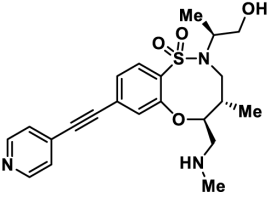
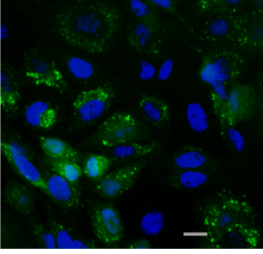
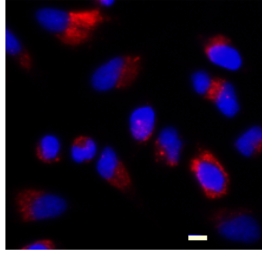
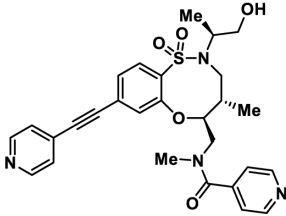
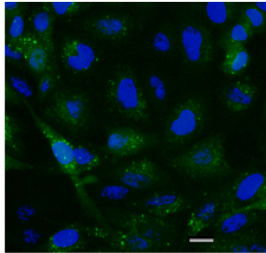
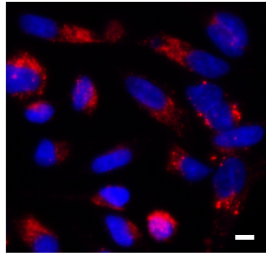
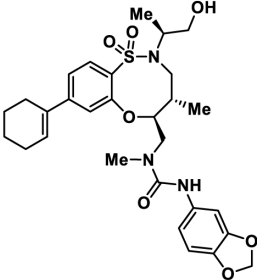
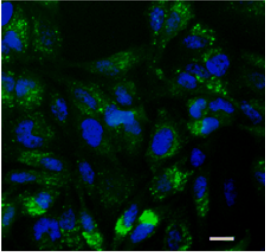
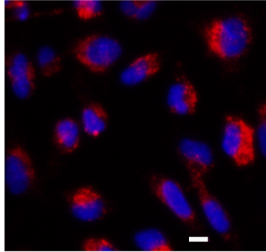
Broad ID		GFP-LC3 (20 $\mu$ M)	LysoTracker (20 $\mu$ M)
DMSO			
BRD6840			
BRD9117			
BRD7039			
BRD2852			

Table S3.1. (Continued)

Broad ID	GFP-LC3 (20μM)	Lysotracker (20μM)	
BRD0237			
BRD1609			
BRD1240			
BRD1295			
BRD5960			

Table S3.1. (Continued)

Broad ID	GFP-LC3 (20 $\mu$ M)	Lysotracker (20 $\mu$ M)	
BRD73146	 <p>Chemical structure of BRD73146: A 1,3-dioxane ring substituted with a methyl group, a hydroxymethyl group, a sulfonamide group, and a 4-(4-pyridyl)but-1-yn-1-yl group. The sulfonamide nitrogen is also substituted with a methyl group and a 4-pyridyl group.</p>	 <p>Fluorescence microscopy image showing GFP-LC3 (green) and DAPI (blue) staining of cells treated with BRD73146. A white scale bar is present in the bottom right corner.</p>	 <p>Fluorescence microscopy image showing Lysotracker (red) and DAPI (blue) staining of cells treated with BRD73146. A white scale bar is present in the bottom right corner.</p>
BRD7020	 <p>Chemical structure of BRD7020: A 1,3-dioxane ring substituted with a methyl group, a hydroxymethyl group, a sulfonamide group, and a 4-(cyclohex-1-en-1-yl)phenyl group. The sulfonamide nitrogen is also substituted with a methyl group and a 4-(2,3-dihydrobenzofuran-5-yl)butanamide group.</p>	 <p>Fluorescence microscopy image showing GFP-LC3 (green) and DAPI (blue) staining of cells treated with BRD7020. A white scale bar is present in the bottom right corner.</p>	 <p>Fluorescence microscopy image showing Lysotracker (red) and DAPI (blue) staining of cells treated with BRD7020. A white scale bar is present in the bottom right corner.</p>

# **Appendix C**

**Supplementary Materials for Chapter IV**

## Supplementary Methods

**Determining optimal 25°C incubation time for HTS AlphaLISA assay.** Lysates of dual-tagged T300A HeLa cells were prepared at 3,000 cells per  $\mu\text{L}$  in lysis buffer (25 mM Tris-HCl pH 7.6, 0.5% NP-40, 150 mM NaCl, 1mM EDTA, 1mM Pefabloc SC, 10 $\mu\text{g}/\text{mL}$  Aprotinin) supplemented with 10mM DTT. If compound treatment was applied, compounds were mix with lysates to desired concentrations. Caspase-3 was diluted to 0.004 units per  $\mu\text{L}$  in lysis buffer supplemented with 10mM DTT, and then incubated at 25°C for 15 minutes. Strep-Tactin Alpha donor beads (PerkinElmer, AS106), anti-FLAG AlphaLISA acceptor beads (PerkinElmer, AL112) and z-DEVD-FMK were diluted in PBS supplemented with 0.1% BSA to the final concentration of 60  $\mu\text{g}/\text{mL}$ , 15  $\mu\text{g}/\text{mL}$  and 30  $\mu\text{M}$ , respectively. 5  $\mu\text{L}$  of lysates was added into each well of AlphaLISA plates (PerkinElmer, 6008350), and then 5 $\mu\text{L}$  caspase-3 was added for 75, 60, 50, 40, 30, 20, 10 and 0 minute incubations at 25°C. 5  $\mu\text{L}$  beads were then distributed into each well, followed by 1 hour incubation at room temperature. Plates were read on Wallac Envision plate reader (PerkinElmer) with “AlphaScreen” protocol.

**Optimizing combi dispensing speeds for HTS AlphaLISA assay.** The initial automation protocol of HTS AlphaLISA assay used slow speed for all combi-dispensing speeds. Starting from the second batch of experiments, it was observed that the tubes of combi cassette used for dispensing beads were sometimes clogged and affected the volume of reagent dispensed. Using a new combi cassette did not significantly improve the clogging conditions. After experimentally tested various factors, the dispensing speed was the most relevant factor to the clogging conditions. Based on this observation, the combi-dispensing speed of beads was changed to medium for the last batch of primary screen and for the confirmation assay. The dispensing speed of lysate and caspase were kept at low speed, since no clogging conditions were observed and a medium dispensing speed could generate bubbles in wells when used for either of these two reagents.

## Supplementary Figures

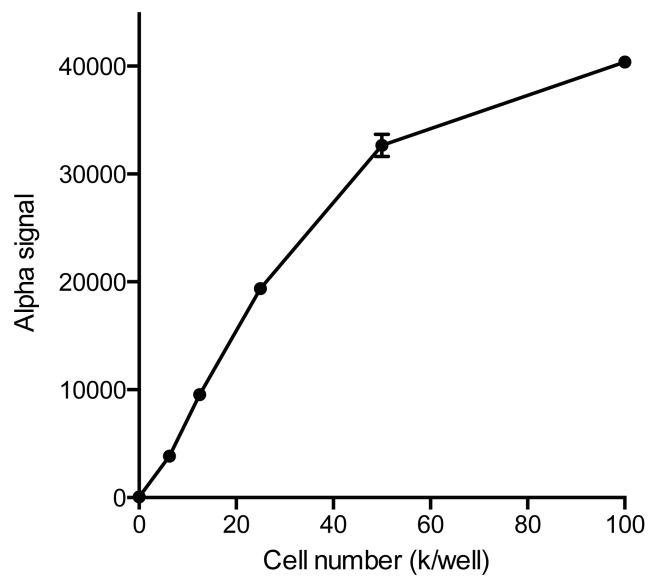


**Figure S4.1. Measurement of level of full-length ATG16L1 T300A in the AlphaLISA assay.** Cell lysates of HeLa cells stably expressing dual-tagged ATG16L1 T300A were plated at various concentrations. Levels of full-length ATG16L1 were measured by AlphaLISA. Data are presented as mean  $\pm$  SD,  $n = 2$ . All data are representative of multiple independent experiments.

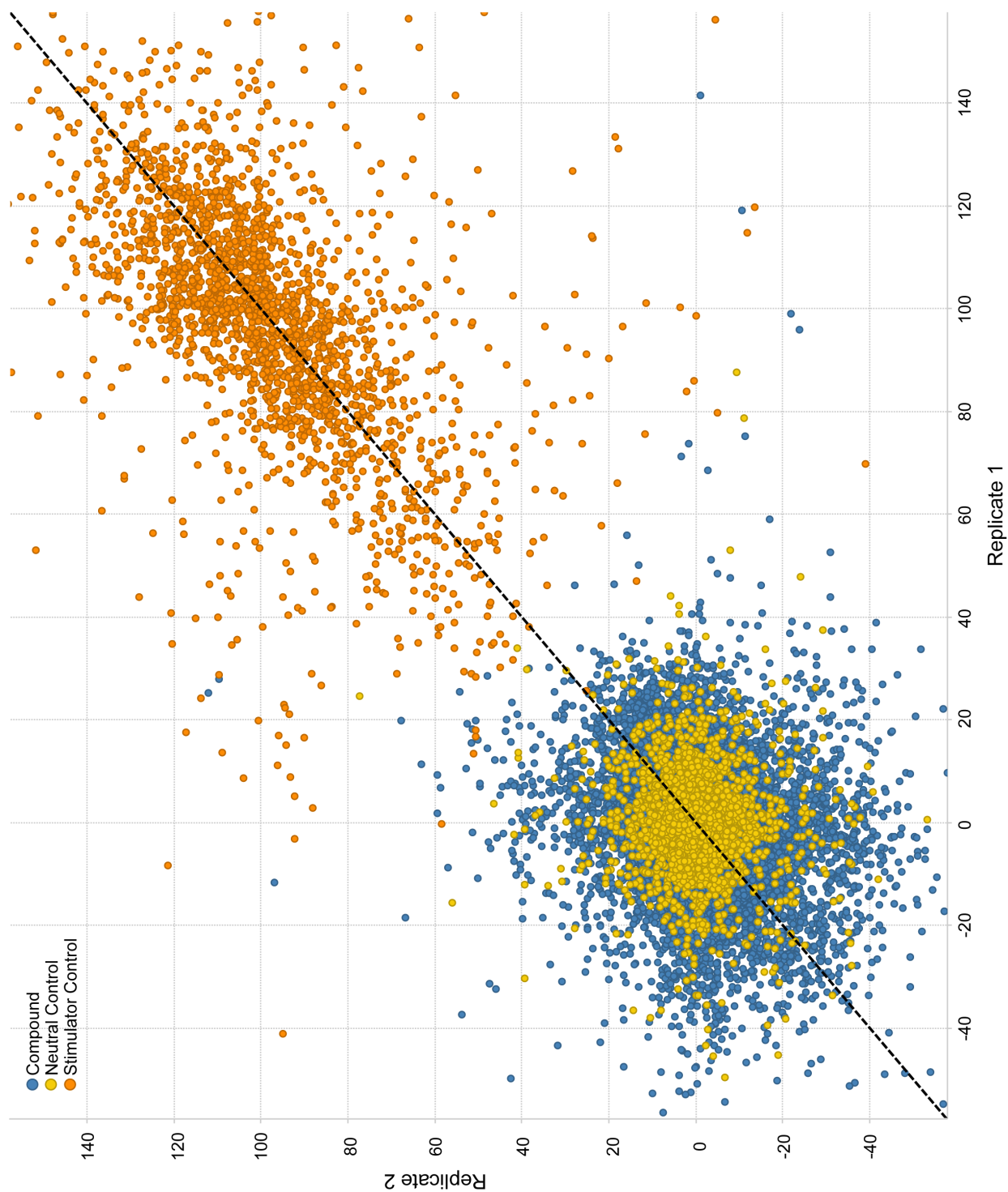


**Figure S4.2. Performances of 20,876 small molecules in protecting ATG16L1 from caspase-3 cleavage.** Percent effects of positive controls, neutral controls and compounds were plotted.

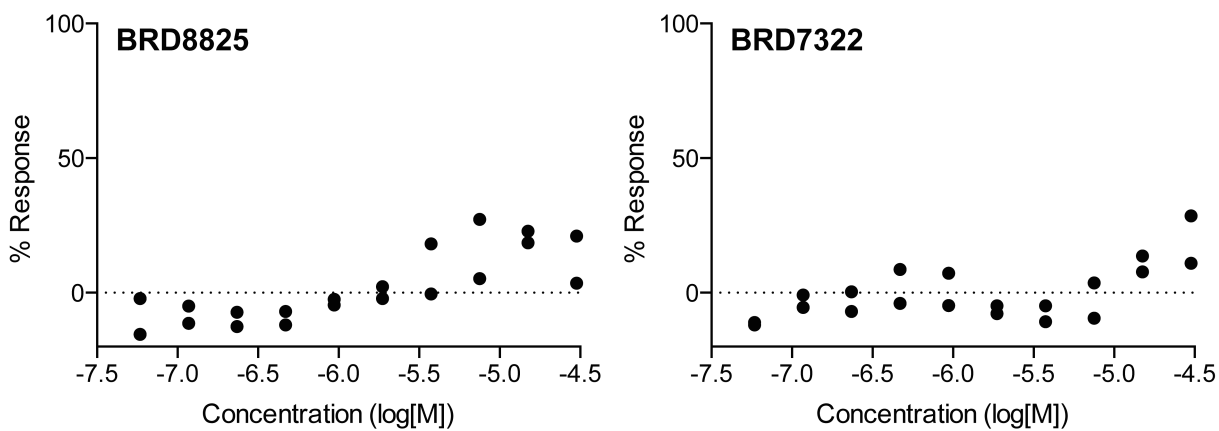


**Figure S4.3. Performances of 3 weak hits in the confirmation screen.** Compounds were tested in-dose in duplicate in the automated AlphaLISA assay. The values of % response were calculated as following: the average value of Alpha signal of in-plate neutral control wells was subtracted from the value of each well, and then the subtracted value was normalized to the average Alpha signal of in-plate positive control wells.